

DEVELOPMENT OF INNOVATIVE BURN RATE ADDITIVES FOR
DOUBLE BASE PROPELLANT

A Thesis
Submitted to
the Temple University Graduate Board

In Partial Fulfillment
of the Requirements for the Degree of
DOCTOR OF PHILOSOPHY

by
Carl E. Lundell
May 2023

Examining Committee Members:

Dr. Michael Zdilla, Dissertation Supervisor, Temple University
Dr. Robert Levis, Dissertation Advisory Chair, Temple University
Dr. Frank Spano, Dissertation Examining Chair, Temple University
Dr. Sam Cowart, External Committee Member, United States Military Academy

©
Copyright
2023

by

Carl Lundell

All Rights Reserved

ABSTRACT

It was accidentally discovered in the 1940s that the addition of lead to double-base propellants, resulted in beneficial burn rate phenomena. However, due to its toxicity the Department of Defense has been trying to find a replacement for lead over the last decade. Research efforts with this goal in mind have generally used the same methodology of either adding different metals, using different grain sizes, or using different concentrations to obtain the same burn rate effects as lead. Although some metal oxides demonstrated significant promise, they also depleted the double-base propellant stabilizer faster than acceptable, decreasing shelf life. The research explored herein does not take the same approach, but rather attempts to replace lead and solve the stability problem at the molecular level using a novel design. The new method was to synthesize a stabilizer ligand complex with a less toxic metal to create a complex that both stabilized the propellant and provides a burn rate modifying agent. First, the syntheses of two leaded complexes, tetrakis (μ_3 -(4-methyl-3-nitrophenyl imido lead (II))) and bis(dinitrophenyl imido lead(II)) are reported as both a proof of concept and to determine a feasible synthetic pathway. After various unsuccessful attempts using common stabilizer molecules as ligands, n-phenylurea was identified as a suitable analogous stabilizer molecule and was bonded to a cobalt center to create hexa-1-phenylurea cobalt(II) nitrate. Additionally and serendipitously, unreported complexes of metal ions with dicyanamide were discovered, which generated a discussion between ligand strength and metal center. Each of the complexes are characterized in depth and many physical properties determined.

DEDICATION

This thesis is dedicated most importantly to my wife Lisa and children Kira and Mia. I have put them through a lot both being in the Army and simultaneously trying to complete this undertaking. I would also like to dedicate this to my mom, and in-laws who always remained encouraging through many a long day and sometimes weekends. I couldn't have asked for a better team of cheerleaders.

ACKNOWLEDGMENTS

I cannot express enough gratitude to my research advisor Dr. Michael Zdilla. His flexibility, patience and insight were critical to me completing this endeavor – many others would have become frustrated with my very atypical research path, but he remained supportive and positive throughout. For that, I owe him a very sincere, “Thank You”. I need to mention my wife Lisa and children Kira and Mia. Their patience through this process and support were a constant support when things became difficult. I would also like to thank my friend Taylor Keller who I had the good fortune of sitting next to my first day of class. Her help through the years answering general chemistry and crystallography questions at all hours of the day and days of week made this possible. The few lunches and drinks I bought her throughout graduate school didn’t come close to providing the appreciation she deserves.

I mentioned my old lab mates in my Masters Thesis and so I would like to say it has been great getting know my new lab group: Chris, James, Laura, Alex & Alex, Brody, and Jacob. I need to give a special acknowledgement to Chris and to Alex Beebe who helped get my final complex over the finish line.

Lastly, Shiva – thanks for always graciously giving me your x-ray time when we both tried to use the XRD and providing me those little chemistry tips and tricks that made my research that much easier.

PREFACE

Chapter 1 exposes the reader to a history of propellants, their various types and components. Double-base propellants and the burn rate phenomena observed from the addition of a lead burn rate additive are discussed in depth. A research gap is found, and a research question is proposed.

Chapter 2 is a literature review and examines previous efforts to remove lead in double-base propellant. A methodology to answer the research question is provided.

In chapter 3, a proof of concept using lead and propellant stabilizers results in the successful crystallization of two lead complexes. Each lead product is discussed in depth and how their synthesis could provide insight into answering the research question.

Chapter 4 is a discussion of the failed pathways to combine a transition or p-block metal with a double-base propellant stabilizer to solve the research question. The eventual success of the n-phenylurea cobalt(II) complex is discussed, and its potential as a burn rate additive.

Chapter 5, is a short discussion on collaboration efforts and their results. The first discussed is a short examination of geometries and ligand competition between dicyanamide and pyridine. The second discussion is focused upon iridium complexes produced by the United States Military Academy and Army Research Laboratory that were characterized using x-ray diffraction.

Chapter 6 provides the reader with results of the endeavor, discusses each novel complex of interest what questions remain unanswered.

Chapter 7, the final chapter, is the experimental section of the manuscript.

TABLE OF CONTENTS

	Page
ABSTRACT.....	iii
DEDICATION.....	iv
ACKNOWLEDGMENTS	v
PREFACE.....	vi
APPENDICES	xi
LIST OF FIGURES	xii
LIST OF EQUATIONS	xiv
1. INTRODUCTION: PROPELLANTS AND BURN RATE PHENOMENA.....	1
1.1 Propellants.....	1
1.1.1 Types of Propellants	1
1.1.2 Solid Propellant Chemical Energy.....	3
1.1.3 Double-Base Propellants.....	4
1.1.4 Burn Rate Catalysts and Burn Rate Modifiers.....	6
1.2 Burn Rate Phenomena.....	7
1.2.1 Super-rate, Plateau, and Mesa Phenomena	7
1.2.2 Double-Base Combustion Reactions	9
1.3 Propellant Stabilizer Reactions.....	10
1.3.1 Use of Propellant Stabilizers.....	10
1.3.2 Proposed Stabilizer Reactions	11

1.4 Research Question	12
1.5 References.....	13
2. LITERATURE REVIEW	15
2.1 Ballistic Modifiers	15
2.1.1 Leaded Ballistic Modifiers.....	15
2.1.2 Unleaded Alternatives.....	17
2.2 Double-base propellant stabilizers.....	19
2.3 Methodology.....	21
2.4 References.....	21
3. LEAD METAL AND STABILIZER LIGAND COMPLEXES	23
3.1 Metal Bis(trimethylamine) Reactions	23
3.2 Reagents.....	24
3.3 Products.....	25
3.3.1 Tetrakis(μ_3 -(4-methyl-3-nitrophenyl imido lead(II)))	26
3.3.2 Bis(dinitrophenyl imido lead(II)).....	30
3.4 Summary of Results	34
3.5 Unexpected High Energy Lead Species.....	35
3.6 Discussion.....	35
3.7 References.....	36
4. SYNTHESIZING AN INNOVATIVE METAL LIGAND COMPLEX	37
4.1 Transition Metals with Stabilizer Ligand Complexes	37
4.1.1 Deprotonation Using N-butyllithium.....	37
4.1.2 Deprotonation Using Trimethylamine	38

4.1.3 Deprotonation Using NaOH	38
4.2 <i>n</i> -Phenylurea Ligand.....	39
4.2.1 Hexa-1-Phenylurea Cobalt(II) Nitrate	39
4.3 Results of DoD Compatibility Testing	43
4.4 Discussion.....	44
4.5 References.....	44
5. CRYSTAL STRUCTURES FOR FUTURE STUDY	45
5.1 Bis(dicyanamide) Tetrakis(pyridine) Cobalt (II)	45
5.2 Bis(dicyanamido) Tetrakis(pyridine) Nickel (II)	46
5.3 Tetrakis(dicyanamido) Dipyridine Manganese (II)	47
5.4 Zinc Dicyanamide	48
5.5 Lead Dicyanamide	49
5.6 Dimethylimidopyridine Dicynamido Copper (II).....	49
5.7 Bis(dicyanamido) Tetrakis(pyridine) Palladium(II)	50
5.7 Discussion	51
5.7.1 The Geometry of the Crystal Complexes.....	51
5.7.2 Describing the Pyridine Dicyanamide Ligand Competition	52
5.8 Iridium Coordination Crystals	54
5.8.1 Ir[(6-(4-methoxyphenyl)-2-pbt) ₂ (acac)]	54
5.8.2 Ir[(6-(3,5-difluorophenyl)-2-pbt) ₂ (acac)]	55
5.9 References.....	56
6. CONCLUSION.....	57
6.1 A Summary of Results	57

6.2 Lead Complexes 1 and 2.....	57
6.3 Hexa-1-phenylurea Cobalt(II) Nitrate.....	58
6.4 Metal dicyanamides and Ir Complexes.....	59
6.5 Future Research	59
7. EXPERIMENTAL.....	60
7.1 Experimental Details.....	60
7.2 Synthesis of Reactants	61
7.2.1 Lead Bis(trimethylsilyl)amide	61
7.2.2 Tin Bis(trimethylsilyl)amide.....	61
7.2.3 Bismuth Bis(trimethylsilyl)amide.....	62
7.2.4 Zinc Bis(trimethylsilyl)amide.....	62
7.3 Synthesis of Novel Products	62
7.3.1 Tetrakis(μ_3 -(4-methyl-3-nitrophenyl imido lead (II)))	62
7.3.2 Bis(dinitrophenyl imido lead (II)).....	63
7.3.3 Hexa-1-Phenylurea Cobalt (II) Nitrate	64
7.3.4 Bis(dicyanamido) Tetrakis(pyridine) Cobalt(II).....	64
7.4 Calorimetry	65
7.5 Stabilization Testing	66
7.6 References.....	66
BIBLIOGRAPHY.....	67

APPENDICES

A. Crystal data for Tetrakis (μ_3 -(4-methyl-3-nitrophenyl imido lead(II)).....	70
B. UV-vis spectra for Tetrakis (μ_3 -(4-methyl-3-nitrophenyl imido lead(II)))	81
C. Crystal data for Bis(dinitrophenyl imido lead (II))	82
D. UV-vis spectra for Bis(dinitrophenyl imido lead(II))	88
E. Crystal data for Hexa-1-phenylurea Cobalt(II) Nitrate	89
F. Crystal data for Bis(dicyanamide) Tetrapyridine Cobalt(II)	96
G. Crystal data for Bis(dimethylimidopyridine) Tetrakisdicyanamide Cobalt(II)	103
H. Crystal data for Ir[(6-(4-methoxyphenyl)-2-pbt) ₂ (acac)]	108
I. Crystal data for Ir[(6-(3,5-difluorophenyl)-2-pbt) ₂ (acac)]	119

LIST OF FIGURES

Figure	Page
1. HELLFIRE missile.....	2
2. Structures of NG and NC	5
3. Sketch of 'n'.....	8
4. Wave zones.....	9
5. Wang crystal.....	16
6. Common Propellant Stabilizers.....	20
7. Stab-5 and Retinyl acetate.....	20
8. Metal reactant.....	23
9. 4-methyl-3-nitroaniline.....	24
10. 2-nitrodiphenylamine.....	24
11. Thermal ellipsoid plots of 1.....	27
12. ¹ H NMR spectra of 1.....	28
13. Energy densities of nitroamines and 1.....	30
14. Thermal ellipsoid plots of 2.....	31
15. ¹ H NMR spectra of 2.....	32
16. FTIR spectra of 2.....	33
17. Bomb calorimetry of 2.....	33
18. Energy densities of nitroamines and 2.....	34
19. Thermal ellipsoid plots of 3.....	40
20. ¹ H NMR spectra of 3.....	41
21. TGA and DSC Spectrum of 3.....	42

22. FTIR spectra of 3.....	42
23. Thermal ellipsoid plots of 4.....	45
24. Thermal ellipsoid plots of 5.....	47
25. Thermal ellipsoid plots of 6.....	48
26. Thermal ellipsoid plots of 7.....	48
27. Thermal ellipsoid plots of 8.....	49
28. Thermal ellipsoid plots of 9.....	50
29. Thermal ellipsoid plots of 10.....	51
30. Thermal ellipsoid plots of 11.....	55
31. Thermal ellipsoid plots of 12.....	56

LIST OF EQUATIONS

Equation	Page
1. Specific Impulse.....	3
2. Exit Velocity.....	3
3. Saint Robert's Law.....	9
4. Metal Bis(trimethylamine) Reactions.....	24
5. Formation of Tetrakis (μ_3 -(4-methyl-3-nitrophenyl imido lead (II)).....	26
6. Formation of Bis (dinitrophenyl imido lead (II)).....	30
7. Formation of Hexa-1-phenylurea Cobalt (II) Nitrate.....	40

CHAPTER 1

INTRODUCTION: PROPELLANTS AND BURN RATE PHENOMENA

[This introduction was adapted from Lundell, C.E. M.A. Thesis, Temple University, Philadelphia, PA, 2017.]

1.1 Propellants

1.1.1 Types of Propellants

For more than 800 years, chemical propellants have powered objects through the air. Nuclear power as a source of energy for propulsion remains in its nascent stages and has high hurdles to overcome; for the time being, conversion of chemical reactants into high temperature gases remains by far the best performing method of propulsion.¹ The primary components of propellants are an oxidizer and fuel, in addition to a number of other components, to ensure maximum effectiveness and simplicity of use. The fuel's chemical bonds break and form new product bonds, releasing heat and a large number of gas molecules. The motor nozzle is used to deliver thrust by passing the high pressure generated by the expanding gas and heat.

The propellants first discovered used solid fuel, but three primarily distinct types have been developed: solid, liquid, and hybrid.¹ Although solid propellants were the first to be developed, they still possess numerous advantages over later-developed liquid and hybrid types. Solid propellants are more dependable, less expensive, and their counterparts simpler to maintain. Solid propellants, on the other hand, are temperature-sensitive, unable to restart once stopped, and rely on the shape of the propellant grain to generate thrust. Their higher density also makes it possible for the designs to be smaller. During production, solid propellants must be inspected for cracks and voids. Rocket performance will suffer as a result of the loss of propellant density caused by trapped pockets of air.



Figure 1. HELLFIRE missile. MQ-9 Reaper firing HELLFIRE missile filled with minimum-smoke cross linked double base (XLDB) solid propellant

Additionally, air pockets or "worm hole" gaps have the potential to significantly increase the burn surface area, which can lead to an explosion and over pressurization of the rocket motor.¹ Cruise missiles like the Tomahawk, AGM-114 Hellfire, and AIM-9E Sidewinder all make extensive use of solid propellants (Figure 1). Solid propellants can be broken down into the following categories, each of which is intended for a specific purpose: single, double, triple, and composite.² The primary goal of this research effort will be to modify a double base (DB) propellant.

Since the 1920s, liquid propellants have outperformed solid propellants - more thrust is produced for the same volume of solid propellant, and combustion can be restarted once it has stopped. However, liquid propellants are more complicated systems that frequently fail. This is due to the renowned fragility of the seals and valves needed for liquid propellants. Monopropellants and bipropellants are the two main types of liquid propellants.¹ Hybrid systems, on the other hand, are the most recently developed propellants. In a hybrid propellant system, the fuel is kept in another phase before being combined with the oxidizer. This rocket system can

perform better than designs that use liquid or solid propellant. Although they are not as expensive as other types, they are still the most complicated and least reliable, so they haven't been widely used.¹ Propellant performance (next section) is measured the same way regardless of the propellant system.

1.1.2 Solid Propellant Chemical Energy

Propellants are commonly measured using two different metrics: heat of combustion (ΔH_c) and specific thrust or specific impulse (I_{sp}). ΔH_c is the potential chemical energy released from the propellant mixture at 25°C. The second metric, I_{sp} , measures the efficiency of the working substance. Since calorimetry is both temperature and pressure dependent, I_{sp} is most commonly used when comparing propellant performance.³

To determine the I_{sp} , the exit velocity of the propellant combustion product must be determined. The ideal exhaust velocity equation is used to calculate the V_e (Equation 1 below):

$$V_e = \sqrt{\left(\frac{2k}{k-1}\right)\left(\frac{R^*T_c}{M}\right)\left(1 - \left(\frac{P_e}{P_c}\right)^{(k-1)/k}\right)} \quad \text{(Equation 1)}$$

In the equation above, k is the specific heat ratio, R^* is the ideal gas constant (8,314.4621 J/kmol)-K, T_c is the combustion temperature, M is the molecular weight of the exhaust gases, P_c is the combustion chamber pressure, and P_e is the pressure at the nozzle exit. Once determined, the I_{sp} can be calculated by the V_e divided by gravitational acceleration of the earth (g_e) found in Equation 2 below.³

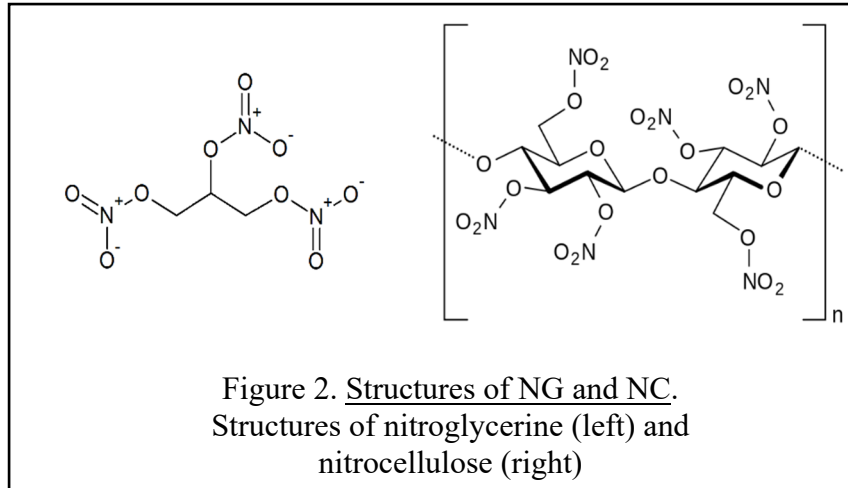
$$I_{sp} = V_e/g_e \quad \text{(Equation 2)}$$

Because specific impulses represent thrust per mass flow, they are preferable to total impulse for measuring thrust. Sutton uses the comparison of specific impulse to that of automobile miles per gallon.² Specific impulse is time averaged and results in a unit per second, so it is unaffected by changes in thrust over time.² The burn rate is a measured characteristic of propellant combustion and is crucial to the research presented here. The burn rate, which is expressed as a distance per second, is the rate at which solid propellant is consumed. Temperature and pressure, among other factors, can have a significant impact on burn rates. A phenomena of burn rate and pressure, which will be covered in greater detail later in this thesis, will serve as the foundation for the research question to be answered.

1.1.3 Double-Base Propellants

Solid propellants for rockets and missiles are either composite modified double-base (CMDB), modified double-base (MDB) or simply double-base (DB).

Double base propellants consist of: 50% nitrocellulose (NC) (12.6% nitrogen), 34.9% nitroglycerine (NG) or more commonly 1,2,4-Butanetriol trinitrate (BTTN), 10.5% diethyl phthalate, 2% 2- nitrodiphenylamide, 1.2% Lead Salicylate, 1.2% lead 2- ethyl hexoate, .2% candelilla wax (Figure 2).⁴ DB propellants are doped with High Velocity Military Explosive (HMX), triactin, ammonium perchlorate or aluminum metal are called modified DB propellants and can perform better in particular situations. The most complicated type, composite propellants, use ammonium perchlorate as an oxidizer with an added composite polymer. Cross-linked (XLDB) is an additional type of composite modified double-base propellant which has an increase in tensile strength and structural integrity by use of a polymer binder.⁵



The term "smoke-less" propellant is also used to describe 50/50 NC and NG blends. This is because double-base propellant produces much less smoke than other formulations. Smoke signatures are reduced and the missile's source and path are obscured by excluding non-volatile energetic additives.

Although the nature of DB propellants appears to be straightforward at first glance, their actual composition is complex, with a variety of additives in small amounts determining its performance. The primary components, along with a brief description of each one, are as follows:⁶

(1) Nitroglycerine serves as the propellant's fuel and oxidizer. It is relatively stable, easy to mass produce, and has a high potential chemical energy, but it is too sensitive to use unblended.

(2) The primary function of the nitrocellulose is to act as an energetic binder that holds the propellant together.

(3) An additional plasticizer is diethyl phthalate.

(4) A stabilizer for propellants are molecules such as 3-Methyl-1,1-diphenylurea

(Akardite II) or 2-nitrodiphenylamide (NDPA). The benzylic N-H slows down the autocatalytic decomposition of the propellant's nitrocellulose resulting from the release of nitrogen-oxide-based radicals. The DB propellant's shelf life is significantly extended when a stabilizer is added. This is an important part of the motivation of the research presented here, and the mechanisms that are related to decomposition of nitrocellulose will be explained in detail later in this chapter.⁷

(5) Lead salicylate, also known as lead 2-ethyl hexoate, is added as a ballistic modifier. It is crucial to the burn rate phenomena that have been observed, which are extensively discussed in the next section, and it is also crucial to the research hypothesis that will be presented in later sections.

(6) The candelilla wax aids in molding and serves as a lubricant.

Each of these components has been the subject of a lot of research into how to improve performance. To reduce toxicity and lengthen storage times, for instance, various stabilizers have been studied.⁸ However, the ballistic burn rate modifiers, also known as burn rate catalysts, have arguably received the greatest amount of research funding.

1.1.4 Burn Rate Catalysts and Burn Rate Modifiers

Many solid DB propellants contain burn rate catalysts (BRCs) or burn rate modifiers, which are necessary components. They eliminate a significant amount of the smoke that is produced and improve the propellant's burn rate at pressure ranges needed for specific application. Burn rates are greatly enhanced by copper organic chelates or lead-iron double metal chelates.^{9,10} However, ferrocene-based BRCs migrate within the propellant, reducing shelf life and altering designed burning parameters.^{9,10} Ferrocene derivatives containing alkyl, acyl, and ester functional groups demonstrate additional improved performance in butyl hydroxide

propellants containing ammonium perchlorate (AP), aluminum powder, and Royex Demolition Explosive (RDX). Substances like lithium fluoride are occasionally added to propellants to slow the burn rate in order to tailor the propellant grain and thrust requirements.⁹ Recent research has revealed that ferrocene-based BRCs do not diffuse within the propellant under storage conditions.

During World War II, it was discovered that when added to double-base propellants, lead produced very desirable ballistic effects on burn rate and pressure. During the propellant excursion process, it was observed that adding a small amount of lead increased burn rates at low pressures or “super-rate” burning. Then burn rate is independent of pressure (plateau), followed lastly by mesa burning when burn rate decreases with an increase in pressure.

1.2 Burn Rate Phenomena

1.2.1 ‘Super-Rate’, ‘Plateau’, and ‘Mesa’ Phenomena

Burn rate is profoundly affected by chamber pressure. The usual representation of the pressure dependence on burn rate can be demonstrated in Saint-Robert's Law;

$$r = ap^n \quad (\text{Equation 3})$$

where r is the burn rate, a is the burn rate coefficient, n is the pressure exponent, and p is the combustion chamber pressure. The values of a and n are determined experimentally for a propellant formulation and cannot be easily predicted. It is important to realize that a single set of a and n values are typically valid over a distinct pressure range. Typical burn rates increase linearly with an increase in pressure (Figure 3).¹¹ However, under plateau conditions a burn rate phenomenon occurs, and the burn rate does not increase with pressure. The pressure exponent (n), is approximately zero for plateau burning and is negative for mesa burning, as shown below

in Figure 3. The physical and chemical properties of the lead additive and amount used greatly effect pressure exponent of super-rate, plateau, and mesa burning. Furthermore, as the density of the NC-NG compound is varied, or heat of explosion is altered, the pressure exponent of the burn rate (n) remains unchanged (~ 0.64).¹²

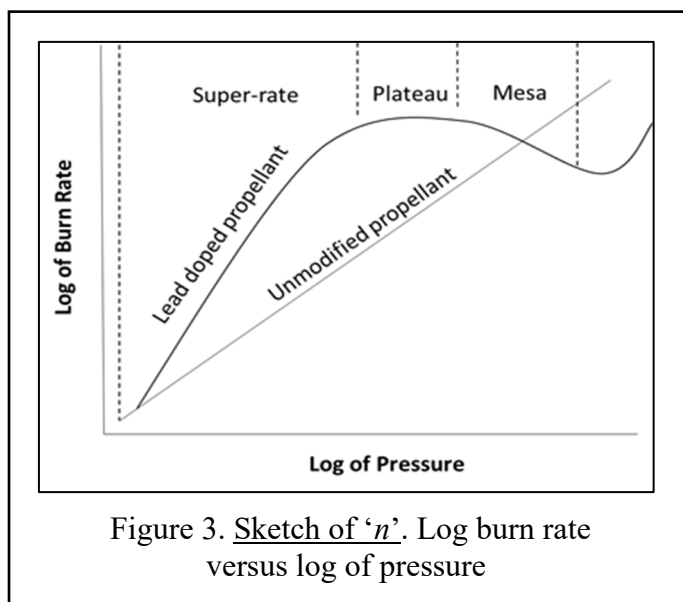


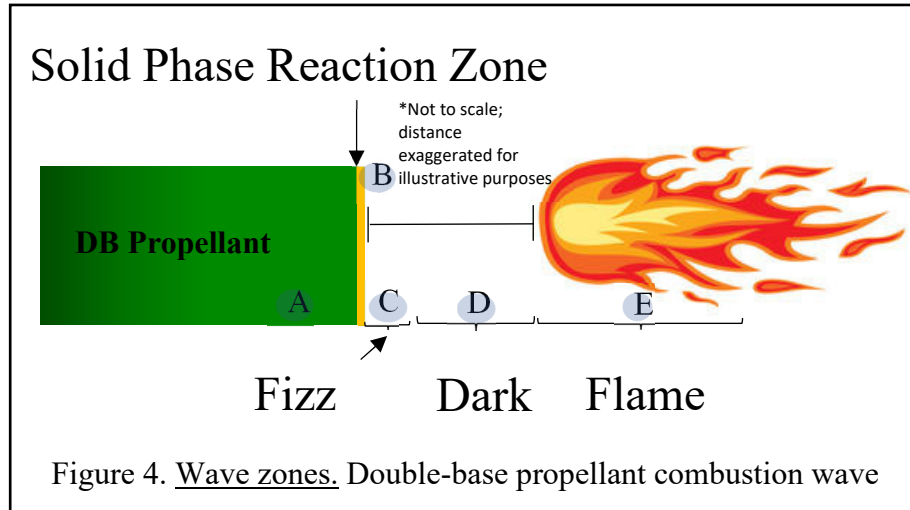
Figure 3. Sketch of 'n'. Log burn rate versus log of pressure

When n is greater than 0.8 at low pressures, lead-catalyzed propellant experiences super rate burning. As a result, motor performance immediately following ignition is enhanced when the burn rate is higher than that of unleaded propellant at low pressure. However, burning can become erratic when " n " is greater than 1, so the value n must be stopped. Fortunately, a plateau zone exists where the burn rate is independent of the combustion chamber pressure. The rocket motor's stress will be significantly reduced as the burn rate drops at higher temperatures.

However, not all Pb compounds result in these shifts in burn rate. Some lead compounds, like PbBr_2 , PbI_2 , and PbCl_2 , do not, for instance. However, lead salicylic acid and lead 2-ethylhexoate do.¹¹ The exact cause of this phenomenon has not yet been determined, but some research supports the hypothesis that band gap is a factor.^{13,14}

1.2.2 Double-Base Combustion Reactions

Double-base propellant combustion is achieved over several sequential chemical reactions that take place within different burn “zones” (Figure 4).



In zone A, the propellant increases in temperature but does not start to degrade until the solid phase reaction zone, (B) when enough energy is applied to break chemical bonds within the fuel. The atoms recombine to form NO_2 , aldehydes, and NO , making the reaction exothermic. In the fizz zone (C) nitrogen dioxide, aldehydes and other C, H, O species react to produce nitric oxide, carbon monoxide, water, hydrogen, and carbonaceous materials. This reaction process occurs very rapidly just above the burning surface. In the dark zone the same reactions as (D) take place but much slower. Finally, in the flame zone (E), N_2 , CO , CO_2 , H_2O and H_2 are formed, with the formation of N_2 releasing much of the energy in the form of heat and completing the reaction.¹¹

However, lead doped propellants create lead oxides at the solid phase reaction zone, creating conditions for super-rate burning. Sharma et al., proposed that metallic lead reacts with NO_2 to form lead oxide (Sharma observed this oxide in post-mortem XPS studies). Sharma

concluded that the lead oxides greatly increase the oxidation rate of carbon by five orders of magnitude producing more CO₂ and thus “super-rate” burning.¹⁵

Similarly, Sharma supports conclusions from Otto et al., that Pb(s) eventually saturates the burning surface, plugging gaps within the carbon structure on the surface and slowing the burn rate regardless of pressure, creating the “plateau” and “mesa” regions.¹⁶

This is a simplified version of one hypothesis of how lead effects DB combustion, but many others exist including the examination of band gap by Warren et al. In their work, a direct and small band gap is observed between the Pb(II) d-orbital and oxygen p-orbital within PbO. However, when comparing PbO₂, SnO₂ and Bi₂O₃ the band gap was found to be much larger and indirect – leading the researchers to hypothesize that the small band gap observed influence lead catalytic burn rate activity.¹⁷ The chemistry is not fully understood and still debated, with numerous hypotheses attempting to answer this question.

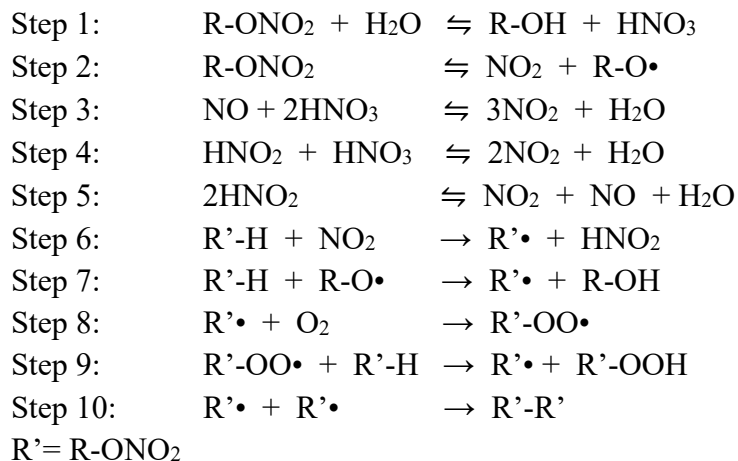
1.3 Propellant Stabilizer Reactions

1.3.1 Use of Propellant Stabilizers

Any propellant that contains nitrate esters, has a small amount of propellant stabilizer added to inhibit the decomposition of the material. Although only added in quantities in <5% of volume, they are instrumental in keeping the propellant safe for long periods of time. It is generally believed that conventional stabilizers and phenol containing compounds trap •NO₂ and produces nitro or nitroso derivatives.¹⁸ Additionally, there is an observed heat release of NC during shelf-decomposition but it was reported that O₂ rather than •NO₂ was the more likely factor in producing the exothermic reaction.¹⁸

1.3.2 Proposed Stabilizer Reactions

Katoh, et al. did a number of thermal stability experiments in 2007 comparing common stabilizers such as diphenylamine (DPA) versus various phenol compounds such as diphenyl urea.¹⁹ From these experiments they proposed the following reaction mechanism that is similar to that of many other publications:



Steps 1-5 generate NO₂ and RO• which in turn, abstracts a hydrogen from the NC in steps 6 and 7. The produced R' and O₂ start autoxidation in steps 8 and 9. This mechanism explained the experimental results that Katoh observed for steps 8-10 creating the most heat released.

Katoh and his fellow researchers were also able to make a number of important observations from differences discovered between DPA and phenol compounds. Although conventional stabilizers likely trapped NO₂ in the initial process (steps 1-5) this only contributed a minor amount of heat release. The phenol compounds decreased the heat release more than the stabilizer, possibly from trapping ROO generated in steps 8 and 9, preventing autoxidation which contributed the preponderance of heat. The observed success of phenol compounds in arresting the decomposition of nitrocellulose will become important in chapter four.

1.4 Research Question

In any solid rocket motor design, the type of solid propellant is the largest performance factor. Solid propellants should exhibit a high I_{sp} , be a dense matter, have predictable burning characteristics, be affordable, have a low smoke profile, possess a long shelf life and importantly, produce desirable thermal effects. However, toxicity has become a concern as well.

Since the 1990s the Department of Defense has attempted to replace the lead used in ballistic modifiers and replace it with a less toxic element to decrease handling precautions, ease recycling of propellants and reduce personnel exposure. Several other chemical elements have been pursued, including tin, bismuth, cobalt and copper in achieving the same effects as lead, but with limited success.^{18, 19} A useful substitute to create the same ballistic effects appears to be a mix of both copper and bismuth.¹⁶ This is an obvious area of research need, and resources are available. However, the chemistry is poorly understood and already routinely studied by numerous groups. Of particular importance was the discovery that transition metals such as cobalt oxide produced desirable burn rate effects, but depleted the stabilizers at unacceptable rates.²⁰

After close examination of these recent efforts, a research gap was identified. A literature review didn't reveal any efforts to synthesize a product that would combine a transition metal and propellant stabilizer. Successful synthesis of unleaded complexes could create a pathway to make less toxic additives that the DoD has been trying to achieve for almost 30 years. A thesis question was formed and research focus developed: *could a propellant stabilizer and a metal as ballistic modifier be combined to create a replacement double-base propellant additive?* This work builds upon research done in 2017 in pursuit of the same goal.²¹

1.5 References

1. Ramnarace, J. *Rocket Propellant Technology*, Page publishing: New York, NY, 2015.
2. Sutton, G. *Rocket Propulsion Elements*, Wiley: Hoboken, New Jersey, 2017.
3. Braeunig, R. A., Rocket and Space technology, <http://www.braeunig.us/space/propuls.htm> (accessed 5 January 2017).
4. Composition of Type N5 Nitrocellulose-based Double Base Propellant, courtesy of Island Pyrochemical Industries, http://www.islandpyrochemical.com/military/rocket_propellants.php.
5. Bhat, V.K.; Singh, H. Cross-Linked Slurry Cast Composite Modified Double Base Propellants: Mechanical Properties. *Def Sci J.*, **1987**, 37,1, 39-445.
6. Yang, V. Thakre, P. Encyclopedia of Aerospace Engineering, Blockley, R. and Shyy, W., Ed; John Wiley and Sons, Ltd: **2010**.
7. Apatoff, J. B.; Norwitz, G. *Role of Diphenylamine as a stabilizer in propellants; analytical chemistry of diphenylamine in propellants*; US Army Armament Command, Test Report T73-12-1, 1973.
8. Tunestål, E.; Hafstrand, A.; Lindborg, A.; Krumlinde, P.; Ek, S.; Goede, P.; Schragen, C. New stabilizers for NC-propellants Evaluated in Rocket Propellants. FOI, Swedish Defense Research Agency, Department of Energetic Materials and Modelling, SE-147 25 Tumba, Sweden.
9. Zain-ul-Abdin, L.W.; Yu, H.; Saleem, M.; Abbasi, N.; Ullah Khan, R.; Ullah, R. S.; Haroon, Mu. Synthesis of ferrocene-based saccharides and their anti-migration and burning rate catalytic properties. *RSC Adv.*, **2016**, 6, 97469–97481.
10. Gao, J.; Wang, L.; Yu, H.; Xiao, A.; Ding, W. Recent Research Progress in Burning Rate Catalysts. *Propellants, Explos. Pyrotech.* **2011**, 36, 404 – 409.
11. Sketch redrawn from Kubota, N. *Propellants and Explosives*, WILEY-VCH Verlag GmbH & Co. KGaA, Weinheim, 2007.
12. Kubota, N. *Propellants and Explosives*, WILEY-VCH Verlag GmbH & Co. KGaA, Weinheim, 2007.
13. Fifer, R.A. *Workshop Report: Fundamental Reactions in Solid Propellant Combustion*; ARBRL-TR-02166; 1979.
14. Warren, L.; Pulham, C.; Morrison, C. *Phys. Chem. Chem. Phys.* **2020**, 22, 25502-25513.

15. Sharma, J.; Wilmot, G.B.; Campolaattro, A. A., Santiago, F. *Combust Flame*. **1991**, 85, 416-426.
16. Otto, K.; Lehman, C.; Bartosiewicz, L.; Shelef, M. *Carbon*. **1982**, 20, 243-251.
17. Katoh, K.; Yoshino, S.; Kubota, S.; Wada, Y.; Ogata, Y.; *Propellants, Explos. Pyrotech.* **2007**, 32, 4, 314-321.
18. Katoh, K.; Le., L.; Itoh, M.; Arai, M.; Tamura, Spontaneous Ignition of Cellulose Nitrate: The Effect of the Type of Storage Atmosphere (I), *Sci. Tech. Energ. Mater.* **2003**, 64, 236.
19. Magill, B. T.; Naufflett, G. W.; Furrow, K. W. *Lead-Free Double-Base Propellant for the 2.75 Inch Rocket Motor*; 20000116525; Cocoa Beach, FL, 2000.
20. Raman, K.V., Singh, H., Rao, K.; *Combustion Science and Technology*, **1985**, 45, 213-219.
21. Lundell, C. E.; Master's Thesis, Temple University, Philadelphia PA, 2017.

CHAPTER 2

LITERATURE REVIEW OF BALLISTIC MODIFIER AND STABILIZER

[This chapter was adapted from Lundell, C.E. M.A. Thesis, Temple University, Philadelphia, PA, 2017.]

2.1 Ballistic Modifiers

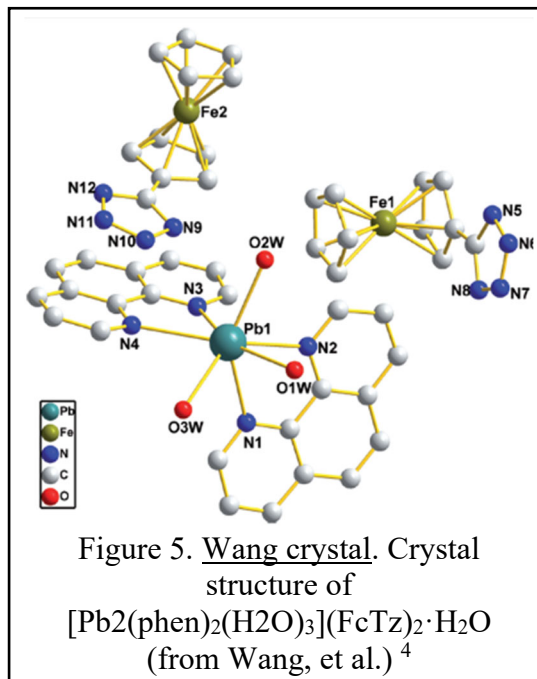
There have been decades of research into developing better lead containing compounds for plateau/mesa burn rate effects and in burn rate catalysts. Furthermore, aggressive research efforts have been underway since the 1990s to find alternatives to lead – with some success. It would be impossible to summarize them all here in a literature review, but an assortment of research efforts is summarized that were both noteworthy and significant to the research undertaken to answer the thesis question.

2.1.1 Leaded Ballistic Modifiers

Extensive research into using lead complexes for burn rate modifiers began in the 1950s and carries through today.¹ Over time, and likely due to financial factors as much as performance, several different lead ballistic modifiers are used today. More conventional and older compounds being: lead salicylate, lead 2-ethyl hexoate and lead beta resorcylate. However, several lead-copper compounds are in use for many military applications: LC-12-0, LC-12-5, LC-12-6, LC-12-7, LC-12-10, LC-12-15 and LC-12-20.² A quick investigation of LC-12-15 for example, reveals a copper content between 10-13%, and lead of 35.8%-39.4% with salicylic acid and resorcylic acid making up all but 4% of the rest.³

A recently created crystallographically characterized lead complex $[\text{Pb}_2(\text{phen})_4(\text{CO}_3)][\text{FcTz}]_2 \cdot \text{phen} \cdot 9\text{H}_2\text{O}$ was synthesized in 2015 as a potential burn rate catalyst due to the various drawbacks exhibited by commercially available ballistic modifiers *n*-butylferrocene, *tert*-butylferrocene and 2,2-bis(ethylferrocenyl)propane.⁴ The

[Pb₂(phen)₂(H₂O)₃](FcTz)₂·H₂O (Figure 5), crystallizes in the triclinic $P\bar{1}$ spacegroup. It contains two Pb (II) cations, four phenol ligands, one carbonato ligand, two FcTz anions, one phenol molecule and nine lattice water molecules.



The authors propose that arrangement of atoms around the Pb center suggests that a hole exists around the metal ion that is occupied by a stereo active lone pair of electrons on the Pb(II) ion. This group also successfully synthesized other transition metal complexes, [Cu₂(bpy)₂(FcTz)₄]·2C₂H₅OH, [Cu(phen)₃](FcTz)₂·8H₂O, [Ni(phen)₃](FcTz)₂·9H₂O and [Co(phen)₃](FcTz)₂·9H₂O. Each complex comprised several water molecules in the lattice, leading the authors to believe that packing of each crystal was influenced by strong intra- and intermolecular hydrogen bonds. Furthermore, each complex stability is increased by the π - π interaction between phenol and Cp molecules.⁴

The manganese-containing crystals [Mn(phen)₂(H₂O)₂](FcTz)₂ and

[Mn(bpy)(H₂O)₄](FcTz)₂] that the Wang group produced for the purpose of modifying burn rate showed stabilization effects that were comparable.⁴ However, despite being structurally relevant to the chemistry discussed in this manuscript, each of these crystals was designed specifically for use as catalysts for AP and RDX. Since this was not the focus of the research, it was not mentioned if these structures had plateau/mesa effects.

Raman and Singh conducted additional research in 1988 by adding lead and copper salts to RDX-doped composite modified double-base propellant (CMDB).⁵ It was found that lead stannate, basic copper salicylate (BCS), lead methylene disalicylate (LMDS), and cobalt oxide produced higher burning rates than non-doped CMDB by 10% to 16%, and burn rates were even higher when the CMDB was primarily nitramines rather than. The addition of lead salts, carbon black, and transition metal oxides only resulted in a modest increase in the burn rate, and fluorides of chromium, iron, and lead had no effect on burn rates. However, neither a plateau nor a mesa effect was observed in any of the complexes examined.⁵

2.1.2 Unleaded Alternatives

As previously mentioned in Chapter 1, the Department of Defense has attempted to remove lead from ballistic propellants since the 1990s. Several research efforts have been made with that goal in mind.

Since their discovery in the 1950's, ferrocene derivatives have been used as solid propellant as burn rate catalysts.⁶ These iron complexes produced superior burn rates and could be used in larger quantities over previous compounds, such as iron oxide. However, a disadvantage of ferrocene burn rate additives is their tendency to diffuse within the propellant affecting, mechanical and chemical properties during storage.⁶ Several ferrocene derivatives were developed over the past 60 years. *tert*-Butyl ferrocene (TBF), catocene, 2,2-

bis(butylferrocenyl) propane (BBFPr) and 2,2-bis(butylferrocenyl) pentane (BBFPe) are but a few examples, all developed with high burn rate properties.⁶ These compounds, however, were not evaluated for, nor expected to demonstrate plateau/mesa effects due to the inability of iron metal complexes to exhibit that burn rate phenomena.

Research by Deisyuk and Demidova found lead, tin, titanium oxides and bismuth also to increase burn rates of DB propellants, providing optimism that these elements could also be used to replace lead.⁷ Unfortunately in their research, plateau/mesa effects were not investigated using these metals.

Researcher in 1983 studied the influence of barium and cobalt salts on the burn rate and pressures in DB propellants. Barium and cobalt salts produced both catalytic and significant plateau effects. Cobalt stearate was most successful in replicating lead in the low-pressure range, and cobalt salicylate in the high-pressure range. Both additives has detrimental effects on the stability of the nitrate esters.⁸

One of the more successful unleaded compounds was made for 2.75-inch rockets. The Navy Surface Warfare Center (NSWC), Radford Army Ammunition Plant, and Alliant Tech systems created a lead-free double-base ballistic modifier with plateau and mesa burn rate characteristics. The double-base additive developed consists of four components: 1.5% bismuth subsalicylate, 1.0% copper salicylate, 0.77% copper stannate, and 0.1% carbon black. This compound's specific impulse output was not an exact match for existing propellant within the 2.75-inch Rocket Motor (NOSIH-AA-2), but inventors believed a close enough match to be an acceptable replacement. However, this lead-free compound exhibits a significant drawback from current propellant: The stabilizer within the lead-free compound exhibited a much higher rate of depletion than current NOSIH-AA-2. Although the analysis from the group demonstrated that a

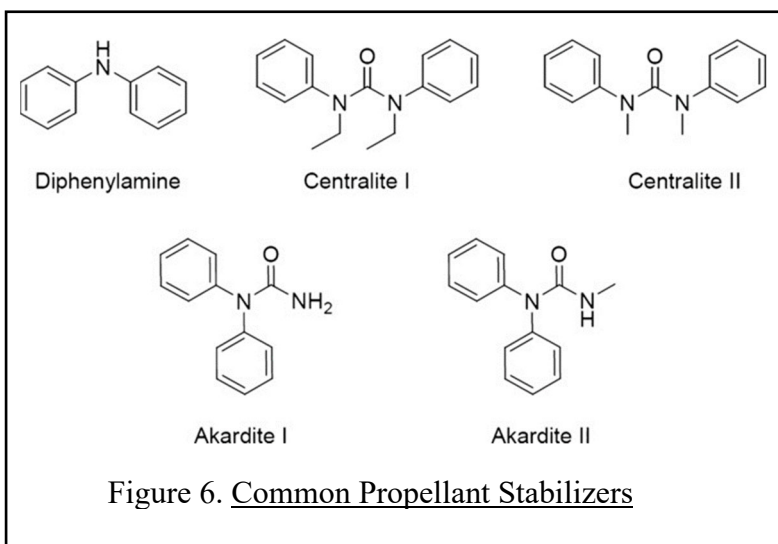
mixture of bismuth subsalicylate and copper salicylate reduced the depletion rate of the stabilizer by half, the presence of the copper salicylate catalysed the decomposition of the nitrocellulose. Although patented, efforts were underway to protect the ballistic modifier from the nitrocellulose with a coating to make it a truly viable alternative to NOSIH-AA-2.²

The ability to eliminate lead entirely from ballistic modifiers may not be possible. A research group at the Naval Surface Warfare Center conducted XPS studies between leaded and unleaded DB propellant. What was observed corroborated earlier research: that lead plays two pivotal roles in producing plateau/mesa effects:⁹ First, it creates soot on the burning surface of the propellant – a requirement for pressure and burn rate effects. Secondly, the lead increases the oxidation rate of the of carbon by five orders of magnitude for super-rate burning.⁹ It was suggested by Otto et al. that lead eventually becomes saturated at the burning surface thereby plugging holes within the soot carbon structure and arresting the super-rate burning.¹⁰ The Navy group later observed that during the onset of plateau/mesa burning, there was a sudden decrease in lead to carbon ratio suggesting that the amount of lead on the burning surface is a key driver of plateau/mesa burn characteristics.¹⁰

2.2 Double-base Propellant Stabilizers

The nitrocellulose component of double-base propellants undergoes an autocatalytic decomposition process whereby it decomposes to form NO and then evolves NO₂ with contact to air. This process creates heat and promotes the degradation of the propellant. The propellant grains show a discolored roughened surface at the ends and edges of the grains.¹¹ To prevent that process and to increase shelf-life and maintain chemical integrity of the propellant, a few stabilizers are commonly used: Diphenlamine (DPA), 2-nitrodiphenyl amine (NDPA), Centralite

I&II and Akardite I&II (Figure 6).¹² However, these stabilizers form N-nitrosoamines within the propellant, which are toxic.

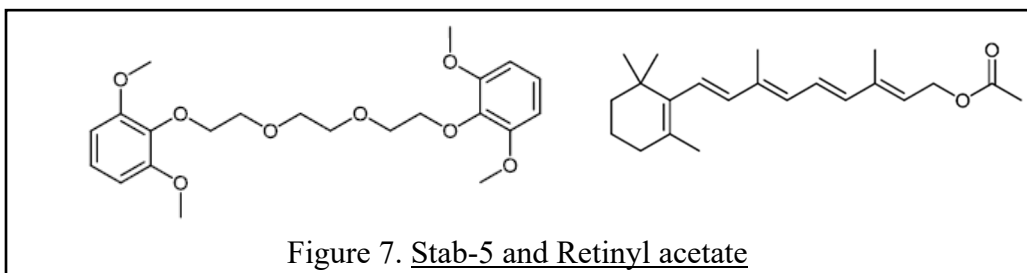


Any new stabilizer would need to meet the following conditions for world-wide acceptance:¹²

1. Be compatible with other energetics.
2. Be stable at normal surface temperatures (-70°C to 55°C).
3. Be a good absorber of free radicals and acids but needed only in small quantity.
4. Not affect the manufacturing of the propellant (softening or stiffening of cast).
5. Most recently, be non-toxic.

Some research has been conducted to find nitrogen free, aromatic free stabilizers.

Researchers at the Swedish Defence Research Agency successfully synthesized a few unique stabilizers in 2015 that appear as good replacements.¹³ Stab-5 (bis-(2,6-dimethoxyphenol)) and retinyl acetate (Figure 7), were two produced that had similar burn characteristics, and exhibited



the stabilizing properties as conventional stabilizers without toxic by-product.¹³ Nevertheless, although promising, non-conventional DB propellant stabilizers do not appear to be used often, if at all.

2.3 Methodology

A survey of previous research leads to some conclusions and a hypothesis formed. First, a demand exists for a non-toxic burn rate additive for DB propellants that does not affect the stability of the nitrate ester fuel, and meets industry requirements. Secondly, although important, a mechanistic study on the effects of lead and burn rate would be beyond the scope of this study. Third, metal salts have shown good promise but degrade stabilizer performance. No previous research has synthesized a stabilizing ligand and metal into a single molecule additive.

In summary, could an effort be made to synthesize p-block and transition metals with stabilizers in hopes of achieving a new complex that: (1) serves as both burn rate modifier with super-rate, mesa and plateau rate burn characteristics within useful pressure ranges, (2) stabilizes the DB propellant as well or better than existing compounds such as 2-NDPA, and (3) meets the industry requirements of such a complex (as outlined in previous section)? The endeavor directly builds upon previous progress made in this area and published in 2017.¹⁴

2.4 References

1. A. T. Camp, Patent US 3,088,858, 1963.
2. Magill, B. T.; Naufflett, G. W.; Furrow, K. W. *Lead-Free Double-Base Propellant for the 2.75 Inch Rocket Motor*; 20000116525; Cocoa Beach, FL, 2000.
3. Ballistic Modifier LC-12-15 Mil Spec, courtesy of parchem, www.parchem.com/Ballistic-Modifier-LC-12-15-Mil-Spec-getpdf-013001.aspx (accessed 15 March 2017).
4. Wang, C.; Li, J.; Fan, X.; Zhao, F.; Zhang, W.; Zhang, G.; Gao, Z.; 5-Ferrocenyl-1H-tetrazole-

Derived Transition-Metal Complexes; Synthesis, Crystal Structures and Catalytic Effects on the Thermal Decomposition of the Main Components of Solid Propellants, *Eur. J. Inorg. Chem.*, 2015, 1012-1021.

5. Raman, K.V., Singh, H., Ballistic Modification of RDX-Based CMDDB Propellants, *Propellants Explos. Pyrotech.*, 1988, 13, 5, 149-151.
6. Zain-ul-Abdin, L. W.; Haojie Y.; Muhammad S.; Nasir A.; Rizwan, U.K.; Raja S.; Haroon, M. *RSC Adv.*, 2016, 6, 97469–97481.
7. Denisyuk, A.P.; Demidova, L.A. *Combustion, Explosion, and Shock Waves*, 2004, 40, 3 311-318.
8. Raman, K.V.; Singh, H.; Rao, K. *Combustion Science and Technology*, 1986, 45, 213-219.
9. Sharma, J.; Wilmot, G.B.; Campolattaro, A.A.; Santiago, F. *Combustion and Flame*, 1991, 85, 416-426.
10. Otto, K., Lehman, C., Bartosiewicz, L., Shelef, M., *Carbon*, 1982, 20, 243-251.
11. Apatoff, J. B.; Norwitz, G. *Role of Diphenylamine as a stabilizer in propellants; analytical chemistry of diphenylamine in propellants*; US Army Armament Command, Test Report T73-12-1, 1973.
12. Trache, D.; Tarchoun, A. *Journal of Material Science*, 2018, 53, 100-123.
13. Tunestål, E.; Hafstrand, A.; Lindborg, A.; Krumlinde, P.; Ek, S.; Goede, P.; Schragen, C. New stabilizers for NC-propellants Evaluated in Rocket Propellants. FOI, Swedish Defense Research Agency, Department of Energetic Materials and Modelling, SE-147 25 Tumba, Sweden.
14. Lundell, C.E., O’Sullivan, O., Gau, M., Zdilla, M., *Chemistry Select*, 2017, 2, 35, 11673-11676.

CHAPTER 3

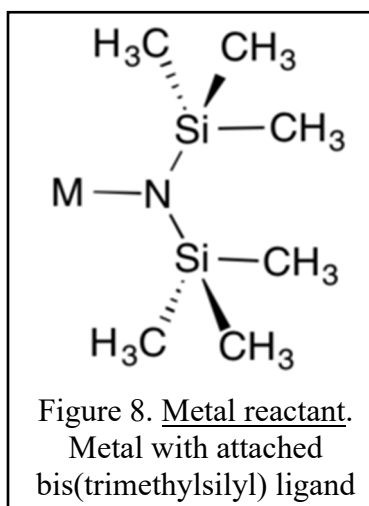
LEAD METAL AND STABILIZER LIGAND COMPLEXES

[This chapter was adapted from Lundell, Lundell, C.E., O'Sullivan, O., Gau, M., Zdilla, M., *Chemistry Select*, 2017, 2, 35, 11673-11676.]

*Note: all experimental details can be found in the final chapter, chapter 7 of this manuscript.

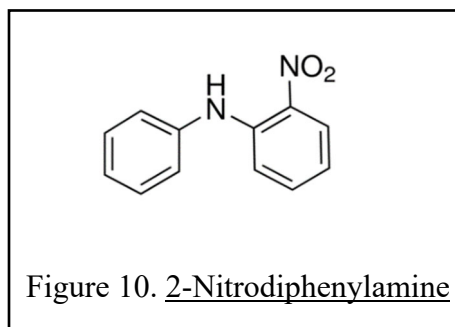
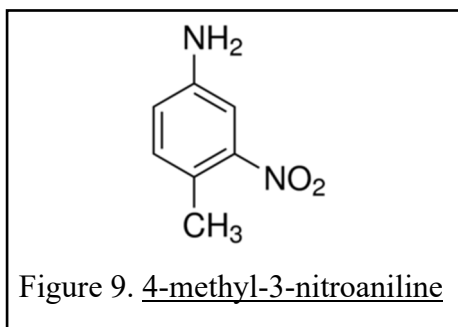
3.1. Metal Bis(trimethylamines) Reactions

The Zdilla research lab was very familiar with Mn clusters and their synthesis using $M(N(SiMe_3)_2)$ (where M=metal) (Figure 8). The metal cation is exchangeable, with dozens of metals having been reported to be coordinated to bis(trimethylsilyl)amide.¹² Metal



bis(trimethylsilyl)amide complexes are nonpolar and have low lattice energies. They are soluble in a range of nonpolar organic solvents, simplifying synthesis. Furthermore, these complexes are strong bases and react with weak protic agents, presenting easy chemistry targets for reactions, and facilitating protolytic ligand replacement reactions. Unfortunately, they are also air-sensitive, and react with water so need to be used in anhydrous environments. Using previous literature for burn rate modifiers mentioned above, and chemical similarity to lead, four metal bis(trimethylsilyl)amides were planned as reactants: lead, zinc, tin, and bismuth.

The choice for a ligand was to use a commonly used double-base stabilizer. N-Methyl-4-nitroaniline is an antiquated yet previously used common stabilizer in older propellants, but to maintain the methyl and nitro groups when reacting with the metal bis(trimethylsilyl)amide, a variant, 4-methyl-3-nitroaniline was purchased and used.



A common and more modern stabilizer was chosen as a second stabilizer reactant, 2-Nitrodiphenylamine (NDPA) (Figure 10). As with N-Methyl-4-nitroaniline, this stabilizer offers an easy target in the deprotonation of the amide.

3.2 Reagents

Formation of metal bis(trimethylsilyl)amides, or $M(N(SiMe_3)_2)$, reactants were generally successful using the commonly-used salt-protolysis reaction of:



$Pb(N(SiMe_3)_2)$ was not available commercially so synthesis from $Na(N(SiMe_3)_2)$ and PbI_2 was required. Approximately 12g (47% yield) was successfully obtained and characterized from indexing the yellow crystals using XRD.¹ It was stored in -30°C in an oxygen and moisture free environment and used in many future reactions.

$\text{Sn}(\text{N}(\text{SiMe}_3)_2)$ was available commercially but was backordered and had a long delivery delay. Therefore, it was ordered but was also synthesized in the lab for expediency. 3.34g (31% yield), of $\text{Sn}(\text{N}(\text{SiMe}_3)_2)$ was successfully synthesized and rudimentarily characterized by comparing FTIR spectra of the synthesized and delivered commercial reagent. Further and more conclusive characterization was not performed because: (1) $\text{Sn}(\text{N}(\text{SiMe}_3)_2)$ commercial product was made available and (2) subsequent reactions were not successful making further analysis, time prohibitive. At room temperature, it is an orange red liquid.

$\text{Zn}(\text{N}(\text{SiMe}_3)_2)$ was not commercially available and so was synthesized. As a cloudy white solid, $\text{Zn}(\text{N}(\text{SiMe}_3)_2)$ melts at room temperature, but product appearance and melting point matched previously reported chemical properties.² 5.496g (49% yield) was produced.

Another $\text{M}(\text{N}(\text{SiMe}_3)_2)$ previously discussed as a reactant was $\text{Bi}(\text{N}(\text{SiMe}_3)_3)$. 1.51g was produced (41% yield). It dried to a primarily yellow powder indicative of the substance. It was characterized by matching melting point range to literature.³

3.3 Products

A total of 36 syntheses were attempted by combining various metal reagents and the two previously mentioned propellant stabilizers. The end goal of each reaction was to produce stable crystals of metal/stabilizer complexes that could be characterized by a minimum of three experimental techniques and suitable for testing at a collaborating lab for burn rate and pressure effects.

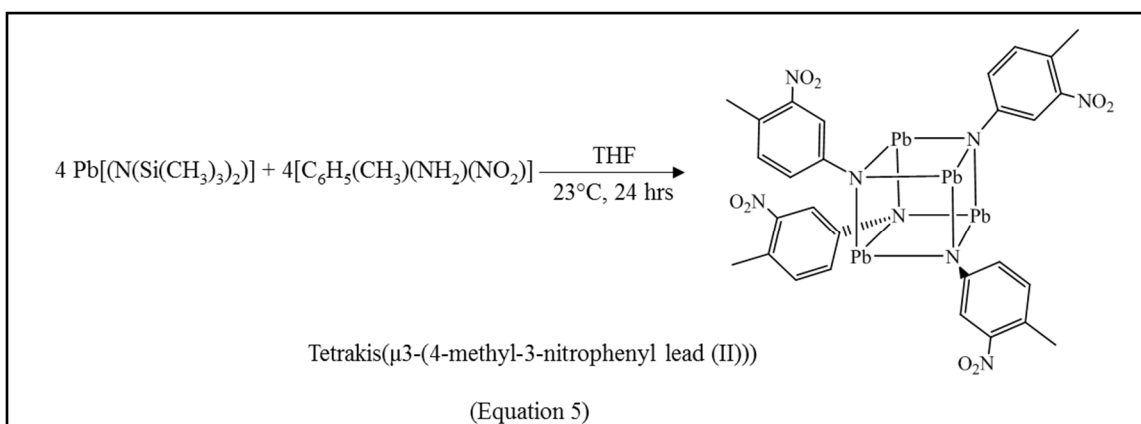
The crystals were grown by a vapor diffusion technique in a double vial apparatus. This method was by far the most effective crystal growing method during this research, and used a two-solvent system. The choice in solvents is to ensure that they are miscible and a significant

difference in polarity is preferable. In most reactions, the products were dissolved in THF and aliquoted into an inner shell vial and pentane was placed in the outer scintillation vial and the outer vial sealed. Varying the temperature during concurrent attempts was used to test crystallization at different speeds. However, when reactions created a color change, and formed product without a crystal, additional crystallization techniques were employed: slow cooling, and convection (by heating the bottom of the solution in an NMR tube). Unfortunately, these attempts never succeeded where vapor-diffusion had failed.

Numerous attempts with various metals and crystallization techniques (usually conducted both at room temperature and at -30°C), yielded two novel crystal structures from the lead precursor. Two novel complexes were synthesized, while pursuing precursors for developing a new family of dual stabilizer/ballistic modifiers, and in the process discovered a high-energy-density lead-based heterocubane compound.

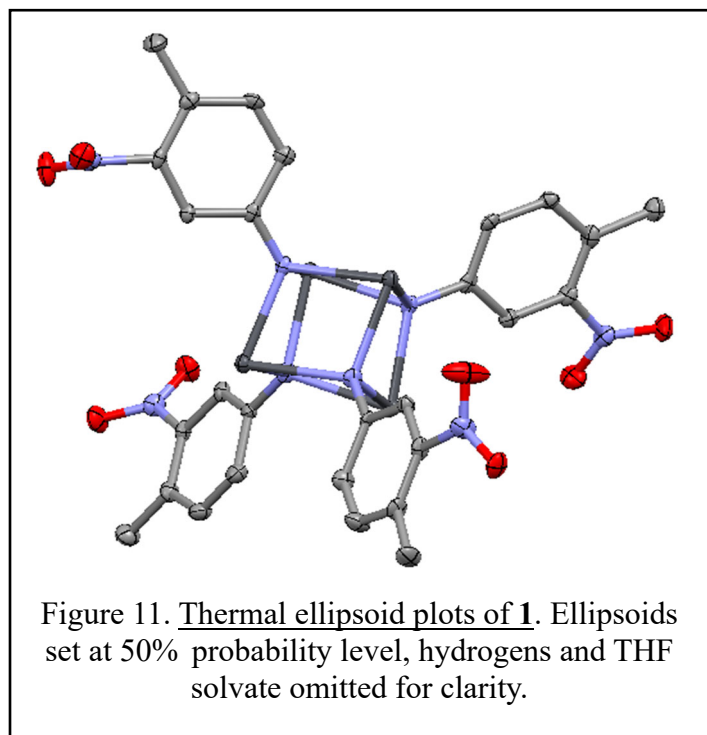
3.3.1 Tetrakis(μ_3 -(4-methyl-3-nitrophenyl imido lead (II)))

A 1:1 stoichiometric reaction of lead bis(trimethylsilyl)amide with 4-methyl-3-nitroaniline produced tetrakis(μ_3 -(4-methyl-3-nitrophenyl imido lead (II))) (**1**). The reaction is illustrated in Equation 5. Single-crystal X-ray diffraction analysis was performed on the dark red



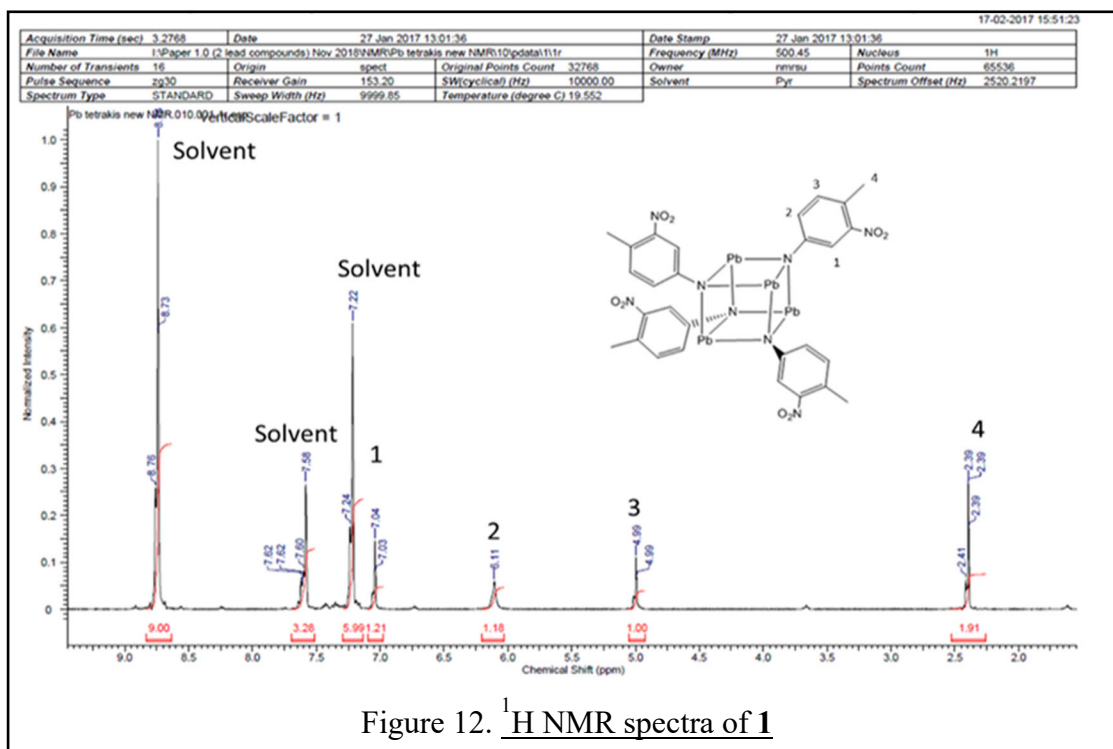
or rust colored crystals, and **1** is a triclinic system with the space group of $P\bar{1}$. It has four Pb^{+2}

ions, surrounded by four 2-nitromethyl aniline ligands. A thermal ellipsoid plot is shown below (Figure 11).



An analogous structure is not reported in the literature to our knowledge. The tetrakis structure is distorted, with bond angles varying between atoms within the cube from 78.6° to 100.0° . This distortion is likely from NO_2 groups weakly coordinating to the Pb of adjacent clusters. However, no π - π stacking is present in the crystal. The N-C bond distances are $\sim 1.4 \text{ \AA}$, slightly shorter but close to expected bond distances, and all C-C bonds are of typical length (see appendix A).

Different solvents were explored for dissolution of **1**, with only pyridine being capable. **1** was not soluble in THF, ACN, HMDS, benzene, toluene, pentane or ethanol. However, using deuterated pyridine produced ^1H NMR spectra that supports the proposed structure and is found below in Figure 12.

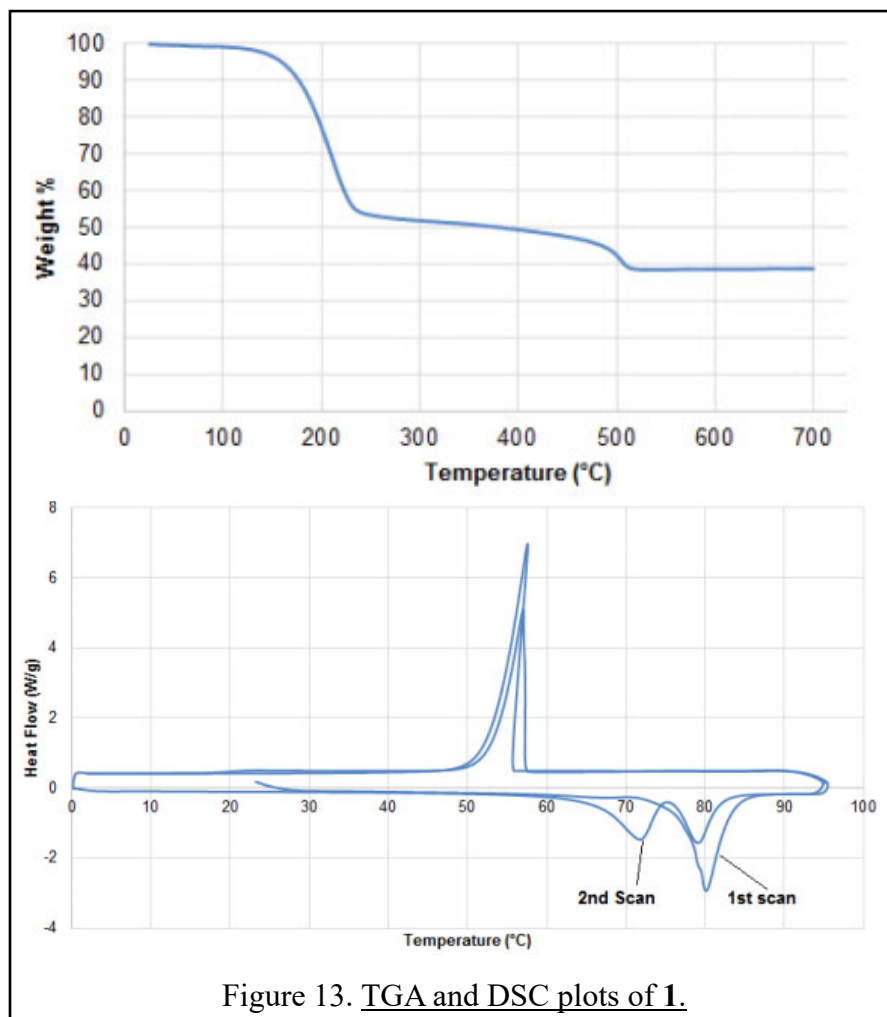


CHN analysis supported the structure with one co-crystallized THF molecule within the lattice.

Thermal Gravimetric Analysis (TGA) on compound **1** shows a weight loss of 91% between 100 and 200°C, suggesting the compound most likely sublimates, leaving behind some residue. Differential scanning calorimetry (DSC) shows a melting point of 808°C on the initial sweep. On subsequent sweeps a second melting event occurs at 72°C which we attribute to the loss of solvate THF, giving an additional, lower-melting solvent-free phase after the first DSC cycle (Figure 13). Unfortunately, the solid dark red crystals when removed from the glove box show a change in color and decomposition to air. Air sensitivity of **1** was confirmed when dissolved in pyridine and monitored through UV-vis absorption spectroscopy, showed significant spectral changes within minutes of exposing the volume to air. The exposed Pb⁺² ions are likely oxidized by ambient oxygen creating lead(IV)-oxo complexes, providing rationale for the

complex's sensitivity.

As stated in the introduction, one measure of propellant effectiveness is the heat of combustion (ΔH_c) of the substance, so calorimetry experimentation was conducted to evaluate the ΔH_c of **1**.

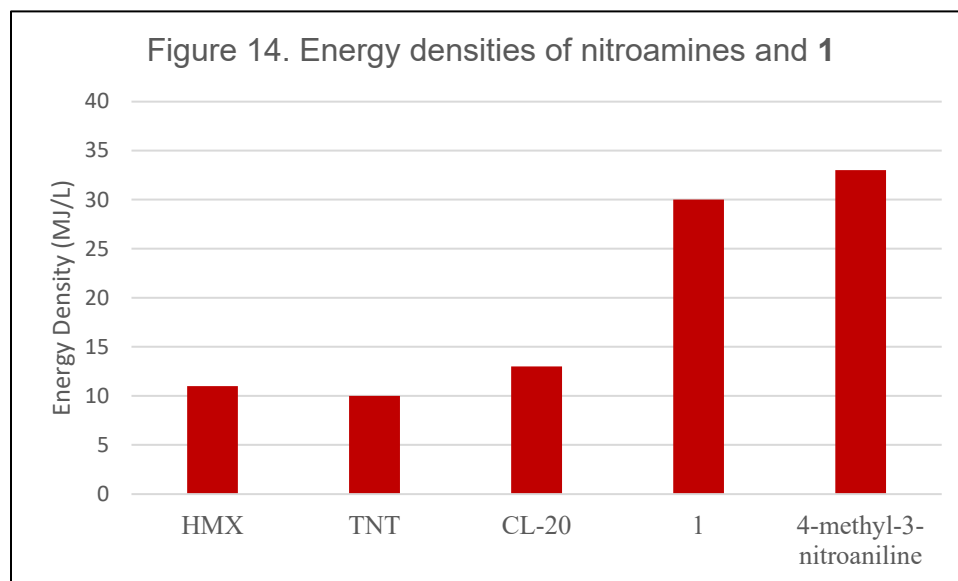


Complex **1** mean ΔH_c was $-7,012.5$ cal/g (± 399.16), 16.5% increase over the stand-alone ligand (-6014.5 cal/g) (Figure 14), which presumably results from the added exothermicity of the combustion of Pb^{II} to $\text{Pb}^{\text{IV}}\text{O}_2$.⁴ This ΔH_c is significantly higher than that of NC (-1606 cal/g).⁵

A measurement not yet discussed, but significant, is the energy density of a complex. The calculation of energy density of **1** assumes a density equivalent to that of the crystal

structure, 2.526 g/cm^3 . This high density is the result of the large atomic mass of lead, the interaction between nitro groups and adjacent Pb atoms, and from hydrogen bonding between adjacent methyl groups. This high density coupled with modest ΔH_c increase with the added lead ions, produces a mean energy density of $30 \pm 2 \text{ MJ/L}$ for complex **1**.

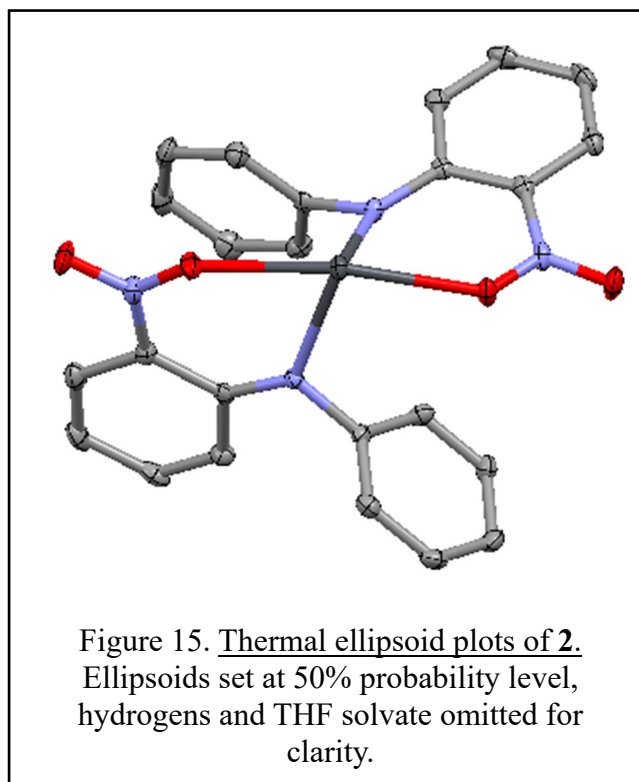
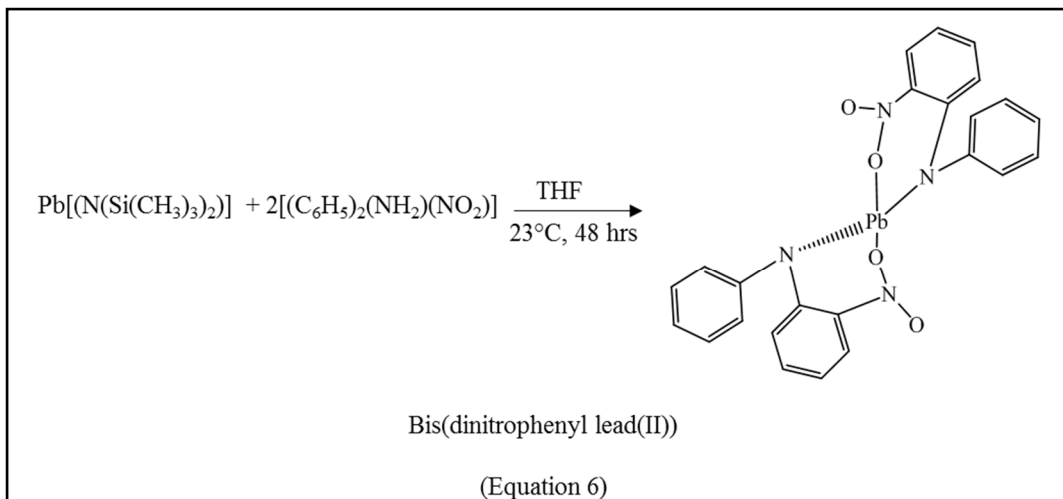
Figure 14 shows that the combustion energy density is more than three times that of the trinitrotoluene (TNT) and the high density of the compound is a driver for the unexpected results. It is possible that the energy density reported is actually lower than the true value due to the various THF solvate within the molecule. Drying over 24-48 hours by vacuum reduced an amount of THF molecules per crystal, but it is unclear if further removal of THF would increase or decrease the heat of combustion. It should be noted also that **1** has a low oxygen balance (-76% for formation of CO_2 , -44% for formation of CO), meaning external oxygen is required to complete combustion of this complex. **1** releases 16% more cal/g than the ligand so the oxidation of the added metal increases heat of combustion as expected.



3.3.2 Bis(dinitrophenyl imido lead(II))

A reaction of lead bis(trimethylsilyl)amide with NDPA produced a second novel crystal **2**.

For charge balance, two equivalents of NDPA were used for the reaction, and the reaction is illustrated below in Equation 6.

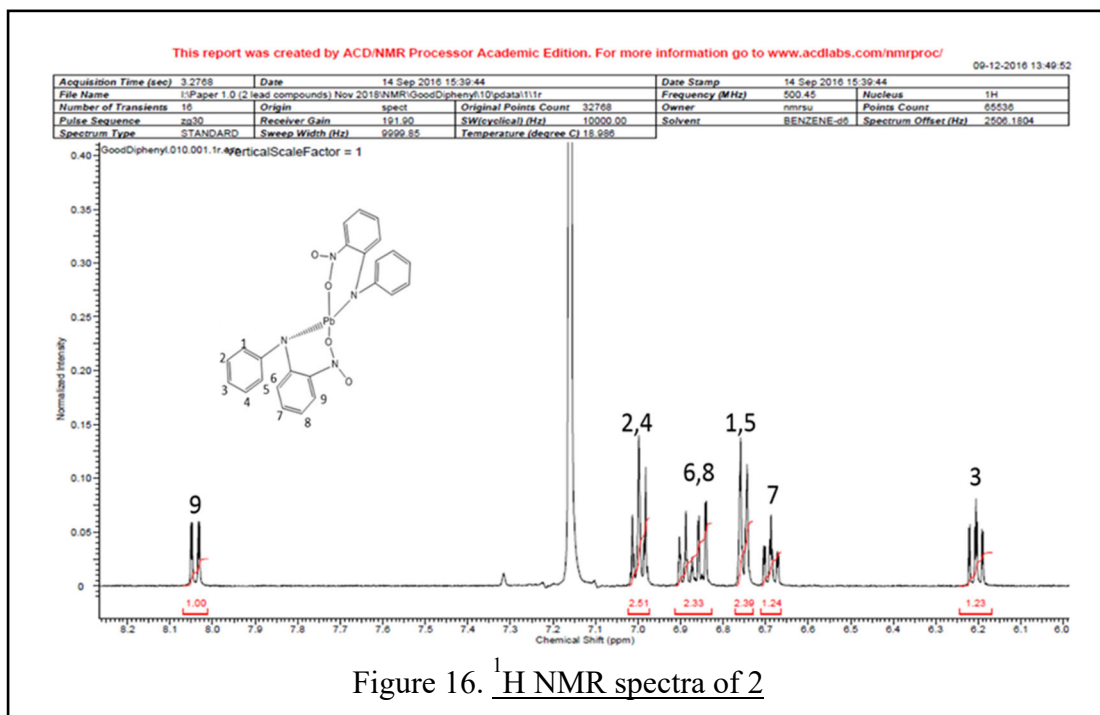


The dark purple crystal complex bis(dinitrophenyl imido lead(II)) is a monoclinic system with the spacegroup of $P2_1/n$. There is one Pb^{+2} cation with two attached nitrodiphenyl ligands

in the asymmetric unit. A thermal ellipsoid plot generated is shown below (Figure 15).

The lead ion in the asymmetric unit has a seesaw geometry with 161.4° between oxygen atoms and the obtuse angle between nitrogen atoms is 82.7° . The **2** Bravais lattice is primitive as in **1** but is less aggregated, than in **1**. The exposed Pb^{+2} atom forms a π -stack with neighboring molecule. Different solvents were attempted to dissolve **2**, with only benzene being capable at room temperature within a few minutes. **2** was not soluble in THF, ACN, HMDS, pyridine, toluene, pentane or ethanol. However, using deuterated benzene produced ^1H NMR spectra that supports the proposed structure and is found below in Figure 16.

CHN analysis supported the structure with one co-crystallized THF molecule within the lattice. Drying the molecule removed some THF but 5 THF were left in the crystal for approximately every 9 lead complex of **2**.



The IR spectrum for crystal **2** provides more supporting evidence of the chemical

structure than observed with **1** (Figure 19). There is a weak signal observed around 3000 cm^{-1} for C-H aromatic stretching although signals at 1250 cm^{-1} and 1100 cm^{-1} indicate a substituted benzene aromatic. A strong signal at the 1500 cm^{-1} supports the presence of a nitroso compound, also found in complex **2**.

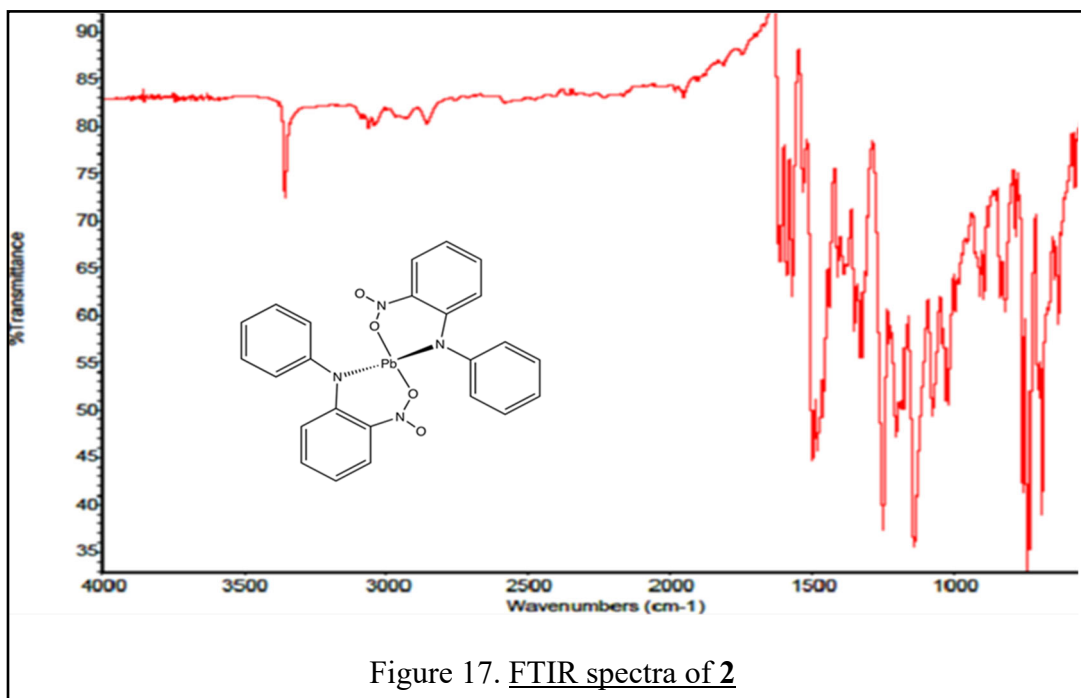
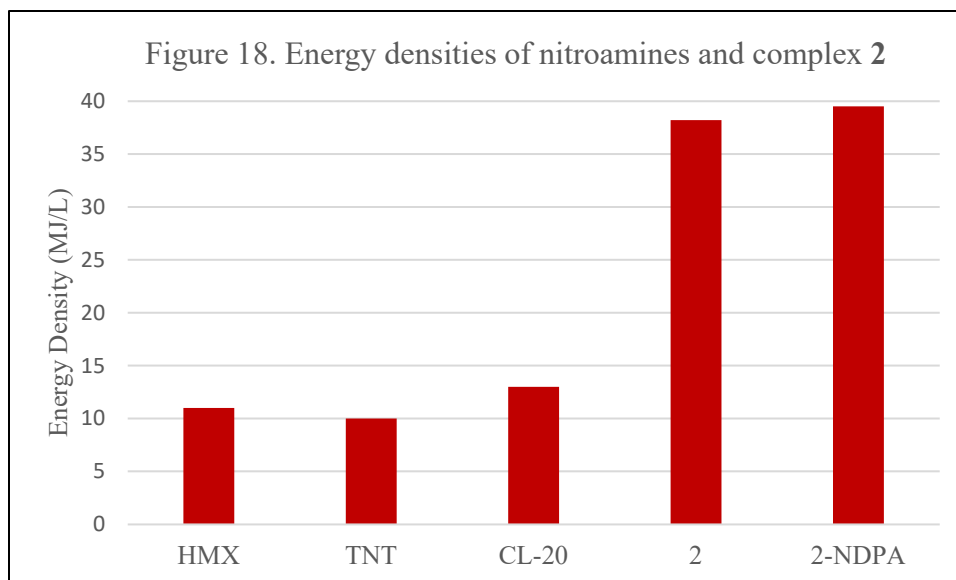


Figure 17. FTIR spectra of **2**

As with complex **1**, the ΔH_c for **2** was determined using a bomb calorimeter. However, complex **2** mean ΔH_c was $-4893.2\text{ cal/g} (\pm 130)$, 29.5% below the NDPA ligand (-6947.8 cal/g) (Figure 18).⁵

Complex **2** energy density was 38.2 MJ/L . Significant when compared to other nitroamines, but possesses lower crystal density of 1.869 g/cm^3 compared to **1** (Figure 19). The oxygen balance was low (-136% for formation of CO_2 , -75% for formation of CO). Unlike **1**, the heat of combustion was lower of the product than the stand-alone ligands so oxidation of the lead did not show similar combustion results.



Neither complex displayed shock or friction sensitivity under rudimentary tests, but were highly air-sensitive making burn rate testing impractical. Determination if **1** or **2** modified DB propellant desirably was not accomplished. Unfortunately, other metal and stabilizer reactions were observed but none crystallized and showed poor ability for characterization using a variety of tools.

3.4 Summary of Results

Only the previously mentioned complexes **1** and **2** were successfully crystallized out of the 36 reactions that were carried out with a variety of metals and two distinct stabilizers at a variety of reaction temperatures. A lot of the results made with different metals produced amorphous solids that looked like crystals until XRD tests showed otherwise. In fact, in each of the 36 attempts, there were color changes and solids formed, indicating that a reaction occurred, but the products were intractable. However, the following questions concerning the thesis question were addressed: Non-lead metal bis(trimethyl)amides do not readily crystallize with the propellant stabilizers mentioned in this manuscript, and organometallic complexes formed using

the reactants described produce products that are sensitive to air. Additionally, it was demonstrated that $\text{Pb}(\text{N}(\text{SiMe}_3)_2)$ reacted with two kinds of double-base propellant stabilizers and can readily form crystalline structures. The products' air-sensitivity prevented them from answering the thesis question. As a result, the question of whether propellant stabilizer and lead or other metals can be combined to create a superior propellant additive remains unanswered.

3.5 Unexpected High Energy Lead Species

The creation of tetrakis(3-(4-methyl-3-nitrophenyl imido lead (II))) (1) resulted in the creation of a novel cubane molecule with a significantly higher energy density than TNT, which are frequently utilized in a variety of military applications. The oxidation of $\text{Pb}(\text{II})$ to $\text{Pb}(\text{IV})$, which results in the formation of $\text{Pb}(\text{IV})\text{O}_2$, and the rise in density brought about by clustering probably contributed to this energy. The number of moles in the ideal gas law is reduced because not all low-weight gases are produced by the material's combustion. A slow combustion reaction is also likely to occur as a result of the low oxygen balance. However, it is possible that the lower number of moles produced and the observed increase in pressure, which was not anticipated from an organometallic complex combustion, could be compensated for by the higher heat of combustion and the denser material.

3.6 Discussion

Although novel, the utility of complexes **1** or **2** within propellant is severely marginalized due to their sensitivity to air, and high lead content. Each was important however in demonstrating proof of principle to the complexation of metals with stabilizers to make unique complexes but did not create a viable synthetic pathway for other metals. The intent to build a

‘proof of concept’ and apply it to other metals and other ligands was ultimately unsuccessful.

The need for a new approach would be required – probably using the same metals and stabilizers as described in this chapter, but with a new way to create the targeted species.

3.7 References

1. Fjeldberg, T.; Hope, H.; Lappert, M.F.; Power, P.P.; Thorne. *J. Chem. Soc. Chem. Comm.*, **1983**, 639-641.
2. Bürger, H.; Sawodny, W.; Wannagat, U.; Darstellung *J. Organomet. Chem.* **3** **1965**, (2): 113–120.
3. Vehkamäki, M.; Hatanpää, T.; Ritala, M.; Leskelä, Ma. *Journal of Materials Chemistry*. **2004**, *14*, 21, 3191.
4. Sullivan, M.V.; Hunt, H. *J. Phys. Chem.*, **1949**, *53*, 497-500.
5. Cox, J.D.; Pilcher, G., *Thermochemistry of Organic and Organometallic Compounds*, Academic Press, New York, **1970**, 1-636.

CHAPTER 4

SYNTHESIZING HEXA-1-PHENYLUREA COBALT(II) NITRATE

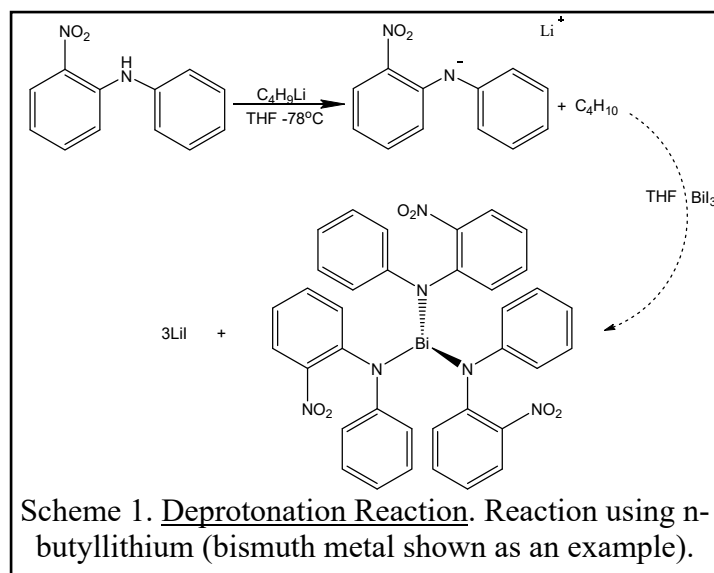
*Note: all experimental details can be found in the final chapter, chapter 7 of this manuscript.

4.1. Transition Metal with Stabilizer Ligand Complexes

Although successful in developing complexes incorporating both lead and propellant stabilizer in the previous chapter (and publishing the results in 2017), any attempt to use the same protolysis reaction with other metals was unsuccessful.¹ Dozens of different combinations were attempted but without success in synthesizing complexes like that of **1** and **2**. Regardless, the original research question aimed to develop non-lead complexes, and therefore the synthetic focus was shifted to a different pathway using transition or p-block metals and other commonly used stabilizers 2-NDPA and MNA.

4.1.1 Deprotonation of Secondary Amine With N-butyllithium

The first attempt following the failure of the protolysis reaction was by deprotonating the ligand directly with a strong base prior to the introduction of the metal. The intent was to remove the secondary amine proton found in 2-NDPA and MNA using *n*-butyllithium, leaving a lone pair on the nitrogen atom to bond with the available metal as shown in scheme 1 below:



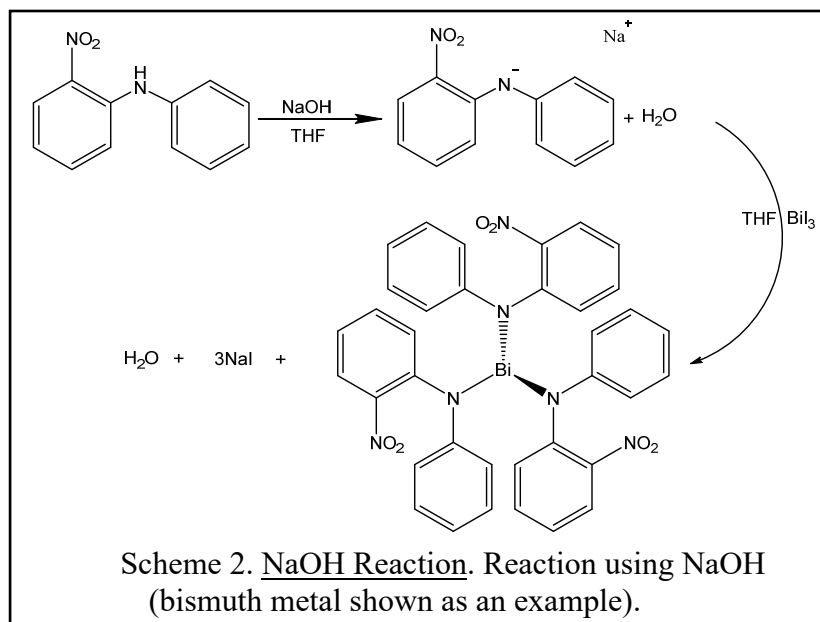
This resulted in an oily product that proved intractable. A black amorphous solid was recovered and although energy dispersive x-ray spectroscopy (EDS) indicated the presence of metal and ligand, ^1H NMR showed no perturbation to the spectra expected for the ligand starting material, aside from broadening due to the presence of the paramagnetic metal. Additionally, mass spectral data did not produce readily identifiable fragments, leading to a conclusion that metal to stabilizer bonding never occurred, but resulted in several unidentified by-products.

4.1.2 Deprotonation of Amine Using Trimethylamine

A second attempt incorporated the use of a gentle base, trimethylamine (TMA) as a deprotonating agent. The advantages of this pathway was that it could be done at ambient conditions, without the need to be in an air-free environment. Unfortunately, no reactions were observed, and only starting material was recovered. The most likely conclusion for this result was that the TMA was not strong enough to deprotonate the targeted amines even though predicted pK_a values would suggest that it was.

4.1.3 Deprotonation of Amine Using NaOH

A third attempt was done using a strong base based on evidence that the TMA was not a strong enough base. This process had advantages over others, specifically the formation of a presumptive NaI salt by-product that can be easily separated (scheme 2 below). Initial addition of NaOH to 2-NDPA solution produced a dramatic color change, indicative of the deprotonation of the 2-NDPA amine, yet whenever metal salts were added, the metal was immediately oxidized. The hope was that by changing the stoichiometric ratios, a small amount of product could be recovered. Unfortunately, using ^1H NMR, IR and recrystallization techniques, only oxidized metal and unreacted ligand were ever identified and recovered.

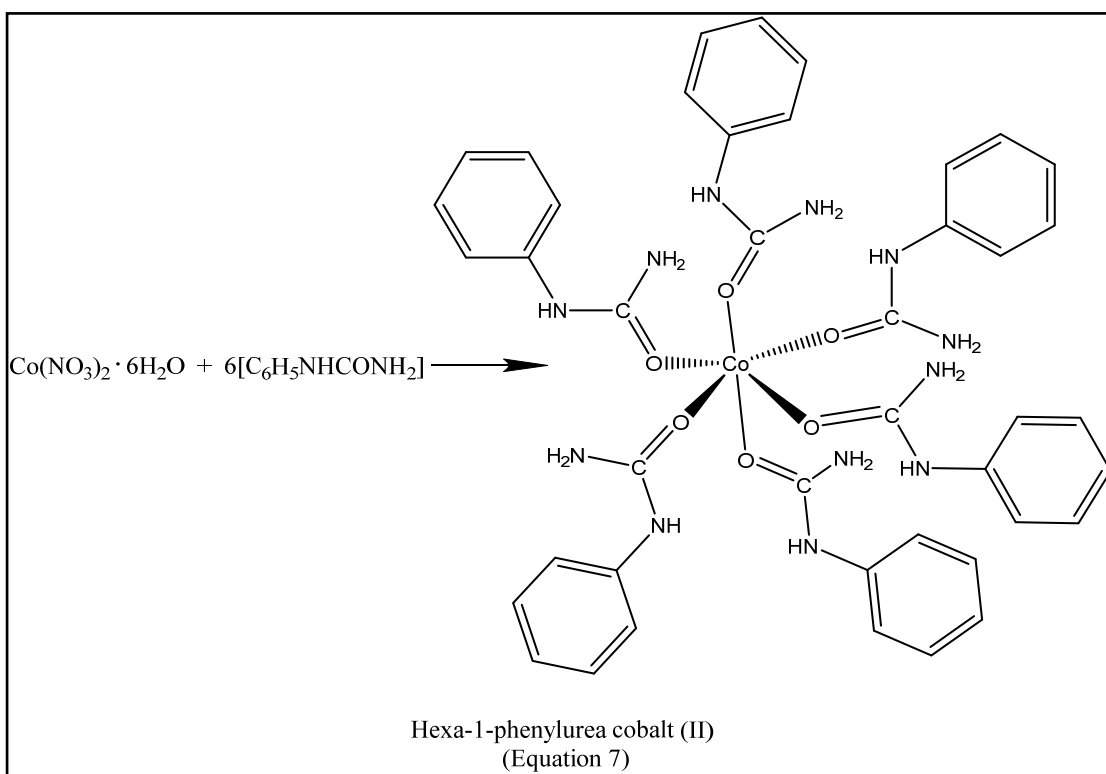


4.2 *n*-Phenylurea Ligand

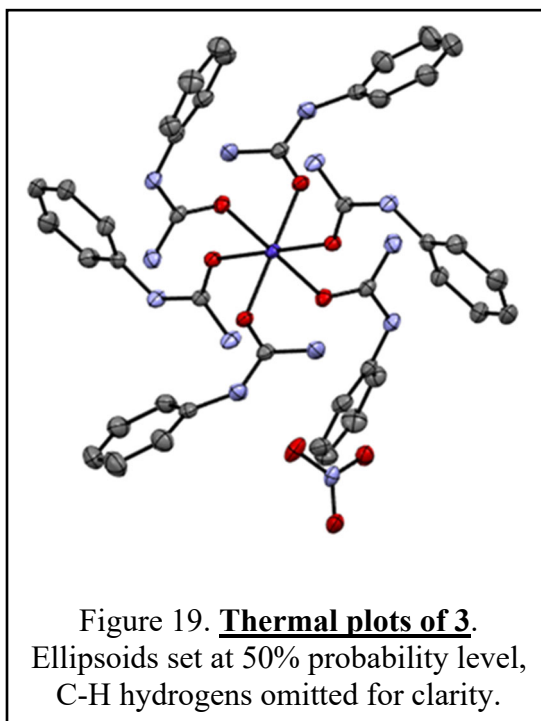
After three separate attempts using different metals and the stabilizers 2-NDPA and MNA, it was concluded that the metal-ligand bond in these complexes may be too weak and therefore unstable. Thus, a search for a new suitable ligand went underway. With the propellant additive requirements in mind as detailed in chapter 2, a non-toxic yet good radical and acid scavenger was needed. Although unproven to the community, Katoh claimed that a phenol based analogous molecule could have similar effects as 2-NDPA and a urea-based ligand was chosen: *n*-phenylurea.² Various metals were chosen to synthesize with the urea ligand, but cobalt was a metal of choice based on the results from Rao et al. in 1983.³

4.2.1 Hexa-1-Phenylurea Cobalt (II) Nitrate

A 6:1 stoichiometric reaction of *n*-phenylurea and cobalt (II) hexahydrate produced hexa-1-phenylurea cobalt (II) nitrate (**3**). The reaction is illustrated in Equation 7. The crystals were grown by vapor diffusion in a double vial apparatus using acetonitrile and tetrahydrofuran solvents,

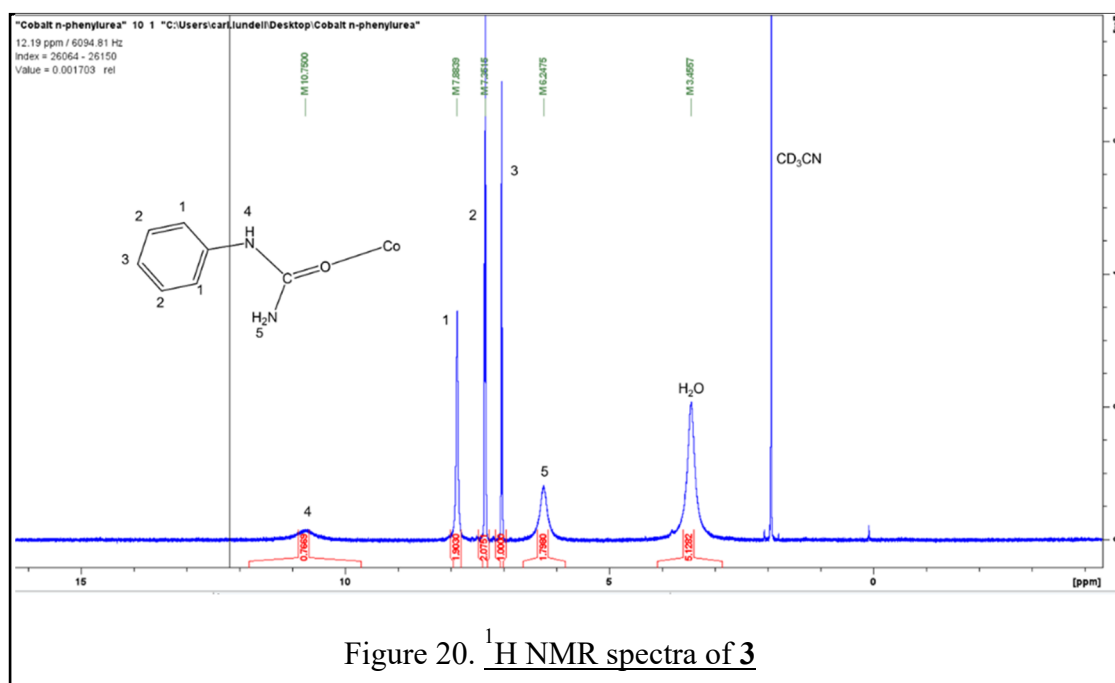


Single-crystal X-ray diffraction analysis was performed on the bright red colored crystals, and **3** is a monoclinic system with the space group of $P-2_1/n$. It has one Co^{II} ion, surrounded by



six *n*-phenylurea ligands. A thermal ellipsoid plot is shown at right (Figure 20). There is covalent bonding between the cobalt and oxygen atoms on the ligands and there are two instances of hydrogen bonding, one between carbonyl and primary amine of adjoining ligands and another between the nitrate and secondary amine likely adding to its stability.

Different solvents were screened to dissolve **3**, and it was found soluble in ethanol, acetone, ethyl acetate, and acetonitrile. It is insoluble in water. The ^1H NMR spectra in d_3 -acetonitrile supports the proposed structure with an added peak of water exchange while in solution is found below in Figure 21.



Thermal Gravimetric Analysis (TGA) on compound **3** shows slow weight loss between 22°C and 200°C , suggesting the slow loss of water which is present in the NMR spectra. Good thermal stability was observed until $\sim 206^\circ\text{C}$ as shown in Figure 22 below. Differential scanning calorimetry (DSC) shows a melting point of 75°C and 145°C on the initial sweep. On subsequent sweeps (purple line) the 75°C melting event disappears at which we attribute to the

loss of water, giving an additional, lower-melting solvent-free phase after the first DSC cycle (Figure 22). The accompanying IR spectrum below provides good supporting evidence of the proposed structure (Figure 23). A broad peak at 3300 cm^{-1} is likely the O-H stretch associated with the hydrogen bonding within the complex. Another peak observed at 1650 cm^{-1} is indicative of the C=O of the carbonyl found on the ligand, and the peak observed at 1538 cm^{-1} is most likely the N-O stretch of the nitrate anion. The bulk material is a pink powder and subsequent red crystals are not sensitive to air, and metal Co^{II} ion is well protected.

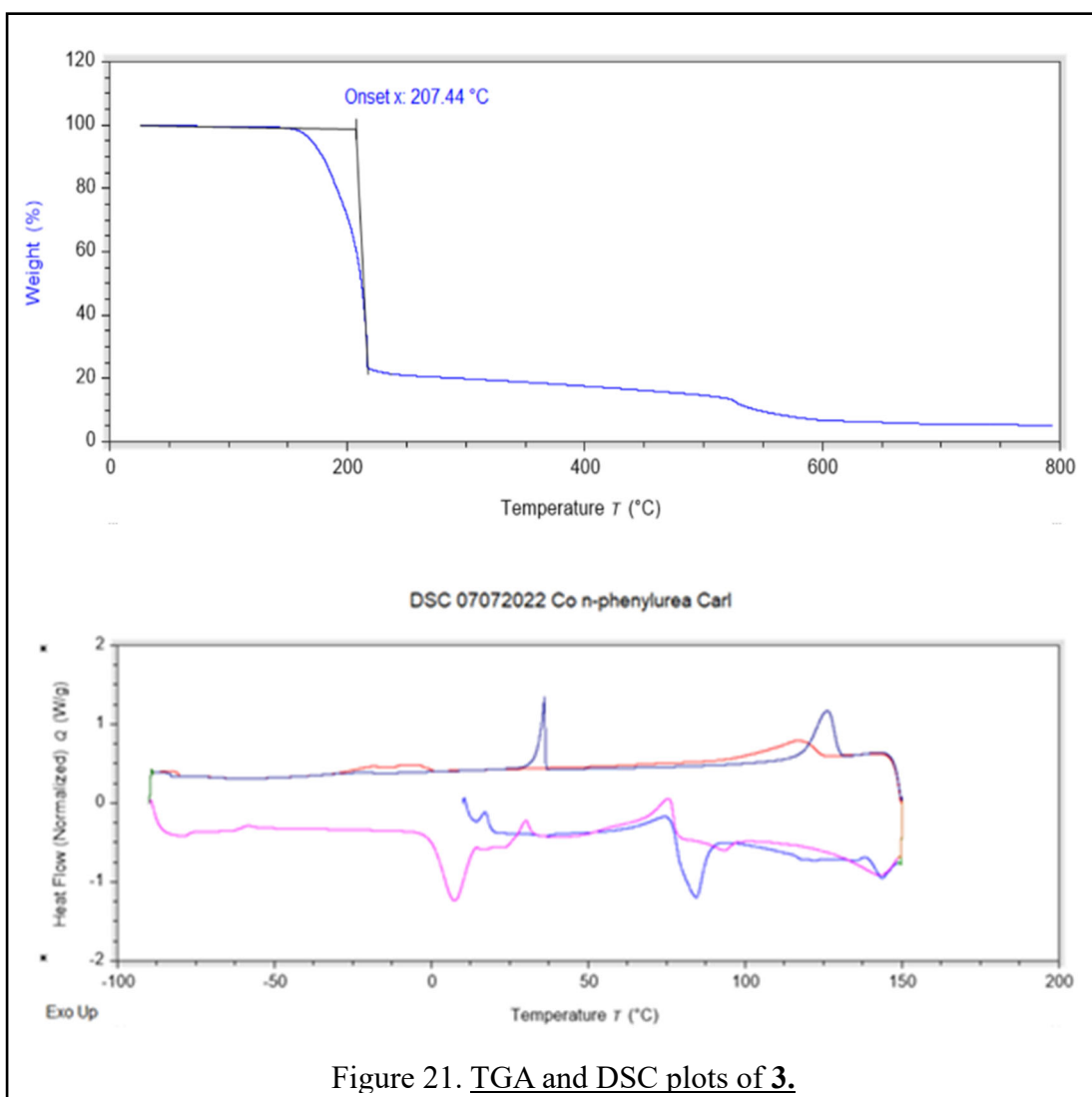
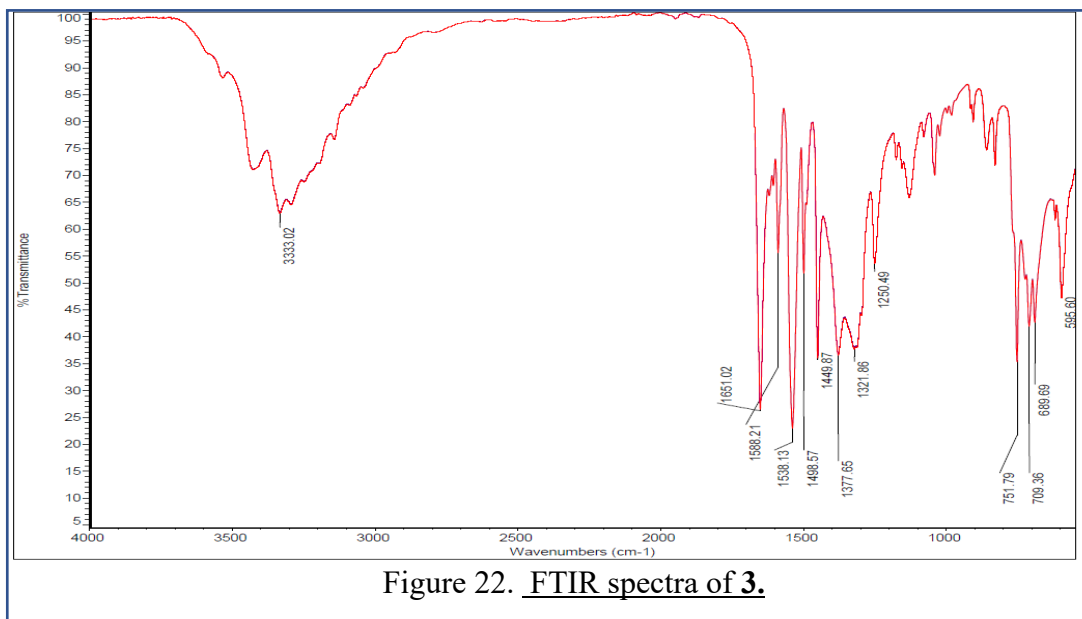


Figure 21. TGA and DSC plots of **3**.



As stated in the introduction, one measure of propellant effectiveness is the heat of combustion (ΔH_c) of the substance, so calorimetry experimentation was conducted to evaluate the ΔH_c of **3**.

Complex **3** mean ΔH_c was $-3,718 \pm 49.7$ cal/g (ΔH_c of the unmetallated ligand has not been reported). Using the crystallographic density of 1.326 g/cm³, combustion energy density of 20.6 MJ/L for complex **3** is obtained (Figure 24).

This ΔH_c is significantly higher than that of NC (-1606 cal/g).⁴ A summary of many physical properties of **3** are listed in table 1 below:

Property	Value
Molecular Weight	937.86 g/mol
Melting Point	145°C
Thermal Stability	205.9°C
Energy Density	20.6 MJ/L

4.3 Results of DoD Compatibility Testing

Compatibility testing of **3** was completed at Indian Head Naval Surface Warfare Center in Maryland using DSC and TGA testing. Nitrocellulose has an exotherm of 203 °C, the mixture

with the cobalt urea material has an event earlier at 177 °C. This could indicate that the materials are incompatible. However, the Co complex alone has an endotherm at the same temperature when run alone and that appears to be what's starting the reaction. That would indicate that the two materials are compatible since the event is due to the Co material not because they were mixed.

4.4 Discussion

The cobalt product **3** is highly reproduceable in good yield and purity. Many of the parameters outlined in Chapter 1 and Chapter 2 are fulfilled with the successful synthetization of **3**. Specifically, it is stable to 200°C, soluble in organics required for the casting process, yet insoluble in water. Additionally, it is far less toxic than lead, and meets DoD suitability criteria for sensitivity and proved compatible with nitrocellulose within DB propellant. In short, **3** is a good candidate for further evaluation as a DB propellant additive, and suitable for both nitrocellulose surveillance and pressure exponent testing.

4.5 References

1. Lundell, C.E.; O'Sullivan, O.; Gau, M.; Zdilla, M.; *Chemistry Select*, **2017**, 2, 35, 11673-11676.
2. Katoh, K.; Le., L.; Itoh, M.; Arai, M. *Sci. Tech.Energ. Mater.* **2003**, 64, 236.
3. Raman, K.V.; Singh, H.; Rao, K. *Combustion Science and Technology*, **1985**, 45, 213-219.
4. D.H. Kim, in *Encyclopedia of Toxicology (Third Edition)*, **2014**.

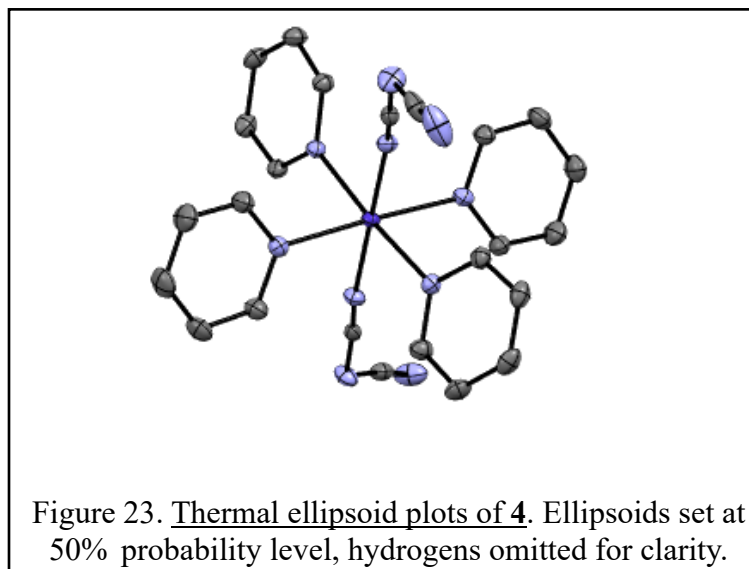
CHAPTER 5

DETERMINING THE CRYSTAL STRUCTURES OF METAL DICYANAMIDO PYRIDINE COMPLEXES AND IRIIDIUM SPECIES FOR FUTURE STUDIES

*Note: all experimental details can be found in the final chapter, chapter 7 of this manuscript.

5.1 Bis(dicyanamido) Tetrakis(pyridine) Cobalt^{II}

Dicyanamide ligands have often been reported in literature as a bridging ligand, adding stability and crystalline character to different complexes.¹ Therefore, dicyanamide was added to various syntheses as a possible way to stabilize and crystallize products described in previous chapters. An unintended product was the formation of bis(dicyanamido) tetrapyridine cobalt^{II} **4**. It was discovered that the complex had not yet been reported. It was observed that the added pyridine ligands took four positions while the dicyanamides bonded axially although no bridging was observed as intended (Figure 25).

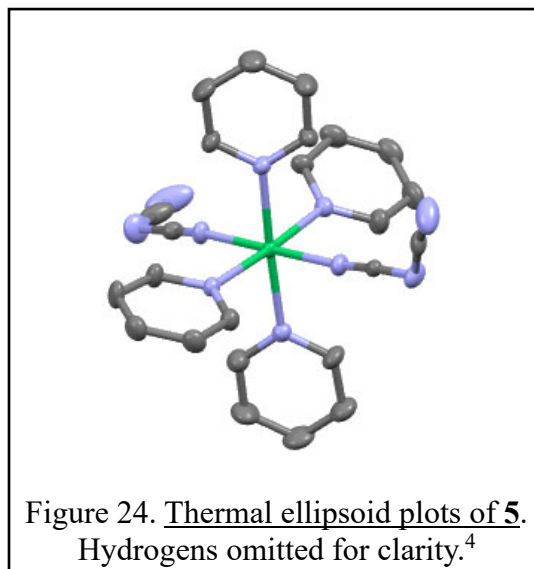


After investigating the synthesis of similar structures, the procedure to produce **4** was refined and was found to be highly reproducible.² Six mmol of dicyanamide was dissolved in 1:1 H₂O/EtOH

solution, and to this 0.5 mmol of $\text{Co}(\text{NO}_3)_2 \cdot 6\text{H}_2\text{O}$ was added, with pyridine added last in excess. With the goal of generating a series of analogous complexes, the same procedure was used but cobalt was replaced with various metal salts. Interestingly, when the same procedure was used for both p-block and transition metals, the ligands in the inner coordination sphere and geometries varied greatly, even among similar elements. Specifically, when using copper, the dicyanamide took each position in the octahedral complex as determined by XRD, as in the same structure reported in 1999 by Batten et al.³ Then when using manganese, a structure of four dicyanamides and two pyridine ligands were observed. Crystal structures of ten separate species were characterized with XRD spectroscopy containing manganese, cobalt, palladium, lead, copper, nickel and zinc. A list of all crystalized products is described below – most of which have been previously reported.

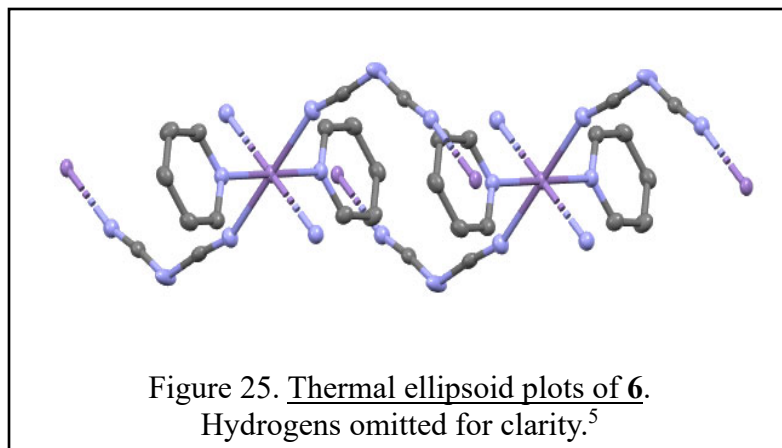
5.2 Bis(dicyanamido) Tetrakis(pyridine) Nickel^{II}

We attempted to synthesize a nickel species analogous to the cobalt complex **4**. The same protocol was used as in **4**, but $\text{Ni}(\text{NO}_3)_2 \cdot 6\text{H}_2\text{O}$ was added in lieu of cobalt. The green solution when dried using slow evaporation and produced large green crystals. The crystals was indexed using x-ray diffraction: $a = 13.0439(6)$, $b = 12.8557(8)$, $c = 15.1294(7)$, $\alpha = 90^\circ$, $\beta = 110.191(5)^\circ$, $\gamma = 90^\circ$, $V = 2381.1(2)$. The unit cell matched the previously reported structure of Wohlert et al. in 2012, and the structure is pseudo-centrosymmetric and can also be refined in the space group $C2/c$, **5**.⁴ The nickel species is six-coordinated by two dicyanamido ligands and four pyridine ligands in a slightly distorted octahedral geometry, with each dicyanamide bonded on the end (Figure 24).



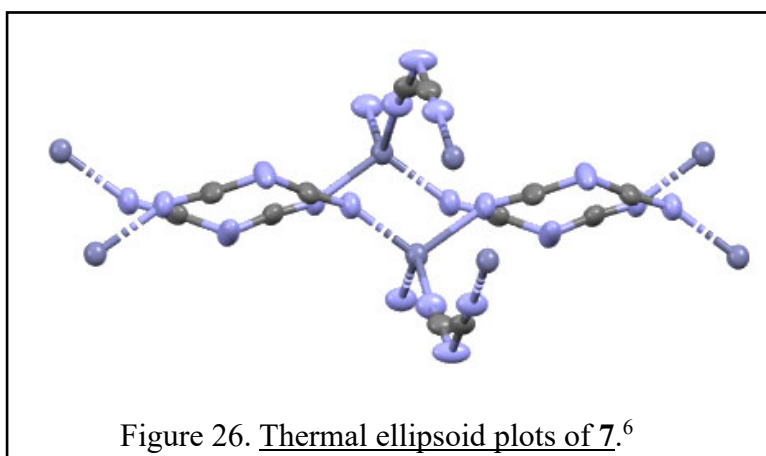
5.3 Tetrakis(dicyanamido) Dipyridine Manganese^{II}

As interest grew in studying the competition between pyridine and dicyanamide ligands, we maintained the same protocols even if stoichiometrically unfavorable. In this case, 0.5 mmol of $\text{Mn}(\text{NO}_3)_2 \cdot 6\text{H}_2\text{O}$ was added as the metal salt. The clear solution produced small amounts of precipitate as the pyridine was added. After several days when dried using slow evaporation, large white “snow flake” like crystals were produced, **6**. The crystals were indexed using x-ray diffraction: $a = 7.5212(3)$, $b = 13.1458(9)$, $c = 8.6087(6)$, $\alpha = 90^\circ$, $\beta = 115.183(9)^\circ$, $\gamma = 90^\circ$, $V = 770.26$. The unit cell matched the previously reported structure of Batten et al.⁵ Unlike **5**, each Mn atom lies on an inversion center, and is connected to two others by four equatorially bound dicyanamide ligands creating a polymer. Two pyridine ligands are axially coordinated with π -stacking interactions between them (Figure 25). As also seen in **5** above, the dicyanamide ligands all bonded on end.



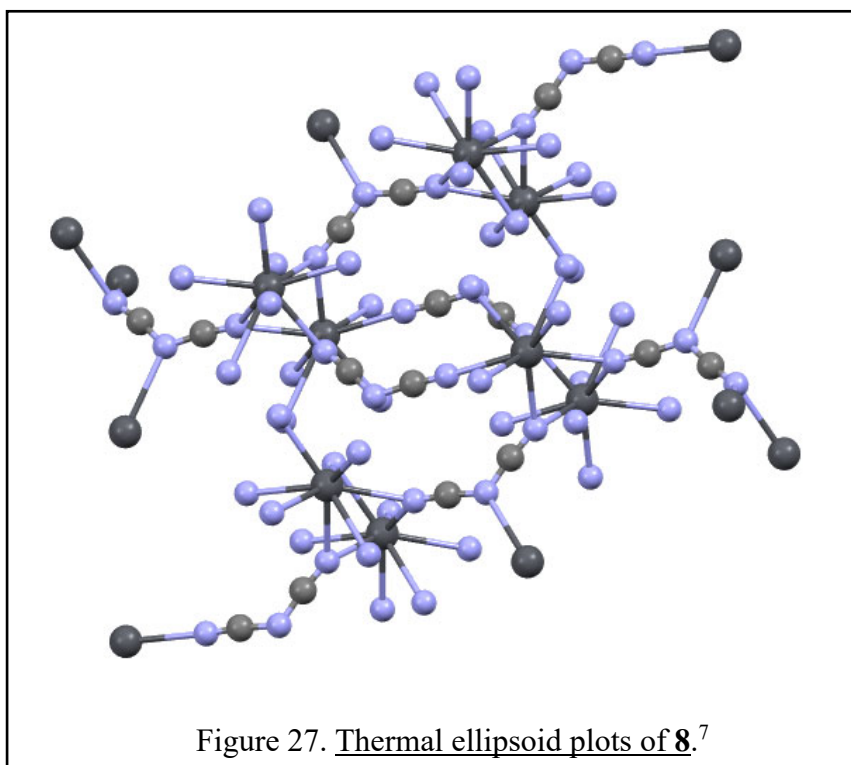
5.4 Zinc Dicyanamide

The next structure observed was by adding $\text{Zn}(\text{NO}_3)_2 \cdot 6\text{H}_2\text{O}$ as the metal salt, again with pyridine added last in excess. After drying for several days using slow evaporation, large clear crystals were produced, **7**. The crystals were indexed using x-ray diffraction: $a = 7.6070(3)$, $b = 7.5828(4)$, $c = 11.8468(6)$, $\alpha = 90^\circ$, $\beta = 90^\circ$, $\gamma = 90^\circ$, $V = 683.35$. The unit cell matched the previously reported structure of Jensen et al.⁶ Unlike both **5** and **6** previously mentioned, the zinc complex (**7**) does not have any pyridine ligands but four dicyanamide – all coordinated on end as in **5** and **6**. A corrugated sheet like structure from the overlapping polymer chains was observed.



5.5 Lead Dicyanamide

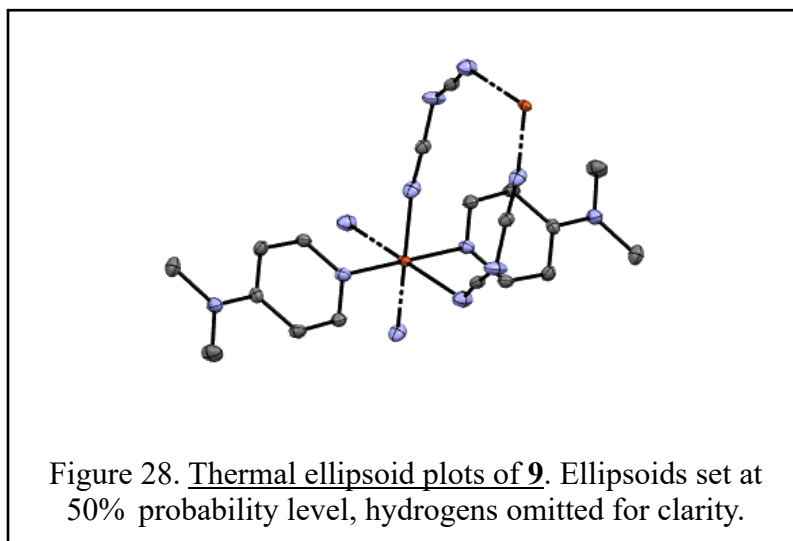
The decision was made to use p-block metals after using transition metals to observe any change in geometry or if the ligands exchanged. Same protocol as the others was used and lead was the p-block metal chosen - 0.5 mmol of $\text{Pb}(\text{NO}_3)_2 \cdot 6\text{H}_2\text{O}$ was added as the metal salt. After drying for several days using slow evaporation, large clear crystals were produced, **8**. The crystals were indexed using x-ray diffraction: $a = 13.5045(10)$, $b = 3.9989(4)$, $c = 11.9939(11)$, $\alpha = 90^\circ$, $\beta = 90^\circ$, $\gamma = 90^\circ$, $V = 647.71$. The unit cell matched the previously reported structure of Jurgens et al.⁷ Again, dicyanamide ligands all bonded on end in an interesting eight coordinate molecular geometry – with bridging ligands between lead atoms forming a polymer (Figure 27).



5.6 Dimethylimidopyridine dicynamido copper (II)

We wanted to observe what geometry was produced and what ligands coordinated when using a slightly more basic ligand. Six mmol of dicyanamide was dissolved in 1:1 $\text{H}_2\text{O}/\text{EtOH}$

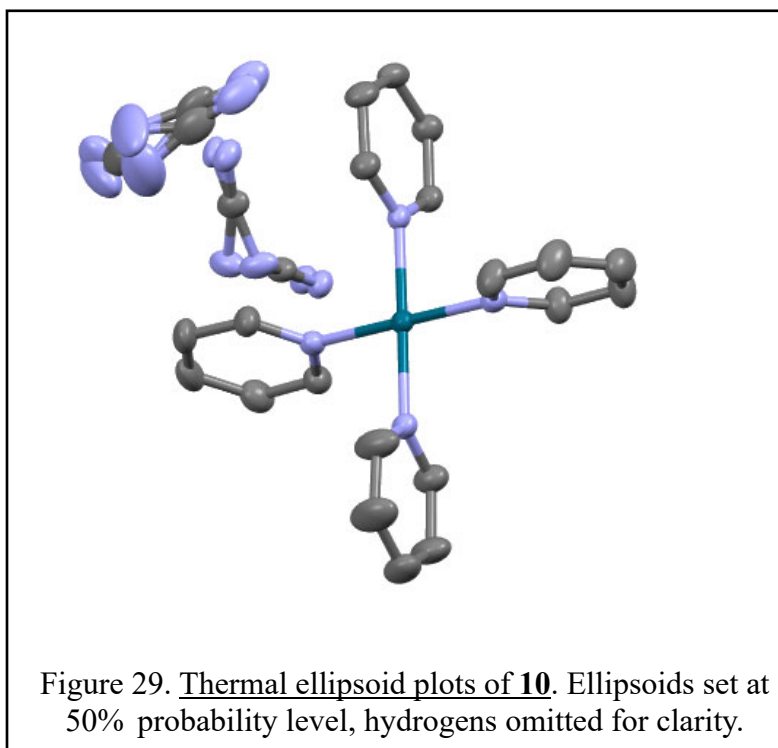
solution as before, and to this 0.5 mmol of $\text{Cu}(\text{NO}_3)_2 \cdot 6\text{H}_2\text{O}$ was added, with dimethylimidopyridine (DMAP) added last in excess. After drying for several days using slow evaporation, large green crystals were produced, **9**. The crystals were indexed using x-ray diffraction: $a = 7.2716(12)$, $b = 8.0636(14)$, $c = 8.9865(15)$, $\alpha = 101.317(4)^\circ$, $\beta = 108.080(3)^\circ$, $\gamma = 95.552(4)^\circ$, $V = 484.09$. Using a slightly more basic ligand resulted in two coordinated DMAP ligands and four dicyanamide each bridging creating a polymer. The coordination environment matched that of **7**, although no π -stacking interactions are apparent. As in every complex in this chapter, the dicyanamide ligands bonded on end to the metal center.



5.7 Bis(dicyanamido) Tetrakis(pyridine) Palladium^{II}

Lastly, Gaby Munoz Sanchez used the same protocol as in the other crystals grown in this chapter but added PdCl_2 as the metal salt. An orange solution was observed with no apparent change after the addition of excess pyridine. After drying for several days using slow evaporation, large clear crystals were produced, **10**. The crystals were indexed using x-ray diffraction: $a = 25.6239(11)$, $b = 25.6239(11)$, $c = 16.823(1)$, $\alpha = 90.0^\circ$, $\beta = 90.0^\circ$, $\gamma = 90.0^\circ$,

$V = 11045.7$. The resulting structure was the first produced that was heavily disordered, and the only metal that ligated to only pyridine ligands with the dicyanamide counterions co-crystallized. The geometry is square planar and single crystal since no dicyanamide allowed for polymerization. Of note, very similar structures have been reported upon but contained different counter anions than **10**.



5.7 Discussion

5.7.1 The Geometry of the Crystal Complexes

The first observation made was that Mn, Co and Ni were six coordinate while Zn, Pb and Pd were four coordinate. Given the common belief that d^8 metals would make square planar complexes based on the moderately strong field pyridine ligand provides a good rationale for the Pd structure observed. A hypothesis could be made that the addition of the dicyanamide ligands

increases the crystal field stabilization energies sufficiently to encourage an octahedral geometry. However, we were unsure why the Pd did not coordinate with the dicyanamide ligands as well. One explanation could be that the larger orbitals of the Pd overlap with the p-orbitals of the pyridine thereby optimizing the stability of the fourfold geometry. Crystal packing could also influence this change in coordination. Of additional interest is the octahedral geometry of Mn, noting that being d^5 metal with strong field ligands would likely favor an octahedral complex as observed. For further insight, dimethylimidopyridine ligand was added in excess in lieu of pyridine affording the structure **9** in Figure 28. Using a more basic ligand resulted in a six-coordinate geometry instead of four coordinate. Kofen et al. argued that sixfold to fourfold coordination among transition metals was due to metal-ligand bond length. In their conclusion they state, “The change from a sixfold (Mn, Fe) to a fourfold coordination (Zn) of the central metal cation was ... caused by a decreasing metal-ligand bond length throughout the first-row transition metals, which decreased the coordination number and ultimately led to steadily decreasing cation radii. The additional increase in steric repulsion of the ligands favors the decrease in the coordination number, supporting the change in coordination.”⁸ This rationale does not articulate why each metal prefers the pyridine over dicyanamide (or vice versa).

5.7.2 Describing the Pyridine Dicyanamide Ligand Competition

A rationale to describe metal ligand preference could be hard-soft acid base theory (HSAB). Ralph Pearson introduced the HSAB theory in the early 1960s, as a qualitative description to help predict factors which drive chemical properties and reactions. Chemical species are described as 'hard' or 'soft', and an 'acid' or 'base' to chemical species. 'Hard' applies to species which are small, have high charge states, while 'soft' applies to species which are big, have low charge states. In crystal structures produced in this chapter, HSAB does not adequately

predict and account for the bonding environments observed although the acids and bases used may perfectly straddle the line between ‘hard’ and ‘soft’. Although not entirely quantitative, Co^{+2} , Ni^{+2} , Zn^{+2} , Pb^{+2} are all ‘borderline’ hard acids. The pyridine ligand is also considered a ‘borderline’ soft base. Dicyanamide is likely softer than pyridine, but not by a significant amount. Nevertheless, the cobalt and nickel complexes were 50/50 mix dicyanamide and pyridine ligands matching expectations, but the zinc and lead species were solely coordinated to dicyanamide ligands. From this result, a logical conclusion would be that the dicyanamide ligand is softer than the pyridine ligand and the slight difference in atomic radius is affecting the bonding outcome. However, when applied to the Pd complex, this proves inaccurate since Pd is certainly the softest acid of the many metals used but only coordinated to the pyridine ligands. Adding the slightly more basic dimethylamidopyridine ligand does not seem to offer any insights since the ‘borderline’ Cu^{+2} once again has an equal mix of ligands. Another rationalization or contributing factors must be involved in the determining ligand bonding affinity in the structures presented in this chapter. Full characterization is being performed on each complex at the time of the writing of this manuscript, and with additional calculations from density functional theory (DFT), more accurate and convincing hypothesis might be provided to explain this competition among ligands.

5.8 Iridium Coordination Crystals

Colonel Chi Nguyen at the United States Military Academy (USMA), West Point New York in collaboration with the Army Research Laboratory in Aldelphi Maryland are developing next generation US Army optics. Organometallic chromophores are of interest due to their photophysical properties in the application of reverse saturable absorption (RSA). RSA occurs

when the excited state of a molecule absorbs more energy than the ground state.⁹ Iridium is a useful transition metal because its many electrons allow for a stronger spin-orbit coupling and metal-to-ligand charge transfer for absorption over a broad wavelength range. The following work focused on the synthesis of iridium(III) cyclometalated chromophores with three different functionalized 2-phenylbenzothiazole (pbt) ligands: 6-(4-methoxyphenyl)-2-pbt, 6-(4-fluorophenyl)-2-pbt, and 6-(3,5-difluorophenyl)-2-pbt. As part of that effort, both products were examined using XRD and their crystal structures were reported.

5.8.1 Ir[(6-(4-methoxyphenyl)-2-pbt)₂(acac)]

The methoxyphenyl iridium crystal structure found below **11** (Figure 30) exhibited minimal disorder, but otherwise proved to be a simple structure to solve.

The iridium metal center takes an octahedral geometry with one methoxyphenyl group perpendicular to the other. The Ir-O bond length to the methoxyphenyl ligand was 2.049Å, well within the usual bond length distance of between 1.5 and 2.5Å. The Ir-N bond lengths were almost identical to the Ir-O, and the Ir-O bonds within the acetate were also equal and similar (2.049Å). The bond angles for octahedral metal center are all between 87.64° and 96.97° - indicating a slight distortion of the octahedral geometry, and also evident from the slight twisting observed of the two directly coordinated and opposite phenol rings to the iridium. One of the aromatic rings displayed some disorder but was split and modeled appropriately – given the very symmetric nature of the crystal it is interesting that the disorder only occurred on one side of the complex.

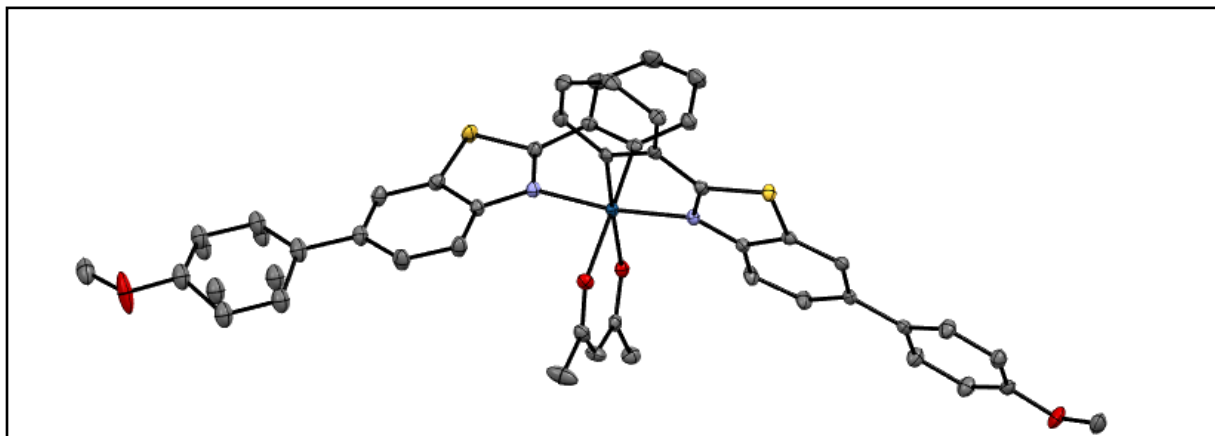
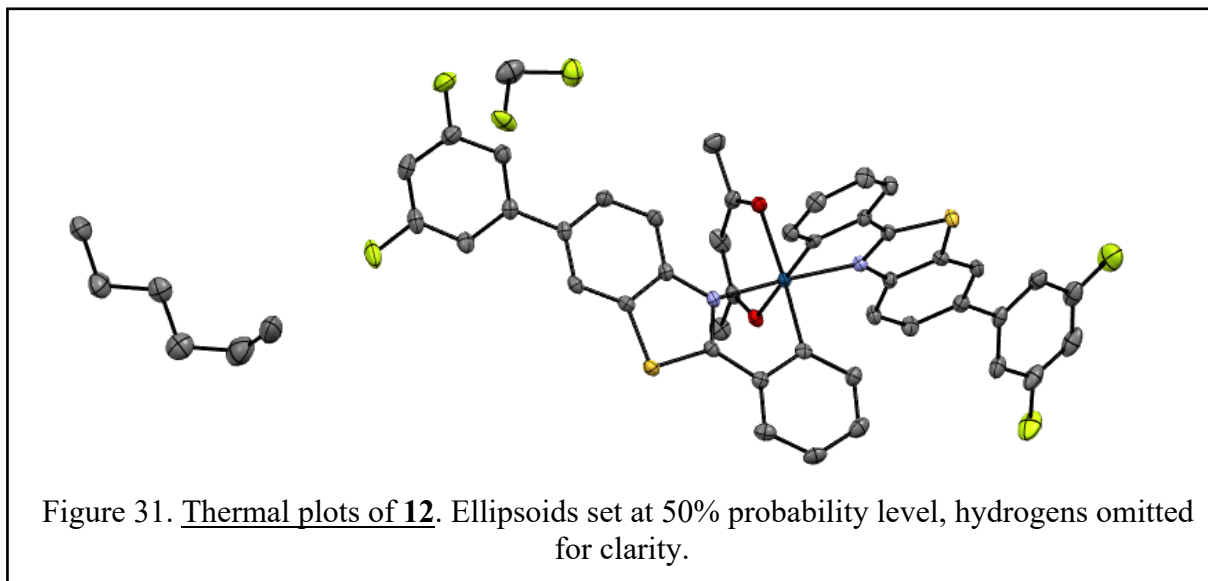


Figure 30. Thermal plots of 11. Ellipsoids set at 50% probability level, hydrogens omitted for clarity.

5.8.2 Ir[(6-(3,5-difluorophenyl)-2-pbt)₂(acac)]

Unlike Figure 30 above, the difluorophenyl iridium complex was solved with little difficulty and crystallized without any disorder. However, both counter anion and hexane solvent were present in the crystal structure **12** (Figure 31).

The dark red crystal structure is built of isolated monometallic molecules. The difluorophenyls bonded axially are perpendicular to each other. As also seen in **11** above, the iridium center has an octahedral geometry and Ir-O, Ir-C, and Ir-N bond lengths only varied by 0.05Å. As also seen in **11**, there is a slight distortion in the octahedral geometry – angles around the metal center ranged from 85.5° to 98.3°. The Ir-N bonds opposite each other positioned axially are 179.1° - indicating most of the distortion to the ideal 90° is made from the other coordination sites. Although containing a number of phenyl rings, no π - π stacking interactions are observed in the crystal structure.



5.9 References

1. Albert, E.; Mautner, F.; Sanz, N.; Vicente, R. *Inorganic Chemistry*, **2000**, 39 (8), 1668-1673.
2. Sun, H.; Wang, Z.; Gao, S. *Inorganic Chemistry*, **2005**, 44 (7), 2169-2176.
3. Batten, R.; Robson, R.; Batten, S.; Jensen, P.; Moubaraki, B.; Murray, K. *Chemical Communications*, **1998**, 439-440.
4. Wöhlert, S.; Wriedt, M.; Jess, I.; Näther, C.; Bis(dicyanamido-κN)tetra-kis-(pyridine-κN)nickel(II). *Acta Crystallogr Sect E Struct Rep Online*. **2012**.
5. Batten, S.; Jansen, P.; Kepert, C.; Kurmoo, M.; Moubaraki, B.; Murray, K.; Price, D.; *J. Chem. Soc., Dalton Trans.*, **1999**, 2987-2997.
6. Jensen, P.; Batten, S.; Fallon, G.; Moubaraki, B.; Murray, K.; Price, D.; *Chemical Communications*, **1999**, 177.
7. Jurgens, B.; Hoppe, H.; Schnick, W.; *Solid State Sciences*, **2002**, 4, 6, 821-825.
8. Kofen, A. G.; Harter, T. M.; Stierstorfer, J. *Energ. Mater. Front.*, **2022**.
9. Verma, N.; Cross, D.; Lundell, C.; Rohrbaugh, T.; O'Donnell, R.; Shensky, W.; Jaffett, V.; Nguyen, C.; Presented at the United States Military Academy, West Point, New York, April, **2022**.

CHAPTER 6

CONCLUSION

6.1 Summary of Results

The effort to create a new double base propellant burn rate modifier that met DoD requirements numerous products were produced along the way and culminated in discovery of a promising cobalt complex **3**. However, as often the case, there were many previously failed attempts for each synthesized and characterized product. In the case of complexes **1** and **2**, no less than 36 reactions using various metals and two different stabilizers under different reaction temperatures and various crystallization techniques were employed. The same could be said about efforts before the discovery and characterization of **3**. Nevertheless, a promising complex to answer the research question was synthesized (**3**) with good yield and reproducibility, and numerous synthetic pathways were reported to help future research efforts in this field.

6.2 Lead Complexes 1 and 2

The formation of tetrakis(μ_3 -(4-methyl-3-nitrophenyl imido lead (II))) (**1**) yielded a novel energy dense cubane molecule that exhibits an energy density above the stand-alone ligand. This energy was probably a result of both the oxidation of Pb(II) to Pb(IV) (forming Pb(IV)O₂ during combustion), and from the increase in density from clustering. The combustion of the material likely does not produce all low-molecular weight gases, thereby decreasing the number of moles available to increase volume according to the ideal gas law. Compound **1** also has a low oxygen balance decreasing energetic performance. The distinctive structures of **1** and **2** with the energy density has interested scientists at Redstone Arsenal, some of whom suspect that the complex could be used for other applications than originally intended. The two lead crystals produced

were both sensitive to air and also contained toxic metal likely limiting their usefulness in propellant application. The investigation using various ligands and metals employing a gentle protolysis reaction was first believed to have proved a viable pathway for future complexes. It was demonstrated that (1) $\text{Pb}(\text{N}(\text{SiMe}_3)_2)$ reacted with two types of double-base propellant stabilizer and can readily form crystalline structures and (2) the lead products could be made fairly easily, in good yield and with good purity not requiring exhaustive separation methods. These positive attributes unfortunately did not translate to the use of other metals using the same ligands. Non-lead metal bis(trimethyl)amides did not readily form crystalline products with the ligands as in the case with lead, although *p*-block and transition metals were all attempted at various stoichiometric ratios and conditions. The toxicity and air-sensitivity of products **1** and **2** dissuaded any further implementation into propellant formulations.

6.3 Hexa-1-phenylurea Cobalt(II) Nitrate

The discovery of hexa-1-phenylurea cobalt (II) (**3**) was pivotal in attempts to answer the research question. The cobalt compound is very easily synthesized without the need for an air-free environment nor expensive reagents. The octahedral shape contains phenol rings, hydrogen bonding and a nitrate counter-ion. The complex also is soluble in a number of organic solvents yet remains insoluble in water – very important quantities if it is to be incorporated into the propellant casting process. Importantly, researchers at the Indian Head Naval Warfare Center determined the material to be suitable for additional propellant testing and found it sufficiently insensitive. Although not completely benign, cobalt is significantly less toxic than lead, and phenylurea ligands are non-toxic making it a promising potential replacement.

6.4 Metal Dicyanamide and Iridium Complexes

The structure of copper dimethylimidopyridine and bisdimethyl tetrapyr dine cobalt (II) were crystallized and are presented. Interesting observations were made between dicyanamide and pyridine ligand competition. The metal ligand geometries could be affected by a number of different factors including crystal stabilization energy, crystal packing, electronics and steric hinderance. At the time of this writing, efforts are underway to better understand each of these complexes and answer many of the questions these complexes raised. Finally, two iridium complexes were solved using XRD and reported to collaborators at the United States Military Academy and the Army Research Laboratory. Although in the nascent stages, these crystal structures may be later reported upon and help future research efforts with reversible saturation absorption materials.

6.5 Future Research

Unfortunately, using the same reaction mechanism for cobalt in **3** did not work for either bismuth or copper in producing crystalline compounds. Although commonly used propellant stabilizers were used as potential ligands – additional stabilizers options such as stab-5 (Figure 7) or vitamin A acetate should be included since each offer good bonding environments. All physical and chemical properties of **3** tested thus far make it a good candidate for further testing. At the time of this manuscript the cobalt complex is being considered for testing in double-base propellant to determine pressure exponent and effects as an additive on nitrocellulose stabilizer longevity. At the completion of those two tests it will be determined if the hexa-1-phenylurea cobalt(II) nitrate is a future additive for DoD ordinance and a solution to a decades old problem.

CHAPTER 7

EXPERIMENTAL

7.1 Experimental Details

Lead bis(trimethylsilyl)amide and synthesized lead compounds are air sensitive. Therefore, those reactions and experiments were conducted in dry, anaerobic conditions using a glovebox and utilizing air sensitive techniques. All reagents were purchased from Sigma-Aldrich. The solvents used were purified by distillation from sodiumbenzophenone ketyl. Solvents were degassed and stored over molecular sieves for 12h before use. X-ray crystal structure determinations were performed using Bruker Kappa APEX II DUO diffractometer equipped with an Oxford Cryostream. Mo K α radiation was used for single-crystal structural determination. The crystals were mounted on MiTeGen loops using Paratone-N oil. Data collection, including strategy, unit cell refinement, integration, scaling, and absorption correction was performed using the Bruker APEX2 suite (Bruker, 2008). Space group determination was performed using XPREP (Sheldrick). The ^1H NMR spectra were obtained on a Bruker Biospin AVANCE 400MHz spectrometer. CHN analysis were performed by the CENTC elemental analysis facility at the University of Rochester (NY). FT-IR spectra was collected from a Thermo Scientific IR with iD5 ATR and the UV-vis spectra was obtained on a Shimadzu UV-1800.

7.2. Synthesis of Reactants

7.2.1 Lead bis(bis(trimethylsilyl)amide)

A lead bis(trimethylsilyl)amide reactant was made using a protolysis reaction to a previously described procedure by Andersen et al.¹ 12.107g of PbI₂ (461.01 g/mol, 25.26 mmol) was dissolved in ~200 mL of THF. 9.817g of K(N(SiMe₃)₂) was dissolved in ~100mL of THF and added drop wise to the PbI₂. After stirring for 12 hours at room temperature the contents were dried under vacuum for 24 hours. Pentane was added to the solid product and filtered through a medium frit. The light-yellow filtrate was and stored at -30°C. Crystals formed and were decanted and rinsed in pentane after 48 hours in storage. The yield produced approximately 6g of lead bis(trimethylsilyl)amide (11.36 mmol, 47%). The resulting structure was indexed and characterized using X-ray diffraction with Mo K α radiation, unit cell (XRD) orthorhombic P, $a = 13.15(3)$, $b = 15.58(3)$, $c = 21.92(5)$, $\alpha = 90.0^\circ$, $\beta = 90.0^\circ$, $\gamma = 90.0^\circ$.

7.2.2 Tin bis(bis(trimethylsilyl)amide)

Tin lead bis(trimethylsilyl)amide was available commercially but was back ordered, so it was synthesized using an analogous protolysis reaction to the previously described procedure. 4.2g of SnBr₂ (278.518 g/mol, 15.0 mmol) was dissolved in ~100 mL of THF. 3.0g (14.9 mmol) of K(N(SiMe₃)₂) was dissolved in ~100mL of THF and added drop wise to the SnBr₂. After stirring for 12 hours at room temperature the contents were dried under vacuum for 24 hours. Pentane was added to the solid product and filtered through a medium frit. The collected light orange filtrate was stored at -30°C. Crystals formed and were decanted and washed in pentane after 48 hours in storage. The yield produced approximately 3.34g of tin bis(trimethylsilyl)amide (10.77 mmol, 31%). The product was characterized by indexing the unit cell using XRD.

7.2.3 Bismuth tris(bis(trimethylsilyl)amide)

A bismuth tris(bis(trimethylsilyl)amide) reactant was made using an analogous protolysis reaction based on a previously described procedure.¹ 3.0g of BiI₃ (589.69 g/mol, 5.01 mmol) was dissolved in ~200 mL of THF. 1.0g (5.0 mmol) of K(N(SiMe₃)₂) was dissolved in ~100mL of THF and added drop wise to the BiI₃. After stirring for 12 hours the contents were dried under vacuum for 24 hours. Pentane was added to the solid product and filtered through a medium frit filter. The light-yellow filtrate was stored at -30 °C. Powder formed and was decanted, washed in pentane and then dried by vacuum. Produced 1.59g of bismuth bis(trimethylsilyl)amide (2.69 mmol, 47%). The resulting structure was characterized using melting point, mp: exp 130-135°C, lit 133-137°C.

7.2.4 Zinc bis(trimethylsilyl)amide

A Zinc bis(trimethylsilyl)amide reactant was made using an analogous protolysis reaction based on a previously described procedure above.¹ 11.10g of ZnBr₂ (225.20.01 g/mol, 49.29 mmol) was dissolved in ~200 mL of THF. 9.832g of K(N(SiMe₃)₂) was dissolved in ~100mL of THF and added drop wise to the ZnBr₂. After stirring for 12 hours at room temperature the contents were dried under vacuum for 24 hours. Pentane was added to the solid product and filtered through a medium frit. The colorless filtrate was stored at -30°C. A white cloudy solid formed and was collected after 48 hours in storage. The yield produced approximately 5.49g of zinc bis(trimethylsilyl)amide (11.36 mmol, 47%). The resulting structure was characterized using melting point, mp: exp 15-20°C, lit 12.5°C.

7.3 Synthesis of Novel Products

Except where otherwise noted, all operations were carried out under rigorous exclusion of air and water, as compound **1**, and compound **2** are air sensitive.

7.3.1 Tetrakis(μ_3 -4-methyl-3-nitrophenylamido)lead (II) (**1**)

To 66 mg (152.1 g/mol, 0.43 mmol) of nitromethylaniline in 2 mL of THF was added 144 mg (527.9 g/mol, 0.28 mmol) lead bis(trimethylsilyl)amine in 2 mL of THF at room temperature giving a color change to dark orange. This solution was then placed in a vapor diffusion double-vial apparatus with the reaction mixture in an inner vial and pentane in the outer vial and left at room temperature. Dark orange crystals were observed 24 hours later. The crystals were subsequently washed 3-5 times with 3 mL aliquots of pentane and dried in vacuo. X-ray diffraction was used to characterize the crystal as a tetrakis complex **1**. Unit Cell (XRD): $a = 10.4265(16)\text{\AA}$ $b = 13.2813(19)\text{\AA}$ $c = 14.624(2)\text{\AA}$, $\alpha = 97.592(3)^\circ$, $\beta = 94.084(4)^\circ$, $\gamma = 99.410(3)^\circ$. $V = 2068.6(4)\text{\AA}^3$ (Appendix A). Yield: 56 mg (0.0373 mmols, 56%). Anal. Calcd for $\text{C}_{28}\text{H}_{24}\text{N}_8\text{O}_8 \text{Pb}_4 \cdot 1 (\text{CH}_2)_4\text{O}$: C, 25.60%; H, 2.15%; N, 7.46%. Found: C, 25.44%; H, 1.99%; N, 7.41%. UV-Vis pyridine: 391 max [nm] $\epsilon = 1.4 \times 10^4$ (Appendix B). ^1H NMR ($\text{C}_5\text{D}_5\text{N}$, ppm, 293K): δ 8.58 (m, pyridine), δ 7.44 (m, pyridine), δ 7.06 (m, pyridine), δ 6.88 (s, 1H), δ 5.93 (m, 1H) δ 4.84 (m, 1H) δ 2.23 (m, Me).

7.3.2 Bis(dinitrophenylamido)lead (II) (**2**)

To 264 mg (527.9 g/mol, 0.5 mmol) of lead bis(trimethylsilyl)amide in 2 mL of THF was added 2 equivalents, 214 mg (214.2 g/mol, 1.0 mmol) of 2-nitrodiphenylamide in 2 mL of THF at room temperature to give a dark purple color. A vapor diffusion double-vial apparatus was used with pentane in the outer vial and reaction mixture in the inner vial and stored at room temperature for 4 days. Purple crystals were formed. The mother liquor was decanted and the

crystals were subsequently washed 3-5 times with 3 mL pentane and dried under vacuum. X-ray diffraction characterized the crystals as bis(dinitrophenylamidolead(II)). Unit Cell (XRD) $a = 11.7362$ (14), $b = 10.8203$ (13), $c = 20.5003$ (2), $\alpha = 90.0^\circ$, $\beta = 104.766(2)^\circ$, $\gamma = 90.0^\circ$. $V = 2514.6(5) \text{ \AA}^3$ (Appendix C). Yield: 264 mg (.0373 mmols, 42%). Anal. Calcd for $\text{C}_{24}\text{H}_{20}\text{N}_4\text{O}_4 \text{ Pb} \cdot 0.55 (\text{CH}_2)_4\text{O}$: C, 46.69%; H, 3.3%; N, 8.32%. Found: C, 45.57%; H, 3.192%; N, 7.99%. UV-Vis benzene: 427 max [nm] $\epsilon = 8.9 \times 10^3$ (Appendix D). $^1\text{H NMR}$ (C_6D_6 , ppm, 293k): $\delta 7.93$ (m, 1H), $\delta 7.06$ (s, C_6D_6), $\delta 6.78$ (t, 1H), $\delta 6.77$ (m, 1H), $\delta 6.65$ (d, 1H) $\delta 6.59$ (m, 1H), $\delta 6.11$ (m, 1H).

7.3.3 Hexa-1-phenylurea Cobalt (II) Nitrate (3)

1-phenylurea was purchased from Sigma Aldrich without further purification and 6 mmol (0.136g) was dissolved in 30 ml of ACN/EtOH 1:1 solution. The solution was stirred for 10 minutes at room temperature – a light blue solution was observed. To this was added 0.5 mmol (0.122) of $\text{Co}(\text{NO}_3)_2 \cdot 6\text{H}_2\text{O}$. The solution turned bright pink was stirred and refluxed for 2 hours. The solution was dried over NaSO_4 and the solvent was removed using rotary evaporation. Crystals were afforded by dissolving the pink powder in THF and using a vapor diffusion technique with pentane. Unit Cell (XRD) $a = 10.549$ (3), $b = 14.371$ (4), $c = 216.525$ (4), $\alpha = 90.0^\circ$, $\beta = 92.0^\circ$, $\gamma = 90.0^\circ$. $V = 2503.6(11) \text{ \AA}^3$ (Appendix E). Yield: 264 mg (0.288g, 78%). Anal. Calcd for $\text{C}_{42}\text{H}_{48}\text{N}_{13}\text{O}_9\text{Co} \cdot \text{C}$: 53.81%, H: 5.16%; N: 18.42%. Found: C: 34.85%, H: 4.40%; N, 16.6%. $^1\text{H NMR}$ (CD_3CN ppm, 293k), $\delta 1.9$, $\delta 10.71$ (s, 1H), $\delta 7.88$ (d, 2H), $\delta 7.36$ (d, 2H), $\delta 6.99$ (s, 1H), $\delta 6.24$ (s, 1H) $\delta 3.48$ (s, 1H).

7.3.4 Bisdicyanamido tetrapyridine cobalt (II) (4)

Sodium dicyanamide was purchased from Sigma Aldrich without further purification and 1 mmol was dissolved in 30 ml of $\text{H}_2\text{O}/\text{EtOH}$ 1:1 solution. The solution was stirred for 10 minutes at room temperature. To this was added 0.5 mmol (0.122) of $\text{Co}(\text{NO}_3)_2 \cdot 6\text{H}_2\text{O}$ also in 30

ml of H₂O/EtOH 1:1 solution. Pyridine was added dropwise in excess, and solution stirred overnight. Unit Cell (XRD) $a = 13.063(2)$, $b = 12.880(2)$, $c = 15.033(2)$, $\alpha = 90.0^\circ$, $\beta = 110.0(3)^\circ$, $\gamma = 90.0^\circ$. $V = 2376.8(6) \text{ \AA}^3$ (Appendix C).

7.3.5 Bisdimethylimidopyridine Tetrakis(dicyanamido) Copper (II) (9)

Sodium dicyanamide was purchased from Sigma Aldrich without further purification and 1 mmol was dissolved in 30 ml of H₂O/EtOH 1:1 solution. The solution was stirred for 10 minutes at room temperature. To this was added 0.5 mmol (0.122) of Cu(NO₃)₂·6H₂O also in 30 ml of H₂O/EtOH 1:1 solution. Pyridine was added dropwise in excess, and solution stirred overnight. Unit Cell (XRD) $a = 7.2716(12)$, $b = 8.0636(14)$, $c = 8.9865(15)$, $\alpha = 101.317(4)^\circ$, $\beta = 108.080(3)^\circ$, $\gamma = 95.552(4)^\circ$. $V = 484.09(14) \text{ \AA}^3$ (Appendix C).

7.4 Calorimetry

Calorimetry experiments were conducted using a 6725 semimicro calorimeter attached to a 6772 calorimic thermometer from Parr Instruments. The combustion reactor was a 1109X oxygen combustion vessel and pressurized with O₂ to 35 atm. Pellets of compounds **1** and **2** were made by use of a Parr pellet press, and five were made of each product weighing between 5mg and 227mg. Each pellet was trapped between two adhesive plastic strips in an anaerobic glovebox to prevent exposure to air prior to combustion initiation, and transferred to the combustion vessel. When determining the internal energies of the lead compounds, the mean specific heat of the plastic strips was determined to be 5,952.33 cal/g and subtracted from gross heat produced. This modified procedure for air sensitive testing was evaluated using the accepted value of -6318.4 cal/g for benzoic acid and plastic strips. The ΔH_c percent error was determined

to be higher by 0.86%. For experimental measurements on **1**, **2** and **3**, heats of combustion in cal/g were converted to MJ/L using their experimental crystallographic densities.

7.5 Compatibility Testing

Compatibility testing of **3** was completed at Indian Head Naval Surface Warfare Center in Maryland. Per CPIA Publ. 597, (1993) 301: “Compatibility of Energetic Materials by DSC and TGA, any downward shift of the peak temperature by the admixture of more than 4°C indicates some interactivity. There is no shift indicating inter-reactivity based on the endothermic peak of the cobalt complex being a decomposition event. However, the mixture does have a lower activation energy relative to NC.”

7.6 References

1. Andersen, R.A.; Faegri, K.; Green, J.; Haaland, A.; Lappert, M. F.; Leung, W.P.; Rypdal, K. *Inorg. Chem.* **1988**, 27, 1782.
2. Fjeldberg, T.; Hope, H.; Lappert, M.F.; Power, P.P. *J. Chem. Soc. Chem. Comm.*, **1983**, 639-641.

BIBLIOGRAPHY

- A. T. Camp, Patent US 3,088,858, **1963**.
- Albert, E.; Mautner, F.; Sanz, N.; Vicente, R.; *Inorganic Chemistry*, **2000**, 39 (8), 1668-1673.
- Apatoff, J. B.; Norwitz, G. *Role of Diphenylamine as a stabilizer in propellants; analytical chemistry of diphenylamine in propellants*; US Army Armament Command, Test Report T73-12-1, **1973**.
- Ballistic Modifier LC-12-15 Mil Spec, courtesy of parchem, www.parchem.com/Ballistic-Modifier-LC-12-15-Mil-Spec-getpdf-013001.aspx (accessed 15 March 2017).
- Batten, R.; Robson, R.; Batten, S.; Jensen, P.; Moubaraki, B.; Murray, K.; *Chemical Communications*, **1998**, 439-440.
- Bhat, V.K.; Singh, H. Cross-Linked Slurry Cast Composite Modified Double Base Propellants: Mechanical Properties. *Def Sci J.*, **1987**, 37,1, 39-445.
- Braeunig, R. A., Rocket and Space technology, <http://www.braeunig.us/space/propuls.htm> (accessed 5 January 2017).
- Bürger, H.; Sawodny, W.; Wannagat, U. Darstellung. *J. Organomet. Chem.* **1965**, (2): 113–120.
- Composition of Type N5 Nitrocellulose-based Double Base Propellant, courtesy of Island Pyrochemical Industries, http://www.islandpyrochemical.com/military/rocket_propellants.php.
- Cox, J.D.; Pilcher, G. *Thermochemistry of Organic and Organometallic Compounds*, Academic Press, New York, **1970**, 1-636.
- D.H. Kim, in *Encyclopedia of Toxicology (Third Edition)*, **2014**.
- Denisyuk, A.P.; Demidova, L.A.; *Combustion, Explosion, and Shock Waves*, 2004, 40, 3 311-318.
- Fifer, R.A. *Workshop Report: Fundamental Reactions in Solid Propellant Combustion*; ARBRL-TR-02166; 1979.
- Fjeldberg, T.; Hope, H.; Lappert, M.F.; Power, P.P.; Thorne, A.J. *J. Chem. Soc. Chem. Comm.*, **1983**, 639-641.
- Gao, J.; Wang, L.; Yu, H.; Xiao, A.; Ding, W. *Propellants, Explos. Pyrotech.* **2011**, 36, 404-409.

- Jensen, P.; Batten, S.; Fallon, G.; Moubaraki, B.; Murray, K.; Price, D.; *Chemical Communications*, **1999**, 177. Katoh, K.; Le., L.; Itoh, M.; Arai, M.; Tamura, *Sci. Tech. Energ. Mater.* **2003**, 64, 236.
- Jurgens, B.; Hoppe, H.; Schnick, W.; *Solid State Sciences*, **2002**, 4, 6, 821-825. Katoh, K.; Yoshino, S.; Kubota, S.; Wada, Y.; Ogata, Y.; *Propellants, Explos. Pyrotech.* **2007**, 32, 4, 314-321.
- Kofen, A. G.; Harter, T. M.; Klapötke.; Stierstorfer, J. *Energ. Mater. Front.*, **2022**.
- Kubota, N. *Propellants and Explosives*, WILEY-VCH Verlag GmbH & Co. KGaA, Weinheim, 2007.
- Lundell, C. E.; Master's Thesis, Temple University, Philadelphia PA, **2017**.
- Lundell, C.E.; O'Sullivan, O.; Gau, M.; Zdilla, M.; *Chemistry Select*, **2017**, 2, 35, 11673-11676.
- Magill, B. T.; Naufflett, G. W.; Furrow, K. W. *Lead-Free Double-Base Propellant for the 2.75 Inch Rocket Motor*; 20000116525; Cocoa Beach, FL, 2000.
- Otto, K.; Lehman, C.; Bartosiewicz, L.; Shelef, M. *Carbon*. **1982**, 20, 243-251.
- Raman, K.V.; Singh, H. *Propellants Explos. Pyrotech.*, 1988, 13, 5, 149-151.
- Raman, K.V., Singh, H., Rao, K.; *Combustion Science and Technology*, **1985**, 45, 213-219.
- Ramnarace, J. *Rocket Propellant Technology*, Page publishing: New York, NY, **2015**.
- Sharma, J.; Wilmot, G.B.; Campolattaro, A.A.; Santiago, F.; *Combustion and Flame*, **1991**, 85, 416-426.
- Sharma, J.; Wilmot, G.B.; Campolaattro, A. A., Santiago, F. *Combust Flame*. **1991**, 85, 416-426.
- Sketch redrawn from Kubota, N. *Propellants and Explosives*, WILEY-VCH Verlag GmbH & Co. KGaA, Weinheim, 2007.
- Sullivan, M.V.; Hunt, H. *J. Phys. Chem.*, **1949**, 53, 497-500.
- Sun, H.; Wang, Z.; Gao, S.; *Inorganic Chemistry*, **2005** 44 (7), 2169-2176.
- Sutton, G. *Rocket Propulsion Elements*, Wiley: Hoboken, New Jersey, **2017**.
- Trache, D., Tarchoun, A., *Journal of Material Science*, **2018**, 53, 100-123.
- Tunestål, E.; Hafstrand, A.; Lindborg, A.; Krumlinde, P.; Ek, S.; Goede, P.; Schragen, C. New stabilizers for NC-propellants Evaluated in Rocket Propellants. FOI, Swedish Defense

Research Agency, Department of Energetic Materials and Modelling, SE-147 25 Tumba, Sweden.

Vehkamäki, M.; Hatanpää, T.; Ritala, M.; Leskelä, Ma. *Journal of Materials Chemistry*. **2004**, 14, 21, 3191.

Wang, C.; Li, J.; Fan, X.; Zhao, F.; Zhang, W.; Zhang, G.; Gao, Z. *Eur. J. Inorg. Chem.*, 2015, 1012-1021.

Warren, L.; Pulham, C.; Morrison, C.; *Phys. Chem. Chem. Phys.* **2020**, 22, 25502-25513.

Yang, V. Thakre, P. Encyclopedia of Aerospace Engineering, Blockley, R. and Shyy, W., Ed; John Wiley and Sons, Ltd: **2010**.

Zain-ul-Abdin.; L. W.; Haojie Y.; Muhammad S.; Nasir A.; Rizwan, U.K.; Raja S.; Haroon, M. *RSC Adv.*, **2016**, 6, 97469–97481.

APPENDIX A

CRYSTAL DATA FOR TETRAKIS (μ_3 -(4-METHYL-3-NITROPHENYL IMIDO LEAD (II)))

Table 1 Crystal data and structure refinement for tetrakis(u3-(4-methyl-3-nitrophenyl imido (II))).

Identification code	tetrakis(u3-(4-methyl-3-nitrophenyl imido (II)))
Empirical formula	C ₃₆ H ₄₀ N ₈ O ₁₀ Pb ₄
Formula weight	1573.52
Temperature/K	99.89
Crystal system	triclinic
Space group	P-1
a/Å	10.6519(13)
b/Å	13.5498(16)
c/Å	14.8146(17)
α /°	97.453(2)
β /°	95.652(2)
γ /°	100.455(2)
Volume/Å ³	2068.6(4)
Z	2
$\rho_{\text{calc}}/\text{cm}^3$	2.526
μ/mm^{-1}	16.294
F(000)	1440.0
Crystal size/mm ³	0.159 × 0.099 × 0.022
Radiation	MoK α ($\lambda = 0.71073$)
2 Θ range for data collection/°	3.092 to 56.022
Index ranges	-14 ≤ h ≤ 13, -14 ≤ k ≤ 17, -17 ≤ l ≤ 19
Reflections collected	24435
Independent reflections	9852 [R _{int} = 0.0308, R _{sigma} = 0.0395]
Data/restraints/parameters	9852/40/527
Goodness-of-fit on F ²	1.056
Final R indexes [I ≥ 2 σ (I)]	R ₁ = 0.0246, wR ₂ = 0.0629
Final R indexes [all data]	R ₁ = 0.0315, wR ₂ = 0.0655
Largest diff. peak/hole / e Å ⁻³	1.88/-1.15

Table 2 Fractional Atomic Coordinates ($\times 10^4$) and Equivalent Isotropic Displacement Parameters ($\text{\AA}^2 \times 10^3$) for tetrakis(u₃-(4-methyl-3-nitrophenyl imido lead (II))). U_{eq} is defined as 1/3 of of the trace of the orthogonalised U_{IJ} tensor.

Atom	<i>x</i>	<i>y</i>	<i>z</i>	U_{eq}
Pb1	4062.6(2)	8475.9(2)	2230.2(2)	13.27(5)
Pb2	2240.7(2)	6137.1(2)	2609.2(2)	14.27(5)
Pb3	4453.1(2)	6170.9(2)	983.9(2)	13.76(5)
Pb4	5589.5(2)	6791.1(2)	3366.4(2)	13.63(5)
O4	10272(4)	7400(3)	2794(3)	29.3(9)
O9	7171(4)	5459(3)	2593(3)	28.7(9)
O6	5091(4)	2344(3)	677(3)	27.8(9)
O5	3600(4)	1227(3)	1068(3)	30.6(10)
O2	-2365(4)	6759(3)	-40(3)	28.7(10)
N7	4299(4)	2078(3)	1190(3)	20.4(10)
O8	3611(4)	10870(3)	6345(3)	25.2(9)
O1	-1797(4)	5369(3)	-532(3)	34.2(11)
O3	11357(4)	8857(3)	2609(3)	31(1)
N8	3313(5)	10422(4)	5556(3)	23.7(10)
N1	2786(4)	6984(3)	1416(3)	14.9(9)
O7	3067(6)	10867(4)	4917(3)	57.8(17)
N3	4132(4)	5565(3)	2335(3)	16.5(9)
C16	3863(5)	4247(4)	3334(4)	20.2(11)
N6	10339(4)	8231(4)	2527(3)	20.5(10)
C5	-203(5)	6815(4)	-151(3)	16.3(11)
C27	3476(5)	8957(4)	4500(3)	16(1)
N5	-1551(4)	6267(3)	-244(3)	18.4(9)
C25	3070(5)	8736(4)	6073(3)	19.5(11)
C26	3274(5)	9327(4)	5379(3)	16.7(11)
C11	9235(5)	9154(4)	1466(4)	19.4(11)
C6	620(5)	6636(4)	579(3)	14.3(10)
C20	4271(5)	3812(4)	1799(4)	16(1)
C18	3919(5)	2496(4)	2792(4)	18.2(11)
C4	149(5)	7436(4)	-787(3)	18.4(11)
C13	8019(5)	7910(4)	2274(3)	15.7(10)
C15	4093(5)	4561(4)	2476(3)	13.9(10)
C22	3500(4)	7939(4)	4244(3)	11.2(9)
C9	6898(5)	8707(4)	1211(3)	16(1)
C19	4161(5)	2820(4)	1968(3)	15.6(10)
N2	5663(4)	7504(3)	2056(3)	14.1(9)
C12	9166(5)	8462(4)	2075(3)	16.0(11)
C8	6837(5)	8032(4)	1857(3)	15.1(10)
C2	2273(5)	7791(4)	78(3)	17.5(11)

C23	3287(5)	7332(4)	4937(4)	20.5(11)
C14	10454(5)	9779(4)	1235(4)	24.2(12)
C7	-765(6)	7559(5)	-1580(4)	26.9(13)
C17	3811(5)	3270(4)	3484(4)	21.4(12)
C10	8053(5)	9244(4)	1027(3)	17.1(11)
C3	1425(5)	7925(4)	-648(3)	17.9(11)
C24	3079(6)	7716(4)	5802(4)	23.5(12)
C29	7523(6)	5319(5)	1684(4)	25.3(12)
C30	8423(6)	4583(5)	1682(4)	28.5(13)
N4	3720(4)	7526(3)	3377(3)	14.7(9)
C28	2789(6)	9102(4)	7023(4)	26.4(13)
C21	3797(6)	1428(4)	2986(4)	26.1(13)
C1	1913(5)	7136(4)	704(3)	14.8(10)
C32	7426(7)	4621(5)	3040(4)	36.1(16)
C31	7890(6)	3903(5)	2338(4)	31.0(14)
O10	9593(14)	7978(12)	4918(9)	210(6)
C35	9921(13)	7246(11)	6204(8)	119(5)
C36	9500(14)	8126(12)	5881(10)	134(5)
C33	9260(20)	6763(14)	4722(12)	199(9)
C34	9388(17)	6212(11)	5542(11)	155(6)

Table 3 Anisotropic Displacement Parameters ($\text{\AA}^2 \times 10^3$) for tetrakis(u_3 -(4-methyl-3-nitrophenyl imido lead (II))). The Anisotropic displacement factor exponent takes the form: $-2\pi^2[h^2a^{*2}U_{11}+2hka^*b^*U_{12}+\dots]$.

Atom	U_{11}	U_{22}	U_{33}	U_{23}	U_{13}	U_{12}
Pb1	13.42(9)	10.91(9)	14.89(9)	-0.91(7)	2.17(7)	2.66(7)
Pb2	13.63(9)	13.04(9)	15.10(9)	-0.14(7)	2.08(7)	1.37(7)
Pb3	15.69(9)	12.51(9)	12.24(9)	-1.75(7)	1.81(7)	3.08(7)
Pb4	14.22(9)	14.12(9)	12.00(9)	-1.28(7)	1.22(7)	3.92(7)
O4	23(2)	32(2)	35(2)	9.3(19)	3.2(17)	9.9(18)
O9	34(2)	30(2)	27(2)	2.1(18)	14.6(18)	16.3(19)
O6	29(2)	24(2)	29(2)	-2.1(18)	12.9(18)	2.4(17)
O5	39(2)	14(2)	33(2)	-2.9(17)	5.0(19)	-2.9(17)
O2	23(2)	34(2)	28(2)	-3.9(19)	6.7(17)	8.3(18)
N7	22(2)	17(2)	22(2)	-1.7(19)	3.9(19)	7.3(19)
O8	26(2)	22(2)	22(2)	-10.9(17)	1.7(16)	1.6(16)
O1	23(2)	16(2)	58(3)	-5(2)	4(2)	-1.0(16)
O3	14.1(19)	34(2)	41(3)	7(2)	-3.1(17)	-2.5(17)
N8	37(3)	17(2)	18(2)	-2.5(19)	10(2)	6(2)
N1	12(2)	15(2)	16(2)	-3.0(17)	1.0(16)	2.3(16)

O7	133(5)	26(3)	23(2)	4(2)	15(3)	37(3)
N3	18(2)	14(2)	17(2)	-1.8(17)	2.8(17)	5.2(17)
C16	21(3)	21(3)	18(3)	1(2)	-1(2)	5(2)
N6	15(2)	26(3)	20(2)	1(2)	3.2(17)	7.4(19)
C5	14(2)	13(2)	18(2)	-6(2)	-1.4(19)	2.1(19)
C27	17(2)	14(2)	16(2)	-0.4(19)	3.9(19)	0.0(19)
N5	19(2)	22(2)	13(2)	0.1(18)	-0.4(17)	4.5(18)
C25	26(3)	16(3)	14(2)	-7(2)	3(2)	1(2)
C26	15(2)	14(3)	19(3)	-6(2)	4.8(19)	2.6(19)
C11	14(2)	22(3)	20(3)	-4(2)	5(2)	2(2)
C6	13(2)	12(2)	17(2)	-1.0(19)	1.4(18)	2.4(19)
C20	13(2)	14(2)	20(3)	0(2)	-0.5(19)	2.6(19)
C18	18(3)	13(2)	23(3)	2(2)	0(2)	4(2)
C4	20(3)	19(3)	16(2)	-1(2)	1(2)	6(2)
C13	19(3)	13(2)	15(2)	-1.0(19)	2.1(19)	5(2)
C15	13(2)	16(2)	13(2)	3.8(19)	0.4(18)	1.1(19)
C22	10(2)	13(2)	9(2)	-3.1(18)	1.0(17)	1.5(18)
C9	18(3)	17(3)	11(2)	-3.5(19)	-2.0(19)	4(2)
C19	12(2)	14(2)	19(3)	-3(2)	2.4(19)	2.0(19)
N2	12(2)	14(2)	15(2)	-3.3(16)	2.5(16)	3.2(16)
C12	12(2)	19(3)	18(2)	-2(2)	2.5(19)	7(2)
C8	17(2)	12(2)	14(2)	-7.5(19)	0.6(19)	4.5(19)
C2	21(3)	15(3)	17(2)	0(2)	5(2)	6(2)
C23	27(3)	14(3)	20(3)	-1(2)	4(2)	6(2)
C14	19(3)	25(3)	27(3)	2(2)	3(2)	2(2)
C7	28(3)	27(3)	24(3)	8(2)	-6(2)	4(2)
C17	27(3)	22(3)	15(3)	4(2)	1(2)	6(2)
C10	18(3)	20(3)	14(2)	2(2)	3.2(19)	5(2)
C3	21(3)	20(3)	14(2)	5(2)	7(2)	4(2)
C24	36(3)	18(3)	19(3)	5(2)	10(2)	5(2)
C29	31(3)	24(3)	23(3)	2(2)	7(2)	10(2)
C30	30(3)	30(3)	29(3)	3(3)	9(2)	11(3)
N4	16(2)	15(2)	13(2)	-3.1(17)	4.9(16)	4.1(17)
C28	41(3)	22(3)	14(3)	-3(2)	9(2)	1(3)
C21	34(3)	18(3)	27(3)	5(2)	2(2)	6(2)
C1	14(2)	14(2)	14(2)	-4.5(19)	1.4(18)	3.7(19)
C32	41(4)	50(4)	26(3)	11(3)	13(3)	23(3)
C31	38(4)	25(3)	36(4)	10(3)	9(3)	15(3)
O10	191(9)	258(10)	175(9)	6(8)	28(7)	51(8)
C35	113(8)	138(9)	106(8)	-2(7)	48(6)	23(7)
C36	105(8)	183(10)	121(9)	40(8)	19(7)	35(7)
C33	200(12)	205(12)	191(12)	43(9)	11(9)	35(9)

C34 169(10) 162(10) 141(10) 28(8) 32(8) 43(8)

Table 4 Bond Lengths for tetrakis(u₃-(4-methyl-3-nitrophenyl imido lead (II))).

Atom	Atom	Length/Å	Atom	Atom	Length/Å
Pb1	Pb2	3.5452(4)	C5	C6	1.399(7)
Pb1	Pb3	3.5303(4)	C5	C4	1.377(8)
Pb1	Pb4	3.5349(4)	C27	C26	1.384(7)
Pb1	N1	2.332(4)	C27	C22	1.388(7)
Pb1	N2	2.350(4)	C25	C26	1.394(8)
Pb1	N4	2.279(5)	C25	C24	1.390(7)
Pb2	Pb3	3.5299(4)	C25	C28	1.507(7)
Pb2	Pb4	3.5460(5)	C11	C12	1.380(8)
Pb2	N1	2.295(5)	C11	C14	1.512(8)
Pb2	N3	2.339(4)	C11	C10	1.392(7)
Pb2	N4	2.310(4)	C6	C1	1.403(7)
Pb3	Pb4	3.5565(4)	C20	C15	1.383(7)
Pb3	N1	2.351(4)	C20	C19	1.385(7)
Pb3	N3	2.293(5)	C18	C19	1.381(8)
Pb3	N2	2.335(4)	C18	C17	1.397(7)
Pb4	N3	2.333(4)	C18	C21	1.498(8)
Pb4	N2	2.280(5)	C4	C7	1.497(7)
Pb4	N4	2.383(4)	C4	C3	1.382(7)
O4	N6	1.233(6)	C13	C12	1.391(7)
O9	C29	1.432(7)	C13	C8	1.394(7)
O9	C32	1.440(8)	C22	C23	1.406(7)
O6	N7	1.226(6)	C22	N4	1.393(6)
O5	N7	1.234(6)	C9	C8	1.405(8)
O2	N5	1.223(6)	C9	C10	1.382(7)
N7	C19	1.465(6)	N2	C8	1.402(7)
O8	N8	1.228(5)	C2	C3	1.387(7)
O1	N5	1.208(6)	C2	C1	1.398(8)
O3	N6	1.234(6)	C23	C24	1.373(7)
N8	O7	1.218(7)	C29	C30	1.503(8)
N8	C26	1.466(7)	C30	C31	1.507(9)
N1	C1	1.397(6)	C32	C31	1.511(8)
N3	C15	1.397(7)	O10	C36	1.431(13)
C16	C15	1.421(7)	O10	C33	1.600(15)
C16	C17	1.363(8)	C35	C36	1.468(14)
N6	C12	1.463(6)	C35	C34	1.578(13)
C5	N5	1.476(6)	C33	C34	1.514(15)

Table 5 Bond Angles for tetrakis(u₃-(4-methyl-3-nitrophenyl imido lead (II))).

Atom	Atom	Atom	Angle/°	Atom	Atom	Atom	Angle/°
Pb3	Pb1	Pb2	59.852(9)	C15	N3	Pb3	125.3(3)
Pb3	Pb1	Pb4	60.449(9)	C15	N3	Pb4	115.7(3)
Pb4	Pb1	Pb2	60.111(9)	C17	C16	C15	122.4(5)
N1	Pb1	Pb2	39.61(11)	O4	N6	O3	122.6(5)
N1	Pb1	Pb3	41.28(10)	O4	N6	C12	118.1(4)
N1	Pb1	Pb4	83.69(11)	O3	N6	C12	119.3(5)
N1	Pb1	N2	81.08(14)	C6	C5	N5	116.1(5)
N2	Pb1	Pb2	82.53(11)	C4	C5	N5	118.4(4)
N2	Pb1	Pb3	40.94(9)	C4	C5	C6	125.5(5)
N2	Pb1	Pb4	39.50(11)	C26	C27	C22	121.4(5)
N4	Pb1	Pb2	39.73(10)	O2	N5	C5	117.7(4)
N4	Pb1	Pb3	83.82(10)	O1	N5	O2	123.5(5)
N4	Pb1	Pb4	41.79(10)	O1	N5	C5	118.8(4)
N4	Pb1	N1	78.89(15)	C26	C25	C28	125.9(5)
N4	Pb1	N2	80.34(15)	C24	C25	C26	113.4(4)
Pb1	Pb2	Pb4	59.800(7)	C24	C25	C28	120.6(5)
Pb3	Pb2	Pb1	59.865(7)	C27	C26	N8	115.2(5)
Pb3	Pb2	Pb4	60.347(9)	C27	C26	C25	124.5(5)
N1	Pb2	Pb1	40.37(10)	C25	C26	N8	120.4(4)
N1	Pb2	Pb3	41.16(10)	C12	C11	C14	125.9(5)
N1	Pb2	Pb4	83.92(10)	C12	C11	C10	114.9(5)
N1	Pb2	N3	80.17(15)	C10	C11	C14	119.2(5)
N1	Pb2	N4	79.01(15)	C5	C6	C1	118.7(5)
N3	Pb2	Pb1	82.41(11)	C15	C20	C19	120.0(5)
N3	Pb2	Pb3	39.87(11)	C19	C18	C17	114.3(5)
N3	Pb2	Pb4	40.56(10)	C19	C18	C21	125.8(5)
N4	Pb2	Pb1	39.10(11)	C17	C18	C21	119.9(5)
N4	Pb2	Pb3	83.41(10)	C5	C4	C7	122.9(5)
N4	Pb2	Pb4	41.69(10)	C5	C4	C3	114.8(5)
N4	Pb2	N3	81.06(14)	C3	C4	C7	122.3(5)
Pb1	Pb3	Pb4	59.839(6)	C12	C13	C8	120.8(5)
Pb2	Pb3	Pb1	60.283(6)	N3	C15	C16	121.4(4)
Pb2	Pb3	Pb4	60.051(9)	C20	C15	N3	122.7(5)
N1	Pb3	Pb1	40.86(10)	C20	C15	C16	115.8(5)
N1	Pb3	Pb2	39.98(11)	C27	C22	C23	114.8(4)
N1	Pb3	Pb4	82.93(10)	C27	C22	N4	124.0(5)
N3	Pb3	Pb1	83.36(10)	N4	C22	C23	121.2(4)
N3	Pb3	Pb2	40.84(10)	C10	C9	C8	122.2(5)

N3	Pb3	Pb4	40.16(10)	C20	C19	N7	115.5(5)
N3	Pb3	N1	79.96(15)	C18	C19	N7	119.4(5)
N3	Pb3	N2	78.59(15)	C18	C19	C20	125.1(4)
N2	Pb3	Pb1	41.26(10)	Pb3	N2	Pb1	97.80(15)
N2	Pb3	Pb2	83.07(10)	Pb4	N2	Pb1	99.54(15)
N2	Pb3	Pb4	39.03(11)	Pb4	N2	Pb3	100.82(17)
N2	Pb3	N1	80.97(14)	C8	N2	Pb1	115.1(3)
Pb1	Pb4	Pb2	60.089(7)	C8	N2	Pb3	119.7(3)
Pb1	Pb4	Pb3	59.712(7)	C8	N2	Pb4	119.8(3)
Pb2	Pb4	Pb3	59.602(6)	C11	C12	N6	120.5(5)
N3	Pb4	Pb1	82.72(11)	C11	C12	C13	124.0(5)
N3	Pb4	Pb2	40.68(10)	C13	C12	N6	115.4(5)
N3	Pb4	Pb3	39.34(11)	C13	C8	C9	115.6(5)
N3	Pb4	N4	79.67(14)	C13	C8	N2	122.3(5)
N2	Pb4	Pb1	40.96(10)	N2	C8	C9	122.0(4)
N2	Pb4	Pb2	83.43(10)	C3	C2	C1	122.7(5)
N2	Pb4	Pb3	40.16(10)	C24	C23	C22	122.7(5)
N2	Pb4	N3	78.90(15)	C16	C17	C18	122.3(5)
N2	Pb4	N4	79.62(15)	C9	C10	C11	122.5(5)
N4	Pb4	Pb1	39.60(11)	C4	C3	C2	122.0(5)
N4	Pb4	Pb2	40.14(10)	C23	C24	C25	123.2(5)
N4	Pb4	Pb3	81.85(10)	O9	C29	C30	106.4(5)
C29	O9	C32	108.5(4)	C29	C30	C31	101.8(5)
O6	N7	O5	123.1(4)	Pb1	N4	Pb2	101.18(16)
O6	N7	C19	117.9(4)	Pb1	N4	Pb4	98.60(15)
O5	N7	C19	118.9(5)	Pb2	N4	Pb4	98.16(15)
O8	N8	C26	119.0(5)	C22	N4	Pb1	122.5(3)
O7	N8	O8	121.7(5)	C22	N4	Pb2	117.7(3)
O7	N8	C26	119.3(4)	C22	N4	Pb4	114.5(3)
Pb1	N1	Pb3	97.85(15)	N1	C1	C6	121.5(5)
Pb2	N1	Pb1	100.02(15)	N1	C1	C2	122.2(5)
Pb2	N1	Pb3	98.86(17)	C2	C1	C6	116.3(5)
C1	N1	Pb1	114.2(3)	O9	C32	C31	106.8(5)
C1	N1	Pb2	124.9(3)	C30	C31	C32	103.2(5)
C1	N1	Pb3	116.5(3)	C36	O10	C33	99.3(12)
Pb3	N3	Pb2	99.30(17)	C36	C35	C34	114.1(12)
Pb3	N3	Pb4	100.50(17)	O10	C36	C35	104.0(12)
Pb4	N3	Pb2	98.76(15)	C34	C33	O10	117.0(13)
C15	N3	Pb2	113.1(3)	C33	C34	C35	91.4(11)

Table 6 Torsion Angles for tetrakis(u₃-(4-methyl-3-nitrophenyl imido lead (II))).

A	B	C	D	Angle/°	A	B	C	D	Angle/°
Pb1	N1	C1	C6	-133.5(4)	C4	C5	C6	C1	1.4(7)
Pb1	N1	C1	C2	46.6(5)	C15	C16	C17	C18	-3.0(8)
Pb1	N2	C8	C13	137.3(4)	C15	C20	C19	N7	176.8(4)
Pb1	N2	C8	C9	-43.8(5)	C15	C20	C19	C18	-2.2(8)
Pb2	N1	C1	C6	-10.4(6)	C22	C27	C26	N8	178.2(4)
Pb2	N1	C1	C2	169.7(3)	C22	C27	C26	C25	-0.5(8)
Pb2	N3	C15	C16	-57.6(5)	C22	C23	C24	C25	-0.6(9)
Pb2	N3	C15	C20	122.3(4)	C19	C20	C15	N3	-177.0(4)
Pb3	N1	C1	C6	113.5(4)	C19	C20	C15	C16	3.0(7)
Pb3	N1	C1	C2	-66.5(5)	C19	C18	C17	C16	3.7(8)
Pb3	N3	C15	C16	-178.8(3)	C12	C11	C10	C9	2.1(7)
Pb3	N3	C15	C20	1.2(7)	C12	C13	C8	C9	2.4(6)
Pb3	N2	C8	C13	-106.6(4)	C12	C13	C8	N2	-178.6(4)
Pb3	N2	C8	C9	72.3(5)	C8	C13	C12	N6	-177.4(4)
Pb4	N3	C15	C16	55.3(5)	C8	C13	C12	C11	-0.2(7)
Pb4	N3	C15	C20	-124.8(4)	C8	C9	C10	C11	0.1(7)
Pb4	N2	C8	C13	18.6(6)	C23	C22	N4	Pb1	179.8(4)
Pb4	N2	C8	C9	-162.5(3)	C23	C22	N4	Pb2	53.3(6)
O4	N6	C12	C11	-155.0(5)	C23	C22	N4	Pb4	-61.2(5)
O4	N6	C12	C13	22.3(6)	C14	C11	C12	N6	-3.6(8)
O9	C29	C30	C31	34.1(6)	C14	C11	C12	C13	179.4(5)
O9	C32	C31	C30	24.5(7)	C14	C11	C10	C9	-179.2(5)
O6	N7	C19	C20	37.3(7)	C7	C4	C3	C2	-178.7(5)
O6	N7	C19	C18	-143.5(5)	C17	C16	C15	N3	179.5(5)
O5	N7	C19	C20	-141.1(5)	C17	C16	C15	C20	-0.5(7)
O5	N7	C19	C18	38.0(7)	C17	C18	C19	N7	179.8(4)
O8	N8	C26	C27	-153.8(5)	C17	C18	C19	C20	-1.2(7)
O8	N8	C26	C25	25.0(7)	C10	C11	C12	N6	175.0(4)
O3	N6	C12	C11	23.4(7)	C10	C11	C12	C13	-2.1(7)
O3	N6	C12	C13	-159.3(5)	C10	C9	C8	C13	-2.4(7)
O7	N8	C26	C27	25.3(8)	C10	C9	C8	N2	178.6(4)
O7	N8	C26	C25	-155.9(6)	C3	C2	C1	N1	178.0(4)
C5	C6	C1	N1	-179.5(4)	C3	C2	C1	C6	-2.0(7)
C5	C6	C1	C2	0.5(7)	C24	C25	C26	N8	-179.1(5)
C5	C4	C3	C2	0.1(7)	C24	C25	C26	C27	-0.4(8)
C27	C22	C23	C24	-0.3(7)	C29	O9	C32	C31	-3.3(7)
C27	C22	N4	Pb1	-0.5(6)	C29	C30	C31	C32	-34.9(6)
C27	C22	N4	Pb2	-127.0(4)	N4	C22	C23	C24	179.4(5)
C27	C22	N4	Pb4	118.5(4)	C28	C25	C26	N8	4.2(8)
N5	C5	C6	C1	-179.9(4)	C28	C25	C26	C27	-177.1(5)

N5 C5 C4 C7	-1.6(7)	C28 C25 C24 C23	177.8(5)
N5 C5 C4 C3	179.7(4)	C21 C18 C19 N7	1.0(8)
C26 C27 C22 C23	0.9(7)	C21 C18 C19 C20	180.0(5)
C26 C27 C22 N4	-178.9(5)	C21 C18 C17 C16	-177.4(5)
C26 C25 C24 C23	1.0(8)	C1 C2 C3 C4	1.8(8)
C6 C5 N5 O2	107.4(5)	C32 O9 C29 C30	-19.5(6)
C6 C5 N5 O1	-74.0(6)	O10 C33 C34 C35	-4(2)
C6 C5 C4 C7	177.1(5)	C36 O10 C33 C34	-18(2)
C6 C5 C4 C3	-1.7(7)	C36 C35 C34 C33	26.4(18)
C4 C5 N5 O2	-73.8(6)	C33 O10 C36 C35	32.1(16)
C4 C5 N5 O1	104.8(6)	C34 C35 C36 O10	-41.5(17)

Table 7 Hydrogen Atom Coordinates ($\text{\AA} \times 10^4$) and Isotropic Displacement Parameters ($\text{\AA}^2 \times 10^3$) for tetrakis(u_3 -(4-methyl-3-nitrophenyl imido lead (II))).

Atom	x	y	z	U(eq)
H16	3742	4737	3821	24
H27	3601	9410	4064	19
H6	309	6184	983	17
H20	4469	3978	1219	19
H13	8042	7444	2700	19
H9	6120	8797	890	19
H2	3134	8160	153	21
H23	3288	6628	4801	25
H14A	10899	10238	1784	36
H14B	10238	10177	755	36
H14C	11016	9326	1014	36
H7A	-1251	6891	-1874	40
H7B	-281	7887	-2026	40
H7C	-1362	7980	-1360	40
H17	3696	3109	4079	26
H10	8040	9692	585	21
H3	1730	8366	-1062	21
H24	2933	7262	6235	28
H29A	7954	5973	1526	30
H29B	6750	5042	1233	30
H30A	9320	4934	1904	34
H30B	8391	4198	1062	34
H28A	3580	9498	7387	40
H28B	2462	8517	7318	40
H28C	2141	9529	6981	40

H21A	2905	1067	2811	39
H21B	4044	1434	3642	39
H21C	4364	1083	2631	39
H32A	6634	4274	3253	43
H32B	8093	4864	3576	43
H31A	8566	3589	2628	37
H31B	7172	3360	2023	37
H35A	9640	7180	6814	143
H35B	10873	7370	6280	143
H36A	8604	8143	5997	160
H36B	10067	8767	6189	160
H33A	8370	6548	4413	239
H33B	9836	6535	4285	239
H34A	10016	5757	5502	186
H34B	8553	5846	5680	186

Experimental

Single crystals of $C_{36}H_{40}N_8O_{10}Pb_4$ [tetrakis(u₃-(4-methyl-3-nitrophenyl imido lead(II)))] were [1]. A suitable crystal was selected and [1] on a 'Bruker APEX-II CCD' diffractometer. The crystal was kept at 99.89 K during data collection. Using Olex2 [1], the structure was solved with the ShelXS [2] structure solution program using Direct Methods and refined with the olex2.refine [3] refinement package using Least Squares minimisation.

1. Dolomanov, O.V., Bourhis, L.J., Gildea, R.J, Howard, J.A.K. & Puschmann, H. (2009), *J. Appl. Cryst.* 42, 339-341.
2. Sheldrick, G.M. (2008). *Acta Cryst. A*64, 112-122.
- 3.

Crystal structure determination of [tetrakis(u₃-(4-methyl-3-nitrophenyl imido lead(II)))]

Crystal Data for $C_{36}H_{40}N_8O_{10}Pb_4$ ($M=1573.52$ g/mol): triclinic, space group P-1 (no. 2), $a = 10.6519(13)$ Å, $b = 13.5498(16)$ Å, $c = 14.8146(17)$ Å, $\alpha = 97.453(2)^\circ$, $\beta = 95.652(2)^\circ$, $\gamma = 100.455(2)^\circ$, $V = 2068.6(4)$ Å³, $Z = 2$, $T = 99.89$ K, $\mu(\text{MoK}\alpha) = 16.294$ mm⁻¹, $D_{\text{calc}} = 2.526$ g/cm³, 24435 reflections measured ($3.092^\circ \leq 2\theta \leq 56.022^\circ$), 9852 unique ($R_{\text{int}} = 0.0308$, $R_{\text{sigma}} = 0.0395$) which were used in all calculations. The final R_1 was 0.0246 ($I > 2\sigma(I)$) and wR_2 was 0.0655 (all data).

Refinement model description

Number of restraints - 40, number of constraints - unknown.

Details:

1. Fixed Uiso
At 1.2 times of:
All C(H) groups, All C(H,H) groups
At 1.5 times of:
All C(H,H,H) groups
2. Restrained distances
C33-O10 = O10-C36
1.43 with sigma of 0.02
C34-C33 = C35-C34 = C36-C35
1.5 with sigma of 0.02
C33-C36
2.33 with sigma of 0.04
C36-C34
2.33 with sigma of 0.04
C33-C35

2.33 with sigma of 0.04
O10-C35
2.36 with sigma of 0.04
O10-C34
2.36 with sigma of 0.04
3. Uiso/Uaniso restraints and constraints
Uanis(O10) \approx Ueq, Uanis(C33) \approx Ueq, Uanis(C34) \approx Ueq, Uanis(C35)
 \approx Ueq, Uanis(C36) \approx Ueq: with sigma of 0.01 and sigma for terminal
atoms of 0.015
4.a Secondary CH2 refined with riding coordinates:
C29(H29A,H29B), C30(H30A,H30B), C32(H32A,H32B), C31(H31A,H31B), C35(H35A,
H35B), C36(H36A,H36B), C33(H33A,H33B), C34(H34A,H34B)
4.b Aromatic/amide H refined with riding coordinates:
C16(H16), C27(H27), C6(H6), C20(H20), C13(H13), C9(H9), C2(H2), C23(H23),
C17(H17), C10(H10), C3(H3), C24(H24)
4.c Idealised Me refined as rotating group:
C14(H14A,H14B,H14C), C7(H7A,H7B,H7C), C28(H28A,H28B,H28C), C21(H21A,H21B,H21C)

This report has been created with Olex2, compiled on 2016.11

APPENDIX B

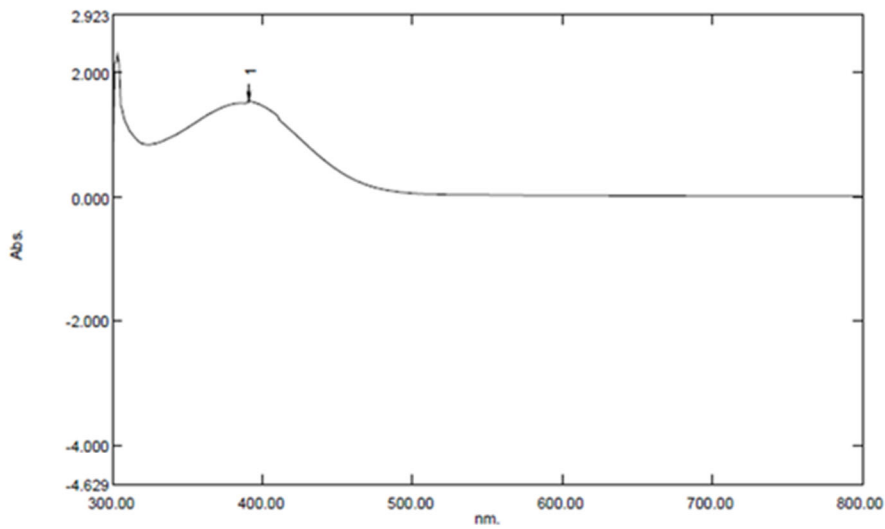
UV-vis Spectra of

Tetrakis(u₃-(4-methyl-3-nitrophenyl imido lead (II)))

Spectrum Peak Pick Report

01/19/2017 01:48:39 PM

Data Set: Pb Tetrakis - RawData



[Measurement Properties]
Wavelength Range (nm.): 200.00 to 800.00
Scan Speed: Medium
Sampling Interval: 1.0
Auto Sampling Interval: Disabled
Scan Mode: Single

No.	P/V	Wavelength	Abs.	Description
1	●	391.00	1.544	

[Instrument Properties]
Instrument Type: UV-1800 Series
Measuring Mode: Absorbance
Slit Width: 1.0 nm
Light Source Change Wavelength: 340.0 nm
S/R Exchange: Normal

APPENDIX C

CRYSTAL DATA FOR Bis(dinitrophenyl imido lead(II))

Table 1 Crystal data and structure refinement for Bis(dinitrophenyl imido lead(II)).

Identification code	Bis(dinitrophenyl imido lead(II))
Empirical formula	C ₆ N ₇ O ₇ Pb ₆ H
Formula weight	705.76
Temperature/K	100.02
Crystal system	monoclinic
Space group	P2 ₁ /n
a/Å	11.7362(14)
b/Å	10.8203(13)
c/Å	20.500(2)
α/°	90
β/°	104.766(2)
γ/°	90
Volume/Å ³	2517.3(5)
Z	4
ρ _{calc} /cm ³	1.8620
μ/mm ⁻¹	6.751
F(000)	1364.1
Crystal size/mm ³	0.095 × 0.065 × 0.060
Radiation	Mo Kα (λ = 0.71073)
2θ range for data collection/°	3.66 to 55.8
Index ranges	-15 ≤ h ≤ 14, -11 ≤ k ≤ 14, -27 ≤ l ≤ 20
Reflections collected	19380
Independent reflections	6006 [R _{int} = 0.0362, R _{sigma} = 0.0376]
Data/restraints/parameters	6006/0/342
Goodness-of-fit on F ²	1.004
Final R indexes [I ≥ 2σ (I)]	R ₁ = 0.0265, wR ₂ = 0.0699
Final R indexes [all data]	R ₁ = 0.0296, wR ₂ = 0.0716
Largest diff. peak/hole / e Å ⁻³	3.66/-1.27

Table 2 Fractional Atomic Coordinates ($\times 10^4$) and Equivalent Isotropic Displacement Parameters ($\text{\AA}^2 \times 10^3$) for mo_3585_0m. U_{eq} is defined as 1/3 of of the trace of the orthogonalised U_{ij} tensor.

Atom	<i>x</i>	<i>y</i>	<i>z</i>	$U(eq)$
Pb1	5078.61 (10)	7882.25 (11)	5111.12 (6)	12.82 (5)
C6	3735 (3)	7296 (3)	6376.2 (18)	13.1 (6)
C50	4259 (3)	11871 (3)	6586 (2)	19.4 (7)
C1	3525 (3)	7684 (3)	7008.3 (18)	16.5 (7)
C21	10029 (3)	7874 (4)	6494 (2)	21.9 (8)
O6	4456 (3)	7667 (3)	9024.7 (16)	29.1 (6)
C19	7878 (3)	8129 (3)	6088.0 (16)	12.9 (6)
C5	3488 (3)	6007 (3)	6232.3 (17)	14.6 (6)
C2	3104 (3)	6927 (4)	7421.6 (19)	20.9 (7)
C4	3019 (3)	5244 (4)	6665.9 (19)	20.2 (7)
C3	2820 (3)	5685 (4)	7244.3 (19)	22.6 (8)
N1	3655 (2)	5407 (3)	5657.1 (15)	16.3 (6)
O5	3410 (2)	4295 (2)	5551.3 (14)	25.3 (6)
N2	4143 (2)	8114 (3)	5994.5 (14)	12.1 (5)
C7	4184 (3)	9382 (3)	6207.5 (16)	13.4 (6)
C9	5218 (3)	9896 (3)	6611.5 (17)	16.7 (7)
C8	3201 (3)	10141 (3)	5986.5 (17)	15.8 (7)
C13	4540 (4)	7930 (4)	9717 (2)	25.7 (8)
C12	5801 (3)	8348 (4)	10004 (2)	25.5 (8)
C11	6122 (3)	8968 (4)	9403 (2)	28.1 (9)
C10	5163 (4)	8557 (5)	8801 (2)	35.8 (10)
N3	6804 (2)	7653 (3)	6026.5 (14)	13.0 (5)
C23	8120 (3)	9347 (3)	5875.7 (16)	14.9 (6)
C20	8917 (3)	7426 (4)	6410.9 (18)	16.7 (7)
C22	10230 (3)	9071 (4)	6276.7 (19)	22.9 (8)
C15	6519 (3)	5441 (3)	6184.0 (18)	18.2 (7)
C16	6337 (3)	4471 (3)	6591 (2)	22.9 (8)
C18	6487 (3)	5869 (4)	7513.3 (18)	21.3 (7)
C17	6305 (3)	4686 (4)	7250 (2)	24.4 (8)
C14	6700 (3)	6634 (3)	6448.3 (16)	13.0 (6)
C25	3237 (3)	11374 (4)	6172.5 (18)	19.1 (7)
C24	5249 (3)	11127 (3)	6800.6 (18)	18.4 (7)
O7	4042 (2)	5997 (2)	5231.7 (13)	18.7 (5)
N6	7233 (3)	10217 (3)	5624.3 (14)	15.0 (5)
O11	6173 (2)	9883 (2)	5381.3 (12)	16.6 (5)
O12	7473 (2)	11338 (2)	5630.7 (15)	25.2 (6)
C26	6694 (3)	6831 (3)	7116.4 (18)	17.2 (7)
C27	9294 (3)	9797 (3)	5980.1 (18)	18.7 (7)

Table 3 Anisotropic Displacement Parameters ($\text{\AA}^2 \times 10^3$) for mo_3585_0m. The Anisotropic displacement factor exponent takes the form: $-2\pi^2[h^2a^*U_{11}+2hka^*b^*U_{12}+\dots]$.

Atom	U ₁₁	U ₂₂	U ₃₃	U ₁₂	U ₁₃	U ₂₃
Pb1	14.03 (7)	13.13 (8)	11.15 (8)	-2.86 (4)	2.95 (5)	0.27 (4)
C6	9.8 (13)	13.7 (16)	15.5 (16)	-0.0 (11)	2.5 (12)	1.6 (12)
C50	25.2 (18)	11.7 (16)	24.0 (19)	-0.4 (13)	11.1 (15)	-2.9 (14)
C1	17.2 (15)	17.9 (17)	14.7 (16)	0.1 (13)	4.6 (13)	-0.2 (13)
C21	13.6 (16)	33 (2)	18.6 (18)	4.6 (13)	2.2 (14)	0.1 (14)
O6	25.1 (14)	35.0 (17)	26.7 (15)	-9.9 (12)	5.8 (12)	-9.2 (13)
C19	14.0 (14)	14.9 (15)	10.0 (14)	-1.5 (12)	3.1 (12)	-0.9 (12)
C5	13.9 (14)	14.7 (16)	14.1 (16)	-1.5 (12)	1.9 (12)	1.7 (12)
C2	15.8 (16)	33 (2)	15.5 (17)	1.2 (14)	7.3 (14)	2.7 (15)
C4	19.2 (16)	17.2 (16)	24.8 (18)	-2.6 (13)	6.4 (14)	5.1 (14)
C3	19.2 (16)	26 (2)	23.7 (18)	-2.4 (14)	8.3 (14)	9.9 (15)
N1	17.4 (13)	13.6 (14)	17.1 (14)	-4.7 (11)	2.5 (11)	-0.0 (11)
O5	36.8 (15)	10.6 (12)	29.0 (15)	-8.6 (11)	9.3 (12)	-2 (1)
N2	13.0 (12)	12.1 (13)	12.0 (13)	-1.7 (10)	4.7 (10)	-0.3 (10)
C7	16.0 (14)	12.3 (15)	13.9 (15)	-0.9 (12)	7.4 (12)	0.3 (12)
C9	16.5 (15)	15.7 (17)	16.8 (15)	3.8 (12)	2.4 (13)	-0.4 (13)
C8	13.1 (14)	20.9 (17)	14.0 (15)	-0.3 (12)	4.3 (12)	1.0 (13)
C13	23.8 (19)	29 (2)	24 (2)	-4.8 (15)	6.2 (17)	-4.2 (15)
C12	20.6 (17)	26 (2)	27 (2)	-1.4 (15)	1.5 (15)	-4.1 (16)
C11	23.5 (18)	24 (2)	38 (2)	-4.6 (15)	9.5 (17)	-4.1 (17)
C10	32 (2)	49 (3)	26 (2)	-11 (2)	6.6 (17)	4 (2)
N3	14.6 (13)	12.5 (13)	11.9 (13)	-1.2 (10)	3.4 (11)	1.6 (11)
C23	15.7 (14)	17.4 (17)	11.5 (15)	-2.8 (13)	3.7 (12)	-0.4 (12)
C20	16.6 (15)	17.4 (17)	16.5 (16)	1.5 (13)	4.9 (13)	0.1 (13)
C22	13.5 (15)	32 (2)	23.8 (19)	-7.5 (14)	6.5 (14)	-3.9 (15)
C15	18.9 (15)	17.4 (17)	18.3 (16)	-1.0 (13)	4.5 (13)	-0.5 (13)
C16	24.4 (17)	10.7 (17)	31 (2)	-2.7 (13)	2.9 (15)	0.5 (14)
C18	22.0 (17)	26.6 (19)	14.9 (16)	3.2 (14)	3.8 (14)	8.1 (14)
C17	22.8 (17)	19.4 (18)	29 (2)	-2.1 (14)	3.4 (15)	12.1 (15)
C14	9.9 (13)	13.6 (16)	14.7 (15)	0.5 (11)	1.5 (12)	2.6 (12)
C25	16.5 (15)	22.1 (18)	21.3 (17)	6.6 (14)	9.5 (13)	3.7 (14)
C24	17.6 (15)	16.0 (17)	21.6 (17)	-3.6 (13)	5.1 (13)	-2.9 (13)
O7	23.8 (12)	17.3 (12)	17.4 (12)	-6.7 (10)	9.7 (10)	-4.1 (10)
N6	18.2 (14)	14.5 (13)	11.9 (12)	-5.9 (11)	3.3 (11)	0.8 (10)
O11	14.4 (11)	14.2 (12)	19.0 (12)	-3.2 (9)	0.2 (9)	4.3 (9)
O12	24.6 (13)	12.8 (12)	35.4 (15)	-6.1 (10)	2.6 (11)	2.6 (11)
C26	18.5 (15)	16.9 (16)	14.9 (16)	2.7 (13)	1.6 (13)	1.1 (13)

C27 19.1 (16) 20.7 (17) 17.8 (16) -7.4 (13) 7.2 (13) -1.6 (13)

Table 4 Bond Lengths for mo_3585_0m.

Atom	Atom	Length/Å	Atom	Atom	Length/Å
Pb1	N2	2.358 (3)	N1	O7	1.255 (4)
Pb1	N3	2.397 (3)	N2	C7	1.436 (4)
Pb1	O7	2.420 (2)	C7	C9	1.399 (5)
Pb1	O11	2.507 (2)	C7	C8	1.394 (5)
C6	C1	1.442 (5)	C9	C24	1.385 (5)
C6	C5	1.440 (5)	C8	C25	1.385 (5)
C6	N2	1.348 (4)	C13	C12	1.516 (5)
C50	C25	1.388 (5)	C12	C11	1.531 (6)
C50	C24	1.390 (5)	C11	C10	1.510 (6)
C1	C2	1.358 (5)	N3	C14	1.426 (4)
C21	C20	1.361 (5)	C23	N6	1.401 (4)
C21	C22	1.410 (6)	C23	C27	1.425 (5)
O6	C13	1.426 (5)	C22	C27	1.361 (5)
O6	C10	1.422 (5)	C15	C16	1.392 (5)
C19	N3	1.338 (4)	C15	C14	1.394 (5)
C19	C23	1.439 (5)	C16	C17	1.380 (6)
C19	C20	1.447 (5)	C18	C17	1.385 (6)
C5	C4	1.423 (5)	C18	C26	1.380 (5)
C5	N1	1.403 (4)	C14	C26	1.388 (5)
C2	C3	1.410 (6)	N6	O11	1.269 (4)
C4	C3	1.352 (6)	N6	O12	1.244 (4)
N1	O5	1.244 (4)			

Table 5 Bond Angles for mo_3585_0m.

Atom	Atom	Atom	Angle/°	Atom	Atom	Atom	Angle/°
N3	Pb1	N2	82.86 (10)	C24	C9	C7	120.3 (3)
O7	Pb1	N2	70.54 (9)	C25	C8	C7	120.9 (3)
O7	Pb1	N3	100.32 (9)	C12	C13	O6	105.0 (3)
O11	Pb1	N2	92.92 (9)	C11	C12	C13	103.6 (3)
O11	Pb1	N3	68.49 (9)	C10	C11	C12	104.1 (3)
O11	Pb1	O7	161.51 (8)	C11	C10	O6	108.1 (3)
C5	C6	C1	113.2 (3)	C19	N3	Pb1	128.4 (2)
N2	C6	C1	119.9 (3)	C14	N3	Pb1	111.65 (19)
N2	C6	C5	126.9 (3)	C14	N3	C19	117.7 (3)

C24	C50	C25	119.4 (3)	N6	C23	C19	122.7 (3)
C2	C1	C6	123.9 (3)	C27	C23	C19	121.7 (3)
C22	C21	C20	121.3 (3)	C27	C23	N6	115.2 (3)
C10	O6	C13	106.7 (3)	C19	C20	C21	122.7 (3)
C23	C19	N3	125.3 (3)	C27	C22	C21	119.4 (3)
C20	C19	N3	120.3 (3)	C14	C15	C16	119.7 (3)
C20	C19	C23	114.3 (3)	C17	C16	C15	120.5 (4)
C4	C5	C6	121.6 (3)	C26	C18	C17	120.0 (3)
N1	C5	C6	123.8 (3)	C18	C17	C16	119.8 (3)
N1	C5	C4	114.6 (3)	C15	C14	N3	120.5 (3)
C3	C2	C1	120.9 (4)	C26	C14	N3	120.1 (3)
C3	C4	C5	121.6 (4)	C26	C14	C15	119.2 (3)
C4	C3	C2	118.7 (3)	C8	C25	C50	120.2 (3)
O5	N1	C5	121.2 (3)	C9	C24	C50	120.6 (3)
O7	N1	C5	120.1 (3)	N1	O7	Pb1	141.2 (2)
O7	N1	O5	118.6 (3)	O11	N6	C23	121.1 (3)
C6	N2	Pb1	132.8 (2)	O12	N6	C23	120.4 (3)
C7	N2	Pb1	110.5 (2)	O12	N6	O11	118.6 (3)
C7	N2	C6	116.1 (3)	N6	O11	Pb1	136.8 (2)
C9	C7	N2	121.1 (3)	C14	C26	C18	120.8 (3)
C8	C7	N2	120.2 (3)	C22	C27	C23	120.6 (3)
C8	C7	C9	118.6 (3)				

Table 6 Hydrogen Atom Coordinates ($\text{\AA} \times 10^4$) and Isotropic Displacement Parameters ($\text{\AA}^2 \times 10^3$) for mo_3585_0m.

Atom	x	y	z	U(eq)
H50	4281 (3)	12712 (3)	6721 (2)	23.3 (8)
H1	3691 (3)	8518 (3)	7143.9 (18)	19.8 (8)
H21	10683 (3)	7369 (4)	6702 (2)	26.3 (10)
H2	3000 (3)	7239 (4)	7835.7 (19)	25.0 (9)
H4	2840 (3)	4404 (4)	6546.2 (19)	24.3 (8)
H3	2496 (3)	5168 (4)	7525.7 (19)	27.1 (9)
H9	5903 (3)	9399 (3)	6756.7 (17)	20.0 (8)
H8	2497 (3)	9809 (3)	5704.7 (17)	19.0 (8)
H13a	3980 (4)	8591 (4)	9760 (2)	30.9 (10)
H13b	4367 (4)	7183 (4)	9954 (2)	30.9 (10)
H12a	5858 (3)	8940 (4)	10379 (2)	30.6 (10)
H12b	6324 (3)	7635 (4)	10169 (2)	30.6 (10)
H11a	6128 (3)	9879 (4)	9449 (2)	33.7 (10)
H11b	6905 (3)	8690 (4)	9363 (2)	33.7 (10)

H10a	5516 (4)	8189 (5)	8455 (2)	42.9 (12)
H10b	4676 (4)	9273 (5)	8598 (2)	42.9 (12)
H20	8820 (3)	6620 (4)	6571.6 (18)	20.1 (8)
H22	11012 (3)	9369 (4)	6336.7 (19)	27.5 (9)
H15	6521 (3)	5292 (3)	5727.5 (18)	21.9 (8)
H16	6233 (3)	3655 (3)	6415 (2)	27.4 (9)
H18	6469 (3)	6020 (4)	7967.1 (18)	25.6 (9)
H17	6159 (3)	4024 (4)	7522 (2)	29.3 (10)
H25	2562 (3)	11881 (4)	6016.8 (18)	23.0 (8)
H24	5952 (3)	11465 (3)	7079.6 (18)	22.1 (8)
H26	6836 (3)	7637 (3)	7302.7 (18)	20.7 (8)
H27	9425 (3)	10611 (3)	5841.4 (18)	22.5 (8)

Experimental

Single crystals of $C_6N_7O_7Pb_6H$ [**Bis(dinitrophenyl imido lead(II))**] were [1]. A suitable crystal was selected and [1] on a 'Bruker APEX-II CCD' diffractometer. The crystal was kept at 100.02 K during data collection. Using Olex2 [1], the structure was solved with the ShelXS [2] structure solution program using Direct Methods and refined with the olex2.refine [3] refinement package using Gauss-Newton minimisation.

1. Dolomanov, O.V., Bourhis, L.J., Gildea, R.J., Howard, J.A.K. & Puschmann, H. (2009), *J. Appl. Cryst.* 42, 339-341.
2. Sheldrick, G.M. (2008). *Acta Cryst.* A64, 112-122.
3. Bourhis, L.J., Dolomanov, O.V., Gildea, R.J., Howard, J.A.K., Puschmann, H. (2015). *Acta Cryst.* A71, 59-75.

Crystal structure determination of [**Bis(dinitrophenyl imido lead(II))**]

Crystal Data for $C_6N_7O_7Pb_6H$ ($M = 705.76$ g/mol): monoclinic, space group $P2_1/n$ (no. 14), $a = 11.7362(14)$ Å, $b = 10.8203(13)$ Å, $c = 20.500(2)$ Å, $\beta = 104.766(2)^\circ$, $V = 2517.3(5)$ Å³, $Z = 4$, $T = 100.02$ K, $\mu(\text{Mo K}\alpha) = 6.751$ mm⁻¹, $D_{\text{calc}} = 1.8620$ g/cm³, 19380 reflections measured ($3.66^\circ \leq 2\theta \leq 55.8^\circ$), 6006 unique ($R_{\text{int}} = 0.0362$, $R_{\text{sigma}} = 0.0376$) which were used in all calculations. The final R_1 was 0.0265 ($I \geq 2\sigma(I)$) and wR_2 was 0.0716 (all data).

Refinement model description

Number of restraints - 0, number of constraints - 48.

Details:

1. Fixed Uiso

At 1.2 times of:

All C(H) groups, All C(H,H) groups

2.a Secondary CH2 refined with riding coordinates:

C13(H13a,H13b), C12(H12a,H12b), C11(H11a,H11b), C10(H10a,H10b)

2.b Aromatic/amide H refined with riding coordinates:

C50(H50), C1(H1), C21(H21), C2(H2), C4(H4), C3(H3), C9(H9), C8(H8), C20(H20), C22(H22), C15(H15), C16(H16), C18(H18), C17(H17), C25(H25), C24(H24), C26(H26), C27(H27)

This report has been created with Olex2, compiled on 2017.01.04 svn.r3372 for OlexSys. Please [let us know](#) if there are any errors or if you would like to have additional features.

APPENDIX D

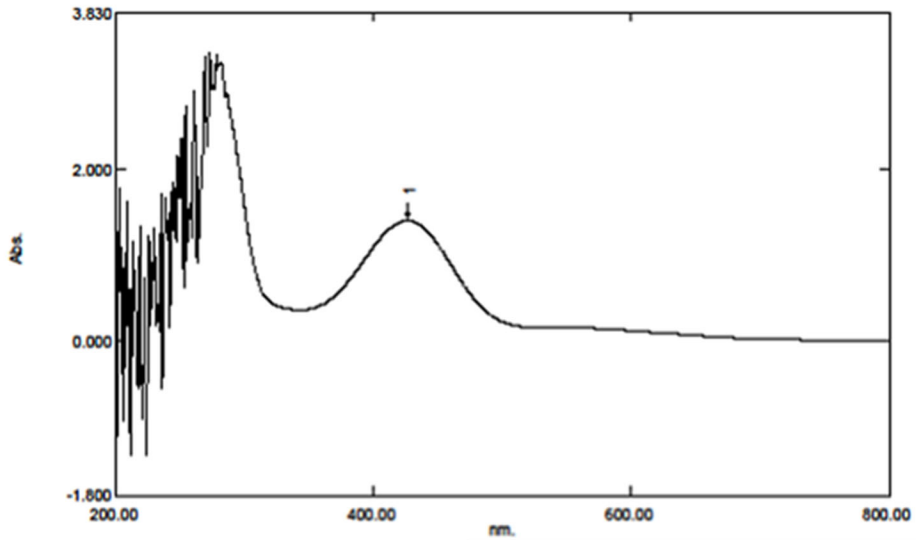
UV-vis Spectra of

Bis(dinitrophenyl imido lead(II))

Spectrum Peak Pick Report

01/25/2017 03:30:10 PM

Data Set: Pb bis - RawData



[Measurement Properties]
Wavelength Range (nm.): 200.00 to 800.00
Scan Speed: Medium
Sampling Interval: 1.0
Auto Sampling Interval: Disabled
Scan Mode: Single

No.	P/V	Wavelength	Abs.	Description
1	☑	427.00	1.396	

[Instrument Properties]
Instrument Type: UV-1800 Series
Measuring Mode: Absorbance
Slit Width: 1.0 nm
Light Source Change Wavelength: 340.0 nm
S/R Exchange: Normal

APPENDIX E

CRYSTAL DATA FOR

HEXA-1-PHENYLUREA COBALT(II) NITRATE

Table 1 Crystal data and structure refinement for Hexa-1-phenylurea cobalt(II) nitrate.

Identification code	Hexa-1-phenylurea cobalt(II) nitrate
Empirical formula	C ₄₂ H ₄₈ CoN ₁₄ O ₁₂
Formula weight	999.87
Temperature/K	99.84
Crystal system	monoclinic
Space group	P2 ₁ /n
a/Å	10.549(3)
b/Å	14.371(4)
c/Å	16.525(4)
α/°	90
β/°	92.036(6)
γ/°	90
Volume/Å ³	2503.6(11)
Z	2
ρ _{calc} /cm ³	1.326
μ/mm ⁻¹	0.414
F(000)	1042.0
Crystal size/mm ³	0.102 × 0.065 × 0.052
Radiation	MoKα (λ = 0.71073)
2θ range for data collection/°	3.756 to 55.856
Index ranges	-13 ≤ h ≤ 13, -15 ≤ k ≤ 18, -21 ≤ l ≤ 21
Reflections collected	38965
Independent reflections	5973 [R _{int} = 0.0326, R _{sigma} = 0.0208]
Data/restraints/parameters	5973/0/314
Goodness-of-fit on F ²	1.054
Final R indexes [I >= 2σ (I)]	R ₁ = 0.0292, wR ₂ = 0.0794
Final R indexes [all data]	R ₁ = 0.0335, wR ₂ = 0.0822
Largest diff. peak/hole / e Å ⁻³	0.40/-0.33

Table 2 Fractional Atomic Coordinates ($\times 10^4$) and Equivalent Isotropic Displacement Parameters ($\text{\AA}^2 \times 10^3$) for Hexa-1-phenylurea cobalt(II) nitrate. U_{eq} is defined as 1/3 of the trace of the orthogonalised U_{ij} tensor.

Atom	<i>x</i>	<i>y</i>	<i>z</i>	U_{eq}
Co1	10000	5000	5000	16.71 (7)
O3	8164.3 (8)	5309.8 (6)	4550.4 (5)	21.67 (17)
O4	9659.9 (8)	3561.7 (5)	4983.0 (5)	20.28 (17)
O6	9466.2 (8)	5131.8 (6)	6201.1 (5)	21.78 (17)
N7	6174.7 (10)	5176.7 (7)	3969.9 (7)	25.8 (2)
N8	7582.7 (11)	3977.3 (8)	3889.9 (7)	29.7 (2)
N9	8318.2 (10)	5515.5 (7)	7296.8 (6)	24.6 (2)
N10	7928.1 (10)	6244.0 (7)	6076.5 (6)	25.6 (2)
N11	9700.1 (11)	2041.2 (7)	5400.6 (6)	24.8 (2)
N12	10115.4 (11)	3216.7 (7)	6303.2 (6)	26.6 (2)
C12	10072.1 (12)	4587.6 (10)	7906.8 (7)	28.3 (3)
C22	6495.6 (14)	6878.2 (9)	3985.7 (8)	32.2 (3)
C23	5952.3 (16)	7762.0 (10)	3968.0 (10)	41.5 (4)
C24	4658.9 (17)	7881.1 (11)	3978.0 (10)	45.2 (4)
C25	3889.3 (16)	7107.0 (12)	4017.4 (11)	47.3 (4)
C26	4411.6 (14)	6217.7 (11)	4045.8 (9)	36.5 (3)
C27	5720.8 (12)	6101.9 (9)	4022.7 (7)	25.2 (2)
C28	7353.1 (12)	4841.3 (8)	4154.2 (7)	22.0 (2)
C29	7912.3 (13)	4333.5 (10)	8288.0 (8)	31.3 (3)
C30	8325.5 (16)	3640.5 (11)	8821.4 (9)	39.7 (3)
C31	9598.6 (15)	3401.4 (11)	8885.0 (9)	38.1 (3)
C32	10462.8 (14)	3873.8 (11)	8427.3 (8)	34.3 (3)
C34	8786.8 (12)	4803.3 (9)	7825.4 (7)	23.4 (2)
C35	8600.2 (11)	5604.1 (8)	6506.7 (7)	21.0 (2)
C36	9751.5 (12)	1952.2 (9)	3907.3 (8)	26.4 (3)
C37	9468.6 (13)	1453.4 (10)	3200.0 (8)	31.2 (3)
C38	8883.2 (14)	593.3 (10)	3231.5 (9)	34.5 (3)
C39	8569.2 (15)	230.0 (10)	3972.7 (10)	37.2 (3)
C40	8815.4 (13)	727.3 (9)	4682.6 (8)	30.7 (3)
C41	9410.8 (11)	1592.8 (8)	4652.2 (7)	22.4 (2)
C42	9819.9 (11)	2971.7 (8)	5540.4 (7)	20.0 (2)
O7	4535.0 (9)	3844.5 (7)	3255.5 (6)	33.9 (2)
O8	3954.8 (9)	3620.2 (7)	1997.8 (6)	32.5 (2)
O9	5895.1 (8)	3333.6 (6)	2407.2 (6)	28.6 (2)
N13	4800.8 (10)	3598.3 (7)	2550.4 (6)	24.3 (2)

Table 3 Anisotropic Displacement Parameters ($\text{\AA}^2 \times 10^3$) for Hexa-1-phenylurea cobalt(II) nitrate. The Anisotropic displacement factor exponent takes the form: - $2\pi^2[h^2a^{*2}U_{11}+2hka^*b^*U_{12}+\dots]$.

Atom	U_{11}	U_{22}	U_{33}	U_{23}	U_{13}	U_{12}
Co1	22.24 (12)	15.25 (11)	12.63 (10)	0.30 (7)	0.44 (8)	-1.81 (8)
O3	25.2 (4)	21.0 (4)	18.5 (4)	-1.3 (3)	-2.7 (3)	-1.8 (3)
O4	27.3 (4)	16.4 (4)	17.0 (4)	1.8 (3)	-1.1 (3)	-2.0 (3)
O6	28.1 (4)	21.2 (4)	16.2 (4)	-0.3 (3)	3.9 (3)	-0.1 (3)
N7	25.7 (5)	23.3 (5)	28.1 (5)	-2.2 (4)	-5.9 (4)	-2.4 (4)
N8	30.6 (6)	23.7 (5)	34.0 (6)	-7.7 (4)	-11.0 (4)	0.9 (4)
N9	29.4 (5)	27.6 (5)	17.0 (5)	-2.4 (4)	4.4 (4)	2.9 (4)
N10	30.0 (5)	25.6 (5)	21.5 (5)	1.0 (4)	5.7 (4)	3.0 (4)
N11	38.7 (6)	16.9 (5)	18.6 (5)	3.2 (4)	-1.7 (4)	-3.0 (4)
N12	44.6 (6)	18.7 (5)	16.4 (5)	3.3 (4)	-1.4 (4)	-5.8 (4)
C12	28.6 (6)	37.0 (7)	19.4 (6)	-3.3 (5)	0.9 (5)	-3.0 (5)
C22	34.5 (7)	27.9 (6)	33.5 (7)	1.2 (5)	-9.7 (5)	-0.9 (5)
C23	54.3 (9)	27.2 (7)	41.9 (8)	0.5 (6)	-13.2 (7)	0.2 (6)
C24	57.3 (10)	34.5 (8)	43.3 (9)	-2.8 (6)	-6.6 (7)	17.2 (7)
C25	40.8 (9)	49.3 (10)	52.1 (10)	1.8 (8)	4.6 (7)	16.3 (7)
C26	32.3 (7)	38.0 (8)	39.3 (8)	2.3 (6)	3.8 (6)	2.8 (6)
C27	31.2 (6)	26.9 (6)	17.3 (5)	-0.1 (4)	-3.0 (4)	2.2 (5)
C28	26.8 (6)	22.4 (5)	16.7 (5)	0.9 (4)	-0.9 (4)	-2.3 (4)
C29	31.0 (7)	33.8 (7)	29.3 (6)	1.9 (5)	4.2 (5)	-2.1 (5)
C30	46.0 (8)	37.6 (8)	35.9 (8)	9.7 (6)	7.8 (6)	-4.5 (6)
C31	50.0 (9)	35.0 (7)	28.9 (7)	4.7 (6)	-3.7 (6)	3.9 (6)
C32	33.9 (7)	43.1 (8)	25.5 (6)	-2.9 (6)	-5.6 (5)	4.3 (6)
C34	29.9 (6)	26.3 (6)	14.1 (5)	-3.9 (4)	0.9 (4)	-1.5 (5)
C35	25.5 (6)	19.6 (5)	18.0 (5)	-2.1 (4)	1.6 (4)	-5.4 (4)
C36	31.0 (6)	23.3 (6)	24.9 (6)	-3.5 (5)	2.5 (5)	-0.7 (5)
C37	36.5 (7)	32.7 (7)	24.6 (6)	-6.3 (5)	1.2 (5)	5.3 (5)
C38	38.1 (7)	31.1 (7)	33.4 (7)	-12.6 (6)	-9.2 (6)	5.4 (6)
C39	42.6 (8)	23.1 (6)	45.0 (8)	-5.1 (6)	-11.0 (6)	-5.3 (6)
C40	39.1 (7)	21.4 (6)	31.1 (7)	2.6 (5)	-5.7 (5)	-4.5 (5)
C41	25.8 (6)	17.9 (5)	23.4 (6)	-1.7 (4)	-3.4 (4)	1.6 (4)
C42	23.5 (5)	18.8 (5)	17.7 (5)	1.8 (4)	1.6 (4)	-2.8 (4)
O7	35.5 (5)	41.0 (5)	25.6 (5)	-14.1 (4)	6.5 (4)	-11.1 (4)
O8	30.1 (5)	38.2 (5)	28.7 (5)	-13.7 (4)	-4.2 (4)	6.7 (4)
O9	25.5 (4)	29.0 (5)	31.1 (5)	-7.2 (4)	0.0 (4)	0.5 (4)
N13	27.9 (5)	19.9 (5)	25.2 (5)	-7.6 (4)	1.6 (4)	-3.8 (4)

Table 4 Bond Lengths for Hexa-1-phenylurea cobalt(II) nitrate.

Atom	Atom	Length/Å	Atom	Atom	Length/Å
Co1	O3	2.0972 (9)	C22	C23	1.393 (2)
Co1	O3 ¹	2.0972 (9)	C22	C27	1.3855 (19)
Co1	O4	2.0979 (9)	C23	C24	1.376 (2)
Co1	O4 ¹	2.0978 (9)	C24	C25	1.380 (3)
Co1	O6 ¹	2.0909 (9)	C25	C26	1.392 (2)
Co1	O6	2.0909 (9)	C26	C27	1.393 (2)
O3	C28	1.2548 (15)	C29	C30	1.390 (2)
O4	C42	1.2588 (14)	C29	C34	1.3932 (18)
O6	C35	1.2583 (14)	C30	C31	1.387 (2)
N7	C27	1.4169 (16)	C31	C32	1.383 (2)
N7	C28	1.3578 (17)	C36	C37	1.3944 (18)
N8	C28	1.3410 (16)	C36	C41	1.3937 (18)
N9	C34	1.4229 (16)	C37	C38	1.383 (2)
N9	C35	1.3554 (15)	C38	C39	1.383 (2)
N10	C35	1.3483 (16)	C39	C40	1.390 (2)
N11	C41	1.4182 (15)	C40	C41	1.3951 (17)
N11	C42	1.3621 (15)	O7	N13	1.2588 (13)
N12	C42	1.3350 (15)	O8	N13	1.2543 (14)
C12	C32	1.392 (2)	O9	N13	1.2461 (14)
C12	C34	1.3926 (19)			

¹2-X,1-Y,1-Z

Table 5 Bond Angles for Hexa-1-phenylurea cobalt(II) nitrate.

Atom	Atom	Atom	Angle/°	Atom	Atom	Atom	Angle/°
O3	Co1	O3 ¹	179.999 (18)	C26	C27	N7	116.83 (12)
O3 ¹	Co1	O4	87.18 (3)	O3	C28	N7	121.91 (11)
O3	Co1	O4 ¹	87.19 (3)	O3	C28	N8	122.62 (11)
O3 ¹	Co1	O4 ¹	92.82 (3)	N8	C28	N7	115.47 (11)
O3	Co1	O4	92.82 (3)	C30	C29	C34	119.76 (13)
O4 ¹	Co1	O4	180.0	C31	C30	C29	120.44 (14)
O6 ¹	Co1	O3	87.67 (3)	C32	C31	C30	119.49 (13)
O6 ¹	Co1	O3 ¹	92.33 (4)	C31	C32	C12	120.88 (13)
O6	Co1	O3 ¹	87.67 (3)	C12	C34	N9	122.36 (11)
O6	Co1	O3	92.33 (3)	C12	C34	C29	120.03 (12)
O6	Co1	O4	92.88 (3)	C29	C34	N9	117.58 (12)
O6 ¹	Co1	O4 ¹	92.88 (3)	O6	C35	N9	121.56 (11)
O6 ¹	Co1	O4	87.12 (3)	O6	C35	N10	122.14 (10)

Table 5 Bond Angles for Hexa-1-phenylurea cobalt(II) nitrate.

Atom	Atom	Atom	Angle/°	Atom	Atom	Atom	Angle/°
O6	Co1	O4 ¹	87.12 (3)	N10	C35	N9	116.28 (11)
O6	Co1	O6 ¹	180.0	C41	C36	C37	119.71 (12)
C28	O3	Co1	132.45 (8)	C38	C37	C36	120.68 (13)
C42	O4	Co1	129.45 (7)	C39	C38	C37	119.47 (13)
C35	O6	Co1	130.83 (8)	C38	C39	C40	120.67 (13)
C28	N7	C27	128.90 (11)	C39	C40	C41	119.91 (13)
C35	N9	C34	125.14 (10)	C36	C41	N11	123.20 (11)
C42	N11	C41	127.57 (10)	C36	C41	C40	119.52 (11)
C32	C12	C34	119.32 (12)	C40	C41	N11	117.18 (11)
C27	C22	C23	119.48 (14)	O4	C42	N11	121.86 (10)
C24	C23	C22	121.36 (15)	O4	C42	N12	122.28 (11)
C23	C24	C25	119.05 (14)	N12	C42	N11	115.86 (10)
C24	C25	C26	120.59 (15)	O8	N13	O7	119.38 (11)
C25	C26	C27	120.03 (15)	O9	N13	O7	119.99 (10)
C22	C27	N7	123.48 (12)	O9	N13	O8	120.63 (10)
C22	C27	C26	119.47 (13)				

¹2-X,1-Y,1-Z

Table 6 Torsion Angles for Hexa-1-phenylurea cobalt(II) nitrate.

A	B	C	D	Angle/°	A	B	C	D	Angle/°
Co1	O3	C28	N7	175.74 (8)	C30	C31	C32	C12	0.3 (2)
Co1	O3	C28	N8	-3.73 (18)	C32	C12	C34	N9	-179.15 (11)
Co1	O4	C42	N11	-171.65 (8)	C32	C12	C34	C29	2.72 (19)
Co1	O4	C42	N12	8.40 (17)	C34	N9	C35	O6	-10.89 (18)
Co1	O6	C35	N9	172.66 (8)	C34	N9	C35	N10	171.03 (11)
Co1	O6	C35	N10	-9.37 (17)	C34	C12	C32	C31	-2.4 (2)
C22	C23	C24	C25	0.9 (2)	C34	C29	C30	C31	-1.2 (2)
C23	C22	C27	N7	174.13 (13)	C35	N9	C34	C12	50.39 (17)
C23	C22	C27	C26	-0.3 (2)	C35	N9	C34	C29	-131.44 (13)
C23	C24	C25	C26	-0.1 (3)	C36	C37	C38	C39	0.4 (2)
C24	C25	C26	C27	-0.9 (2)	C37	C36	C41	N11	177.88 (12)
C25	C26	C27	N7	-173.70 (13)	C37	C36	C41	C40	1.43 (19)
C25	C26	C27	C22	1.1 (2)	C37	C38	C39	C40	1.2 (2)
C27	N7	C28	O3	13.7 (2)	C38	C39	C40	C41	-1.4 (2)
C27	N7	C28	N8	-166.82 (12)	C39	C40	C41	N11	-176.52 (12)
C27	C22	C23	C24	-0.7 (2)	C39	C40	C41	C36	0.1 (2)
C28	N7	C27	C22	25.2 (2)	C41	N11	C42	O4	0.9 (2)

Table 6 Torsion Angles for Hexa-1-phenylurea cobalt(II) nitrate.

A	B	C	D	Angle/°	A	B	C	D	Angle/°
C28	N7	C27	C26	-160.25 (13)	C41	N11	C42	N12	-179.15 (11)
C29	C30	C31	C32	1.6 (2)	C41	C36	C37	C38	-1.7 (2)
C30	C29	C34	N9	-179.14 (12)	C42	N11	C41	C36	30.20 (19)
C30	C29	C34	C12	-0.9 (2)	C42	N11	C41	C40	-153.28 (13)

Table 7 Hydrogen Atom Coordinates ($\text{\AA} \times 10^4$) and Isotropic Displacement Parameters ($\text{\AA}^2 \times 10^3$) for Hexa-1-phenylurea cobalt(II) nitrate.

Atom	x	y	z	U(eq)
H7	5616.01	4762.57	3793.31	31
H8A	8326.44	3717.54	3992.75	36
H8B	6989.58	3670.22	3613.6	36
H9	7804.88	5931.29	7498.76	29
H10A	7892.62	6083.89	5560.5	31
H10B	7150.59	6274.96	6255.29	31
H11	9815.69	1675.7	5824.04	30
H12A	10204.93	3808.28	6430.47	32
H12B	10220.8	2786.71	6678.66	32
H12	10675.94	4924.31	7610.1	34
H22	7390.12	6808.41	3972.54	39
H23	6486.04	8293.44	3948.69	50
H24	4300.58	8487.5	3958.09	54
H25	2995.05	7181.73	4025.27	57
H26	3875	5689.44	4080.85	44
H29	7036.8	4486.23	8238.82	38
H30	7731.66	3328.58	9144.73	48
H31	9875.21	2916.79	9240.25	46
H32	11334.75	3708.76	8468.78	41
H36	10174.57	2534.44	3881.58	32
H37	9680.04	1706.73	2691.22	37
H38	8698.36	255.09	2747.67	41
H39	8181.39	-365.44	3997.16	45
H40	8578.46	478.04	5187.81	37

Experimental

Single crystals of $\text{C}_{42}\text{H}_{48}\text{CoN}_{14}\text{O}_{12}$ [**Hexa-1-phenylurea cobalt(II) nitrate**] were [1]. A suitable crystal was selected and [2] on a '**Bruker APEX-II CCD**' diffractometer. The crystal was kept at 99.84 K during data collection. Using Olex2 [1], the structure was solved with the Unknown [2] structure solution program using Unknown and refined with the Unknown [3] refinement package using Unknown minimisation.

1. Dolomanov, O.V., Bourhis, L.J., Gildea, R.J, Howard, J.A.K. & Puschmann, H. (2009), *J. Appl. Cryst.* 42, 339-341.
- 2.
- 3.

Crystal structure determination of [Hexa-1-phenylurea cobalt(II) nitrate]

Crystal Data for $C_{42}H_{48}CoN_{14}O_{12}$ ($M=999.87$ g/mol): monoclinic, space group $P2_1/n$ (no. 14), $a = 10.549(3)$ Å, $b = 14.371(4)$ Å, $c = 16.525(4)$ Å, $\beta = 92.036(6)^\circ$, $V = 2503.6(11)$ Å³, $Z = 2$, $T = 99.84$ K, $\mu(\text{MoK}\alpha) = 0.414$ mm⁻¹, $D_{\text{calc}} = 1.326$ g/cm³, 38965 reflections measured ($3.756^\circ \leq 2\Theta \leq 55.856^\circ$), 5973 unique ($R_{\text{int}} = 0.0326$, $R_{\text{sigma}} = 0.0208$) which were used in all calculations. The final R_1 was 0.0292 ($I > 2\sigma(I)$) and wR_2 was 0.0822 (all data).

Refinement model description

Number of restraints - 0, number of constraints - unknown.

Details:

1.a Rotating group:

N10 (H10A, H10B)

1.b Aromatic/amide H refined with riding coordinates:

N7 (H7), N9 (H9), N11 (H11), C12 (H12), C22 (H22), C23 (H23), C24 (H24), C25 (H25),
C26 (H26), C29 (H29), C30 (H30), C31 (H31), C32 (H32), C36 (H36), C37 (H37), C38 (H38),
C39 (H39), C40 (H40)

1.c X=CH2 refined with riding coordinates:

N8 (H8A, H8B), N12 (H12A, H12B)

This report has been created with Olex2, compiled on 2022.04.07 svn.rca3783a0 for OlexSys. Please [let us know](#) if there are any errors or if you would like to have additional features.

APPENDIX F

CRYSTAL DATA FOR

Bis(dicyanamide)tetrapyrindine cobalt

Table 1 Crystal data and structure refinement for Bis(dicyanamide)tetrapyrindine cobalt (II).

Identification code	Bis(dicyanamide)tetrapyrindine cobalt (II)
Empirical formula	C _{2.53} H _{2.11} Co _{0.11} N _{1.05}
Formula weight	53.41
Temperature/K	100.01
Crystal system	monoclinic
Space group	Cc
a/Å	13.063(2)
b/Å	12.880(2)
c/Å	15.033(2)
α/°	90
β/°	110.014(3)
γ/°	90
Volume/Å ³	2376.8(6)
Z	38
ρ _{calc} /cm ³	1.418
μ/mm ⁻¹	0.756
F(000)	1044.0
Crystal size/mm ³	0.04 × 0.04 × 0.03
Radiation	MoKα (λ = 0.71073)
2θ range for data collection/°	4.584 to 56.144
Index ranges	-17 ≤ h ≤ 17, -17 ≤ k ≤ 16, -19 ≤ l ≤ 14
Reflections collected	18556
Independent reflections	4781 [R _{int} = 0.0154, R _{sigma} = 0.0140]
Data/restraints/parameters	4781/2/317
Goodness-of-fit on F ²	1.072
Final R indexes [I >= 2σ (I)]	R ₁ = 0.0179, wR ₂ = 0.0481
Final R indexes [all data]	R ₁ = 0.0183, wR ₂ = 0.0483
Largest diff. peak/hole / e Å ⁻³	0.21/-0.25
Flack parameter	0.449(10)

Table 2 Fractional Atomic Coordinates ($\times 10^4$) and Equivalent Isotropic Displacement Parameters ($\text{\AA}^2 \times 10^3$) for Bis(dicyanamide)tetrapyridine cobalt (II). U_{eq} is defined as 1/3 of the trace of the orthogonalised U_{ij} tensor.

Atom	<i>x</i>	<i>y</i>	<i>z</i>	U_{eq}
Co1	4332.7 (3)	7436.6 (2)	4919.0 (3)	13.09 (6)
N1	5577.4 (13)	6583.2 (11)	4682.3 (13)	17.9 (3)
N2	7172.3 (13)	5873.6 (12)	4390.7 (13)	20.8 (3)
N3	8852.6 (14)	6820.6 (14)	4496.4 (16)	30.5 (4)
N4	3075.2 (13)	8261.6 (11)	5179.1 (12)	17.9 (3)
N5	1450.5 (14)	8687.4 (15)	5573.7 (14)	28.5 (4)
N6	1146.5 (19)	7990.2 (17)	6996.3 (17)	44.0 (6)
N7	5541.7 (13)	8660.9 (11)	5568.5 (13)	17.1 (3)
N8	3889.4 (13)	8205.7 (11)	3536.0 (12)	15.2 (3)
N9	3195.6 (13)	6163.0 (11)	4279.4 (12)	17.0 (3)
N10	4765.9 (13)	6781.1 (11)	6347.8 (12)	16.8 (3)
C1	5292.7 (16)	9674.2 (14)	5454.5 (16)	20.6 (4)
C2	6043.6 (18)	10466.0 (15)	5790.7 (17)	27.1 (5)
C3	7116.6 (18)	10205.4 (16)	6275.1 (18)	28.4 (5)
C4	7392.5 (17)	9165.6 (16)	6413.3 (18)	29.1 (5)
C5	6589.4 (16)	8421.5 (14)	6055.5 (16)	21.2 (4)
C6	4589.0 (17)	7345.8 (16)	7034.8 (16)	20.1 (4)
C7	4808.3 (16)	6988.0 (16)	7944.5 (15)	23.3 (4)
C8	5230.1 (17)	6000.7 (17)	8175.0 (16)	25.0 (4)
C9	5411.5 (17)	5403.2 (16)	7479.9 (16)	25.2 (4)
C10	5178.9 (17)	5823.6 (15)	6585.3 (15)	22.4 (4)
C11	3539.3 (17)	5175.6 (14)	4319.5 (17)	22.2 (4)
C12	2849.3 (19)	4339.9 (15)	3957.7 (18)	28.2 (5)
C13	1754 (2)	4528.6 (16)	3526 (2)	34.0 (5)
C14	1386 (2)	5543.1 (18)	3473 (2)	34.4 (5)
C15	2126.0 (17)	6331.9 (15)	3854.1 (17)	24.9 (4)
C16	4257.8 (15)	7864.7 (15)	2857.1 (14)	17.3 (4)
C17	4065.2 (16)	8378.1 (15)	2003.7 (15)	21.4 (4)
C18	3473.1 (16)	9294.7 (15)	1840.0 (15)	22.4 (4)
C19	3084.2 (17)	9652.3 (15)	2531.7 (16)	23.2 (4)
C20	3294.3 (16)	9086.0 (14)	3353.6 (15)	19.2 (4)
C21	2319.2 (15)	8433.6 (13)	5389.2 (14)	16.7 (4)
C22	1316.1 (17)	8285.0 (16)	6338.6 (18)	28.9 (5)
C23	6353.7 (15)	6296.2 (12)	4550.8 (14)	15.2 (3)
C24	8041.2 (15)	6428.5 (14)	4449.8 (14)	18.9 (4)

Table 3 Anisotropic Displacement Parameters ($\text{\AA}^2 \times 10^3$) for Bis(dicyanamide)tetrapyridine cobalt (II). The Anisotropic displacement factor exponent takes the form: - $2\pi^2[h^2a^{*2}U_{11}+2hka^*b^*U_{12}+\dots]$.

Atom	U_{11}	U_{22}	U_{33}	U_{23}	U_{13}	U_{12}
Co1	13.78 (9)	12.05 (9)	14.43 (11)	0.01 (9)	6.10 (8)	1.67 (9)
N1	17.8 (8)	15.5 (6)	21.6 (9)	-0.3 (6)	8.5 (7)	2.9 (5)
N2	19.7 (7)	17.4 (7)	29.2 (10)	-4.5 (6)	13.3 (7)	1.5 (6)
N3	23.5 (8)	27.5 (8)	43.5 (12)	12.3 (8)	15.3 (8)	3.9 (7)
N4	19.5 (8)	16.8 (7)	17.9 (9)	1.6 (6)	7.1 (7)	3.0 (6)
N5	21.9 (9)	38.5 (10)	29.9 (11)	-0.9 (8)	15.2 (8)	4.5 (7)
N6	59.6 (14)	40.2 (11)	49.5 (14)	-18.1 (10)	41.1 (12)	-25.9 (10)
N7	18.7 (8)	15.3 (7)	18.5 (9)	-0.5 (6)	7.9 (7)	0.9 (5)
N8	14.9 (7)	15.0 (7)	15.9 (9)	-0.7 (6)	5.6 (7)	1.1 (5)
N9	17.5 (8)	17.2 (7)	17.2 (9)	-0.5 (6)	7.2 (7)	-0.6 (5)
N10	16.9 (8)	18.0 (7)	16.1 (9)	0.5 (6)	6.4 (7)	0.1 (5)
C1	18.8 (9)	18.0 (8)	24.7 (11)	-0.6 (7)	6.7 (8)	2.0 (7)
C2	30.5 (11)	15.7 (8)	34.0 (13)	-2.9 (8)	9.9 (10)	-1.1 (7)
C3	24.8 (10)	24.0 (9)	33.4 (14)	-4.7 (8)	6.2 (10)	-8.9 (8)
C4	19.4 (10)	27.9 (10)	33.9 (14)	-1.7 (9)	1.2 (9)	-0.7 (7)
C5	17.5 (9)	18.4 (8)	24.7 (12)	-0.2 (7)	3.2 (8)	1.1 (7)
C6	19.6 (9)	21.7 (8)	18.8 (11)	-1.5 (7)	6.5 (8)	0.1 (7)
C7	19.9 (9)	32.9 (10)	17.9 (11)	-3.2 (8)	7.7 (8)	-1.7 (7)
C8	22.7 (10)	35.3 (10)	17.1 (10)	7.1 (8)	6.8 (9)	-3.5 (8)
C9	26.9 (10)	25.8 (9)	21.8 (12)	8.0 (8)	6.8 (9)	3.8 (7)
C10	25.9 (10)	21.2 (8)	21.4 (11)	1.2 (7)	9.8 (9)	3.9 (7)
C11	22.0 (9)	17.9 (8)	27.9 (12)	-1.0 (8)	9.9 (9)	0.2 (7)
C12	33.1 (11)	16.6 (8)	35.9 (14)	-2.0 (8)	13.3 (10)	-3.9 (8)
C13	35.1 (12)	24.4 (10)	40.2 (15)	-6.2 (9)	10.0 (11)	-13.8 (9)
C14	22.3 (10)	32.9 (11)	40.7 (15)	-3.6 (10)	1.4 (10)	-5.4 (9)
C15	23.0 (10)	20.1 (9)	29.3 (13)	-1.4 (8)	5.7 (9)	1.6 (7)
C16	15.7 (8)	18.8 (9)	16.9 (10)	-1.0 (7)	4.9 (7)	3.0 (7)
C17	20.5 (9)	28.5 (9)	17.5 (10)	-0.9 (8)	9.3 (8)	2.5 (7)
C18	22.4 (9)	27.4 (9)	16.2 (10)	5.9 (8)	5.1 (8)	2.9 (7)
C19	26.6 (10)	21.1 (8)	22.5 (11)	3.3 (7)	9.1 (9)	8.6 (7)
C20	20.7 (9)	20.7 (8)	17.1 (10)	0.6 (7)	7.5 (8)	5.3 (7)
C21	17.8 (8)	16.2 (7)	15.0 (10)	-1.7 (6)	4.2 (7)	-0.7 (6)
C22	28.7 (10)	26.1 (9)	39.4 (14)	-16.1 (9)	21.4 (10)	-12.8 (8)
C23	20.2 (9)	11.2 (7)	12.7 (9)	-0.2 (6)	3.7 (7)	-0.4 (6)
C24	21.5 (9)	18.3 (8)	18.9 (10)	5.2 (7)	9.4 (8)	7.1 (6)

Table 4 Bond Lengths for Bis(dicyanamide)tetrapyridine cobalt (II).

Atom	Atom	Length/Å	Atom	Atom	Length/Å
Co1	N1	2.0916 (16)	N9	C15	1.340 (3)
Co1	N4	2.1024 (16)	N10	C6	1.346 (3)
Co1	N7	2.2089 (16)	N10	C10	1.345 (2)
Co1	N8	2.1944 (17)	C1	C2	1.385 (3)
Co1	N9	2.2010 (16)	C2	C3	1.382 (3)
Co1	N10	2.1943 (18)	C3	C4	1.384 (3)
N1	C23	1.158 (3)	C4	C5	1.387 (3)
N2	C23	1.294 (2)	C6	C7	1.377 (3)
N2	C24	1.318 (2)	C7	C8	1.382 (3)
N3	C24	1.154 (3)	C8	C9	1.382 (3)
N4	C21	1.157 (3)	C9	C10	1.384 (3)
N5	C21	1.299 (2)	C11	C12	1.390 (3)
N5	C22	1.327 (3)	C12	C13	1.375 (3)
N6	C22	1.149 (3)	C13	C14	1.385 (3)
N7	C1	1.342 (2)	C14	C15	1.384 (3)
N7	C5	1.348 (3)	C16	C17	1.388 (3)
N8	C16	1.342 (2)	C17	C18	1.386 (3)
N8	C20	1.349 (2)	C18	C19	1.383 (3)
N9	C11	1.343 (2)	C19	C20	1.379 (3)

Table 5 Bond Angles for Bis(dicyanamide)tetrapyridine cobalt (II).

Atom	Atom	Atom	Angle/°	Atom	Atom	Atom	Angle/°
N1	Co1	N4	178.47 (7)	C6	N10	Co1	119.25 (14)
N1	Co1	N7	88.31 (6)	C10	N10	Co1	123.95 (14)
N1	Co1	N8	92.55 (7)	C10	N10	C6	116.78 (19)
N1	Co1	N9	88.96 (6)	N7	C1	C2	124.00 (19)
N1	Co1	N10	90.53 (7)	C3	C2	C1	118.52 (18)
N4	Co1	N7	92.46 (6)	C2	C3	C4	118.64 (19)
N4	Co1	N8	88.76 (6)	C3	C4	C5	119.2 (2)
N4	Co1	N9	90.26 (6)	N7	C5	C4	123.04 (18)
N4	Co1	N10	88.20 (6)	N10	C6	C7	123.3 (2)
N8	Co1	N7	90.77 (6)	C6	C7	C8	119.11 (19)
N8	Co1	N9	90.16 (6)	C9	C8	C7	118.7 (2)
N9	Co1	N7	177.15 (7)	C8	C9	C10	118.66 (19)
N10	Co1	N7	86.34 (6)	N10	C10	C9	123.49 (19)
N10	Co1	N8	175.71 (6)	N9	C11	C12	123.62 (19)
N10	Co1	N9	92.88 (6)	C13	C12	C11	118.58 (19)
C23	N1	Co1	166.88 (14)	C12	C13	C14	118.6 (2)

Table 5 Bond Angles for Bis(dicyanamide)tetrapyridine cobalt (II).

Atom	Atom	Atom	Angle/°	Atom	Atom	Atom	Angle/°
C23	N2	C24	120.46 (16)	C15	C14	C13	119.3 (2)
C21	N4	Co1	160.41 (14)	N9	C15	C14	122.98 (19)
C21	N5	C22	118.11 (19)	N8	C16	C17	123.25 (17)
C1	N7	Co1	122.18 (13)	C18	C17	C16	118.92 (19)
C1	N7	C5	116.64 (16)	C19	C18	C17	118.44 (19)
C5	N7	Co1	121.07 (12)	C20	C19	C18	119.06 (18)
C16	N8	Co1	121.71 (12)	N8	C20	C19	123.43 (19)
C16	N8	C20	116.88 (17)	N4	C21	N5	175.3 (2)
C20	N8	Co1	121.26 (13)	N6	C22	N5	175.2 (2)
C11	N9	Co1	121.39 (14)	N1	C23	N2	173.62 (19)
C15	N9	Co1	121.66 (12)	N3	C24	N2	173.10 (19)
C15	N9	C11	116.93 (17)				

Table 6 Torsion Angles for Bis(dicyanamide)tetrapyridine cobalt (II).

A	B	C	D	Angle/°	A	B	C	D	Angle/°
Co1	N7	C1	C2	-175.10 (18)	C5	N7	C1	C2	1.1 (3)
Co1	N7	C5	C4	174.97 (18)	C6	N10	C10	C9	0.7 (3)
Co1	N8	C16	C17	-174.76 (15)	C6	C7	C8	C9	-0.4 (3)
Co1	N8	C20	C19	173.51 (16)	C7	C8	C9	C10	1.0 (3)
Co1	N9	C11	C12	177.57 (18)	C8	C9	C10	N10	-1.2 (3)
Co1	N9	C15	C14	-177.8 (2)	C10	N10	C6	C7	-0.1 (3)
Co1	N10	C6	C7	178.25 (15)	C11	N9	C15	C14	0.5 (3)
Co1	N10	C10	C9	-177.50 (15)	C11	C12	C13	C14	-0.2 (4)
N7	C1	C2	C3	-0.1 (4)	C12	C13	C14	C15	-0.1 (4)
N8	C16	C17	C18	0.7 (3)	C13	C14	C15	N9	-0.1 (4)
N9	C11	C12	C13	0.6 (4)	C15	N9	C11	C12	-0.8 (3)
N10	C6	C7	C8	-0.1 (3)	C16	N8	C20	C19	-2.1 (3)
C1	N7	C5	C4	-1.2 (3)	C16	C17	C18	C19	-0.9 (3)
C1	C2	C3	C4	-0.8 (4)	C17	C18	C19	C20	-0.2 (3)
C2	C3	C4	C5	0.6 (4)	C18	C19	C20	N8	1.8 (3)
C3	C4	C5	N7	0.4 (4)	C20	N8	C16	C17	0.8 (3)

Table 7 Hydrogen Atom Coordinates ($\text{\AA} \times 10^4$) and Isotropic Displacement Parameters ($\text{\AA}^2 \times 10^3$) for Bis(dicyanamide)tetrapyridine cobalt (II).

Atom	x	y	z	U(eq)
H1	4557	9860	5123	25

Table 7 Hydrogen Atom Coordinates ($\text{\AA}\times 10^4$) and Isotropic Displacement Parameters ($\text{\AA}^2\times 10^3$) for Bis(dicyanamide)tetrapyridine cobalt (II).

Atom	x	y	z	U(eq)
H2	5826	11172	5691	32
H3	7654	10729	6509	34
H4	8123	8964	6749	35
H5	6786	7710	6158	25
H6	4298	8025	6885	24
H7	4672	7414	8407	28
H8	5392	5738	8799	30
H9	5690	4718	7614	30
H10	5319	5414	6114	27
H11	4296	5041	4611	27
H12	3128	3653	4008	34
H13	1261	3975	3270	41
H14	634	5696	3178	41
H15	1864	7025	3812	30
H16	4671	7241	2966	21
H17	4335	8106	1539	26
H18	3338	9668	1266	27
H19	2678	10279	2442	28
H20	3005	9329	3815	23

Experimental

Single crystals of $\text{C}_{2.53}\text{H}_{2.11}\text{Co}_{0.11}\text{N}_{1.05}$ [Bis(dicyanamide)tetrapyridine cobalt (II)] were [1]. A suitable crystal was selected and [1] on a diffractometer. The crystal was kept at 100.01 K during data collection. Using Olex2 [1], the structure was solved with the Unknown [2] structure solution program using Unknown and refined with the Unknown [3] refinement package using Unknown minimisation.

1. Dolomanov, O.V., Bourhis, L.J., Gildea, R.J., Howard, J.A.K. & Puschmann, H. (2009), J. Appl. Cryst. 42, 339-341.
- 2.
- 3.

Crystal structure determination of [Bis(dicyanamide)tetrapyridine cobalt (II)]

Crystal Data for $\text{C}_{2.526316}\text{H}_{2.105263}\text{Co}_{0.105263}\text{N}_{1.052632}$ ($M=53.41$ g/mol): monoclinic, space group Cc (no. 9), $a = 13.063(2)$ Å, $b = 12.880(2)$ Å, $c = 15.033(2)$ Å, $\beta = 110.014(3)^\circ$, $V = 2376.8(6)$ Å³, $Z = 38$, $T = 100.01$ K, $\mu(\text{MoK}\alpha) = 0.756$ mm⁻¹, $D_{\text{calc}} = 1.418$ g/cm³, 18556 reflections measured ($4.584^\circ \leq 2\theta \leq 56.144^\circ$), 4781 unique ($R_{\text{int}} = 0.0154$, $R_{\text{sigma}} = 0.0140$) which were used in all calculations. The final R_1 was 0.0179 ($I > 2\sigma(I)$) and wR_2 was 0.0483 (all data).

Refinement model description

Number of restraints - 2, number of constraints - unknown.

Details:

1. Twinned data refinement

Scales: 0.55098

0.44902

2.a Aromatic/amide H refined with riding coordinates:

C1 (H1), C2 (H2), C3 (H3), C4 (H4), C5 (H5), C6 (H6), C7 (H7), C8 (H8), C9 (H9),

C10 (H10), C11 (H11), C12 (H12), C13 (H13), C14 (H14), C15 (H15), C16 (H16), C17 (H17),
C18 (H18), C19 (H19), C20 (H20)

This report has been created with Olex2, compiled on 2022.04.07 svn.rca3783a0 for OlexSys. Please [let us know](#) if there are any errors or if you would like to have additional features.

APPENDIX G

CRYSTAL DATA FOR

Bis(dimethylimidopyridine)tetrakis(dicyanamide) cobalt(II)

Table 1 Crystal data and structure refinement for Bis(dimethylimidopyridine)tetrakis(dicyanamide) cobalt(II)

Identification code	Bis(dimethylimidopyridine)tetrakis(dicyanamide) cobalt(II)
Empirical formula	C ₉ H ₁₀ Cu _{0.5} N ₅
Formula weight	219.99
Temperature/K	100.09
Crystal system	triclinic
Space group	P-1
a/Å	7.2716(12)
b/Å	8.0636(14)
c/Å	8.9865(15)
α/°	101.317(4)
β/°	108.080(3)
γ/°	95.552(4)
Volume/Å ³	484.09(14)
Z	2
ρ _{calc} /cm ³	1.509
μ/mm ⁻¹	1.156
F(000)	227.0
Crystal size/mm ³	0.098 × 0.085 × 0.072
Radiation	MoKα (λ = 0.71073)
2θ range for data collection/°	4.91 to 55.858
Index ranges	-9 ≤ h ≤ 9, -10 ≤ k ≤ 10, -10 ≤ l ≤ 11
Reflections collected	7497
Independent reflections	2210 [R _{int} = 0.0234, R _{sigma} = 0.0260]
Data/restraints/parameters	2210/0/135
Goodness-of-fit on F ²	1.177
Final R indexes [I ≥ 2σ (I)]	R ₁ = 0.0628, wR ₂ = 0.1782
Final R indexes [all data]	R ₁ = 0.0638, wR ₂ = 0.1786
Largest diff. peak/hole / e Å ⁻³	3.48/-0.66

Table 2 Fractional Atomic Coordinates ($\times 10^4$) and Equivalent Isotropic Displacement Parameters ($\text{\AA}^2 \times 10^3$) for Bis(dimethylimidopyridine)tetrakis(dicyanamide) cobalt(II). U_{eq} is defined as 1/3 of the trace of the orthogonalised U_{ij} tensor.

Atom	x	y	z	$U(\text{eq})$
Cu01	5000	0	0	11.3 (2)
N002	5915 (6)	2099 (5)	1829 (5)	15.5 (8)
N003	2477 (6)	843 (6)	-898 (5)	19.8 (9)
N004	7835 (7)	6515 (6)	5616 (5)	19.3 (9)
N005	-261 (7)	2460 (6)	-1573 (7)	26.1 (11)
N006	-3612 (7)	1570 (6)	-1614 (6)	22.9 (10)
C007	7217 (7)	5087 (6)	4395 (6)	15.0 (9)
C008	6371 (7)	5164 (6)	2770 (6)	17.3 (10)
C009	5754 (7)	3681 (6)	1570 (6)	16.6 (10)
C00A	1124 (7)	1550 (7)	-1203 (6)	16.4 (10)
C00B	7389 (8)	3437 (6)	4661 (6)	16.9 (10)
C00C	-2014 (7)	1922 (6)	-1560 (6)	16.7 (10)
C00D	6723 (7)	2023 (6)	3372 (6)	16.2 (10)
C00E	8754 (8)	6420 (7)	7284 (7)	23.0 (11)
C10	7677 (9)	8190 (7)	5288 (8)	27.6 (13)

Table 3 Anisotropic Displacement Parameters ($\text{\AA}^2 \times 10^3$) for Bis(dimethylimidopyridine)tetrakis(dicyanamide) cobalt(II). The Anisotropic displacement factor exponent takes the form: $-2\pi^2[h^2a^{*2}U_{11}+2hka^*b^*U_{12}+\dots]$.

Atom	U_{11}	U_{22}	U_{33}	U_{23}	U_{13}	U_{12}
Cu01	9.3 (4)	9.1 (4)	13.1 (4)	1.0 (3)	1.1 (3)	3.0 (3)
N002	14.9 (19)	12.7 (19)	17 (2)	2.5 (16)	3.1 (16)	3.0 (15)
N003	12 (2)	27 (2)	18 (2)	5.1 (18)	2.3 (16)	0.0 (17)
N004	23 (2)	15 (2)	17 (2)	1.5 (17)	2.0 (17)	4.3 (17)
N005	20 (2)	27 (2)	40 (3)	20 (2)	13 (2)	12.4 (19)
N006	19 (2)	25 (2)	28 (3)	10 (2)	8.3 (19)	6.4 (18)
C007	13 (2)	15 (2)	15 (2)	0.6 (18)	5.1 (18)	2.1 (17)
C008	19 (2)	13 (2)	19 (2)	4.9 (19)	3.9 (19)	3.6 (18)
C009	17 (2)	16 (2)	16 (2)	4.6 (19)	2.6 (18)	4.2 (18)
C00A	15 (2)	18 (2)	16 (2)	6.3 (19)	5.0 (19)	2.3 (18)
C00B	21 (2)	17 (2)	14 (2)	5.4 (19)	6.1 (19)	3.2 (19)
C00C	20 (2)	17 (2)	15 (2)	8.3 (19)	4.2 (19)	5.7 (19)
C00D	17 (2)	14 (2)	18 (2)	5.6 (19)	4.9 (19)	5.8 (18)
C00E	25 (3)	26 (3)	15 (2)	2 (2)	5 (2)	2 (2)
C10	34 (3)	13 (2)	28 (3)	1 (2)	2 (2)	4 (2)

Table 4 Bond Lengths for Bis(dimethylimidopyridine)tetrakis(dicyanamide) cobalt(II).

Atom	Atom	Length/Å	Atom	Atom	Length/Å
Cu01	N002 ¹	2.005 (4)	N004	C00E	1.461 (7)
Cu01	N002	2.005 (4)	N004	C10	1.446 (7)
Cu01	N003 ¹	2.004 (4)	N005	C00A	1.302 (7)
Cu01	N003	2.004 (4)	N005	C00C	1.310 (7)
Cu01	N006 ²	2.472 (5)	N006	C00C	1.152 (7)
Cu01	N006 ³	2.472 (5)	C007	C008	1.414 (7)
N002	C009	1.351 (6)	C007	C00B	1.408 (7)
N002	C00D	1.344 (7)	C008	C009	1.373 (7)
N003	C00A	1.170 (7)	C00B	C00D	1.380 (7)
N004	C007	1.352 (6)			

¹1-X,-Y,-Z; ²1+X,+Y,+Z; ³-X,-Y,-Z

Table 5 Bond Angles for Bis(dimethylimidopyridine)tetrakis(dicyanamide) cobalt(II).

Atom	Atom	Atom	Angle/°	Atom	Atom	Atom	Angle/°
N002 ¹	Cu01	N002	180.0	C00D	N002	C009	116.2 (4)
N002	Cu01	N006 ²	89.52 (17)	C00A	N003	Cu01	169.1 (4)
N002 ¹	Cu01	N006 ²	90.48 (17)	C007	N004	C00E	121.3 (5)
N002	Cu01	N006 ³	90.48 (17)	C007	N004	C10	120.4 (5)
N002 ¹	Cu01	N006 ³	89.52 (17)	C10	N004	C00E	118.2 (4)
N003 ¹	Cu01	N002	90.17 (18)	C00A	N005	C00C	120.0 (5)
N003	Cu01	N002 ¹	90.17 (18)	C00C	N006	Cu01 ⁴	131.0 (4)
N003 ¹	Cu01	N002 ¹	89.83 (18)	N004	C007	C008	121.9 (5)
N003	Cu01	N002	89.83 (18)	N004	C007	C00B	122.2 (5)
N003	Cu01	N003 ¹	180.0	C00B	C007	C008	115.9 (4)
N003	Cu01	N006 ³	91.84 (17)	C009	C008	C007	120.0 (5)
N003	Cu01	N006 ²	88.16 (17)	N002	C009	C008	124.0 (5)
N003 ¹	Cu01	N006 ³	88.16 (17)	N003	C00A	N005	173.9 (6)
N003 ¹	Cu01	N006 ²	91.84 (17)	C00D	C00B	C007	119.8 (5)
N006 ³	Cu01	N006 ²	180.00 (19)	N006	C00C	N005	173.6 (6)
C009	N002	Cu01	121.4 (4)	N002	C00D	C00B	124.2 (5)
C00D	N002	Cu01	122.5 (3)				

¹1-X,-Y,-Z; ²1+X,+Y,+Z; ³-X,-Y,-Z; ⁴-1+X,+Y,+Z

Table 6 Torsion Angles for Bis(dimethylimidopyridine)tetrakis(dicyanamide) cobalt(II).

A	B	C	D	Angle/°	A	B	C	D	Angle/°
Cu01	N002	C009	C008	-179.3(4)	C009	N002	C00D	C00B	-0.5(8)
Cu01	N002	C00D	C00B	179.3(4)	C00B	C007	C008	C009	0.9(7)
N004	C007	C008	C009	-179.6(5)	C00D	N002	C009	C008	0.5(8)
N004	C007	C00B	C00D	179.6(5)	C00E	N004	C007	C008	-178.3(5)
C007	C008	C009	N002	-0.7(8)	C00E	N004	C007	C00B	1.1(8)
C007	C00B	C00D	N002	0.8(8)	C10	N004	C007	C008	-1.0(8)
C008	C007	C00B	C00D	-0.9(7)	C10	N004	C007	C00B	178.4(5)

Table 7 Hydrogen Atom Coordinates ($\text{\AA} \times 10^4$) and Isotropic Displacement Parameters ($\text{\AA}^2 \times 10^3$) for Bis(dimethylimidopyridine)tetrakis(dicyanamide) cobalt(II).

Atom	x	y	z	U(eq)
H008	6230.65	6241.46	2509.62	21
H009	5178.56	3773.09	491.24	20
H00B	7962.32	3298.27	5723.96	20
H00D	6842.99	924.31	3589.56	19
H00A	7798.37	5792.21	7627.01	35
H00C	9202.01	7582.66	7979.79	35
H00E	9878.73	5821.17	7364.79	35
H10A	8629.63	8484.61	4772.87	41
H10B	7946.3	9046.27	6301.1	41
H10C	6347.62	8176.13	4566.84	41

Experimental

Single crystals of $\text{C}_9\text{H}_{10}\text{Cu}_{0.5}\text{N}_5$ [Bis(dimethylimidopyridine)tetrakis(dicyanamide) cobalt(II)] were [1]. A suitable crystal was selected and [1] on a Bruker APEX-II CCD diffractometer. The crystal was kept at 100.09 K during data collection. Using Olex2 [1], the structure was solved with the Unknown [2] structure solution program using Unknown and refined with the Unknown [3] refinement package using Unknown minimisation.

1. Dolomanov, O.V., Bourhis, L.J., Gildea, R.J., Howard, J.A.K. & Puschmann, H. (2009), J. Appl. Cryst. 42, 339-341.
- 2.
- 3.

Crystal structure determination of [Bis(dimethylimidopyridine)tetrakis(dicyanamide) cobalt(II)]

Crystal Data for $\text{C}_9\text{H}_{10}\text{Cu}_{0.5}\text{N}_5$ ($M=219.99$ g/mol): triclinic, space group P-1 (no. 2), $a = 7.2716(12)$ Å, $b = 8.0636(14)$ Å, $c = 8.9865(15)$ Å, $\alpha = 101.317(4)^\circ$, $\beta = 108.080(3)^\circ$, $\gamma = 95.552(4)^\circ$, $V = 484.09(14)$ Å³, $Z = 2$, $T = 100.09$ K, $\mu(\text{MoK}\alpha) = 1.156$ mm⁻¹, $D_{\text{calc}} = 1.509$ g/cm³, 7497 reflections measured ($4.91^\circ \leq 2\theta \leq 55.858^\circ$), 2210 unique ($R_{\text{int}} = 0.0234$, $R_{\text{sigma}} = 0.0260$) which were used in all calculations. The final R_1 was 0.0628 ($I > 2\sigma(I)$) and wR_2 was 0.1786 (all data).

Refinement model description

Number of restraints - 0, number of constraints - unknown.
Details:

1.a Aromatic/amide H refined with riding coordinates:
C008(H008), C009(H009), C00B(H00B), C00D(H00D)
1.b Idealised Me refined as rotating group:
C00E(H00A,H00C,H00E), C10(H10A,H10B,H10C)

This report has been created with Olex2, compiled on 2022.04.07 svn.rca3783a0 for OlexSys. Please [let us know](#) if there are any errors or if you would like to have additional features.

APPENDIX H

CRYSTAL DATA FOR

Ir[(6-(4-methoxyphenyl)-2-pbt)₂(acac)]

Table 1 Crystal data and structure refinement for Ir[(6-(4-methoxyphenyl)-2-pbt)₂(acac)]

Identification code	Ir[(6-(4-methoxyphenyl)-2-pbt) ₂ (acac)]
Empirical formula	C ₄₅ H ₂₉ IrN ₂ O ₄ S ₂
Formula weight	918.02
Temperature/K	99.99
Crystal system	monoclinic
Space group	P2 ₁ /c
a/Å	9.7527(11)
b/Å	26.827(3)
c/Å	14.5853(16)
α/°	90
β/°	104.776(2)
γ/°	90
Volume/Å ³	3689.9(7)
Z	4
ρ _{calc} /cm ³	1.653
μ/mm ⁻¹	3.780
F(000)	1816.0
Crystal size/mm ³	0.021 × 0.011 × 0.006
Radiation	MoKα (λ = 0.71073)
2Θ range for data collection/°	3.036 to 55.84
Index ranges	-12 ≤ h ≤ 8, -33 ≤ k ≤ 35, -16 ≤ l ≤ 19
Reflections collected	32867
Independent reflections	8727 [R _{int} = 0.0315, R _{sigma} = 0.0268]
Data/restraints/parameters	8727/198/528
Goodness-of-fit on F ²	1.152
Final R indexes [I ≥ 2σ (I)]	R ₁ = 0.0276, wR ₂ = 0.0660
Final R indexes [all data]	R ₁ = 0.0289, wR ₂ = 0.0664
Largest diff. peak/hole / e Å ⁻³	1.19/-2.21

Table 2 Fractional Atomic Coordinates ($\times 10^4$) and Equivalent Isotropic Displacement Parameters ($\text{\AA}^2 \times 10^3$) for solveheavy. U_{eq} is defined as 1/3 of of the trace of the orthogonalised U_{IJ} tensor.

Atom	<i>x</i>	<i>y</i>	<i>z</i>	$U(\text{eq})$
Ir01	3679.4 (2)	6388.9 (2)	5821.7 (2)	10.77 (4)
S002	2934.1 (9)	7807.7 (3)	7258.4 (6)	13.97 (15)
S003	6516.8 (9)	5328.9 (3)	4790.8 (6)	18.92 (17)
O004	1622 (2)	6473.1 (9)	4836.1 (16)	15.0 (5)
N10	3099 (3)	6902.0 (10)	6697.5 (18)	12.0 (5)
O006	2851 (2)	5731.4 (8)	6354.0 (16)	13.8 (4)
O007	-1504 (3)	7041.7 (10)	11993.0 (18)	22.8 (5)
N008	4535 (3)	5926.7 (10)	4994.4 (19)	13.7 (5)
C20	4124 (3)	7454.7 (12)	5789 (2)	12.8 (6)
C21	5566 (3)	6263.8 (12)	6721 (2)	12.8 (6)
C00B	3390 (3)	7369.9 (12)	6521 (2)	12.7 (6)
C00C	1312 (3)	6949.2 (12)	9032 (2)	14.0 (6)
C00D	1703 (3)	7380.3 (12)	8624 (2)	13.7 (6)
O00E	2483 (4)	4436.9 (12)	-1412 (2)	47.2 (10)
C00F	6414 (3)	5911.3 (13)	6400 (2)	15.2 (6)
C00G	4430 (3)	7007.8 (12)	5366 (2)	12.9 (6)
C00H	2207 (4)	6436.7 (12)	7912 (2)	17.8 (7)
C00I	5788 (3)	5742.2 (12)	5445 (2)	15.0 (6)
C00J	5678 (4)	7521.4 (14)	4461 (2)	19.5 (7)
C00K	2307 (3)	7334.4 (12)	7861 (2)	13.0 (6)
C00L	1626 (4)	6483.6 (13)	8681 (2)	18.4 (7)
C00M	5063 (4)	5414.9 (13)	3829 (2)	15.9 (6)
C00N	-398 (4)	6585.8 (14)	11015 (3)	21.0 (7)
C00O	-825 (3)	7048.0 (13)	11276 (2)	16.6 (6)
C00P	6116 (4)	6456.6 (13)	7634 (2)	18.2 (7)
C00Q	4804 (4)	5190.1 (13)	2942 (2)	19.4 (7)
C00R	4556 (4)	7924.6 (13)	5546 (2)	16.4 (6)
C00S	5336 (4)	7955.4 (13)	4878 (2)	19.4 (7)
C00T	2891 (4)	5889.2 (14)	3367 (2)	20.3 (7)
C00U	2515 (3)	6869.7 (12)	7475 (2)	13.0 (6)
C00V	-2066 (4)	7500.9 (15)	12226 (3)	24.9 (8)
C00W	7732 (4)	5752.5 (15)	6959 (3)	22.8 (7)
C00X	-562 (4)	7474.1 (14)	10820 (2)	19.3 (7)
C00Y	1228 (4)	5142.5 (13)	6647 (3)	18.9 (7)
C00Z	298 (4)	6554.6 (13)	10297 (3)	19.3 (7)
C010	1583 (4)	5576.8 (12)	6086 (2)	14.6 (6)
C011	3582 (4)	5316.8 (13)	2243 (2)	18.1 (7)
C012	7439 (4)	6302.8 (15)	8186 (3)	24.5 (8)

Table 2 Fractional Atomic Coordinates ($\times 10^4$) and Equivalent Isotropic Displacement Parameters ($\text{\AA}^2 \times 10^3$) for solveheavy. U_{eq} is defined as 1/3 of of the trace of the orthogonalised U_{IJ} tensor.

Atom	x	y	z	$U(eq)$
C013	499 (4)	5772.4 (13)	5354 (2)	19.0 (7)
C014	2647 (4)	5673.2 (14)	2472 (2)	22.1 (7)
C015	603 (3)	6977.3 (13)	9822 (2)	14.5 (6)
C016	561 (4)	6189.1 (13)	4783 (2)	17.7 (7)
C017	3306 (4)	5077.8 (13)	1293 (2)	23.2 (6)
C018	5243 (4)	7057.8 (13)	4698 (2)	17.0 (7)
C019	155 (4)	7434.9 (13)	10104 (3)	19.9 (7)
C01A	4108 (3)	5755.2 (12)	4058 (2)	13.8 (6)
C01B	3996 (10)	4553 (3)	125 (6)	22.0 (8)
C01C	8232 (4)	5952.2 (16)	7854 (3)	25.8 (8)
C01D	3380 (5)	4051.4 (16)	-1598 (3)	32.6 (9)
C01E	-762 (4)	6324.9 (16)	4038 (3)	32.9 (10)
C01F	2821 (4)	4624.8 (14)	-503 (3)	26.8 (6)
C01G	4245 (10)	4787 (3)	1004 (6)	21.9 (8)
C1	1916 (10)	5135 (3)	619 (6)	26.5 (8)
C2	1599 (10)	4912 (3)	-271 (6)	27.5 (8)
C1A	2371 (9)	5280 (3)	511 (6)	27.3 (8)
C2A	2130 (8)	5037 (3)	-382 (6)	27.8 (8)
C3	3867 (9)	4424 (3)	269 (6)	22.1 (8)
C01H	4110 (9)	4652 (3)	1168 (6)	21.1 (8)

Table 3 Anisotropic Displacement Parameters ($\text{\AA}^2 \times 10^3$) for solveheavy. The Anisotropic displacement factor exponent takes the form: $-2\pi^2[h^2a^*U_{11}+2hka^*b^*U_{12}+...]$.

Atom	U_{11}	U_{22}	U_{33}	U_{23}	U_{13}	U_{12}
Ir01	11.55 (6)	10.85 (6)	9.60 (6)	-0.25 (4)	2.17 (4)	0.36 (4)
S002	18.0 (4)	11.0 (4)	13.5 (3)	-0.5 (3)	5.3 (3)	0.0 (3)
S003	14.2 (4)	25.3 (4)	16.6 (4)	-2.9 (3)	2.9 (3)	6.8 (3)
O004	14.0 (11)	13.9 (11)	15.9 (11)	0.0 (9)	1.6 (9)	1.4 (9)
N10	13.7 (13)	12.0 (13)	9.7 (12)	0.7 (10)	1.9 (10)	0.6 (10)
O006	15.6 (11)	12.0 (11)	13.8 (10)	-0.6 (8)	3.5 (9)	2.0 (8)
O007	26.7 (14)	27.5 (14)	18.8 (12)	3.5 (10)	14.3 (11)	4.0 (11)
N008	14.1 (13)	14.4 (13)	12.2 (12)	-0.2 (10)	3.0 (10)	0.4 (10)
C20	10.1 (14)	17.4 (16)	9.4 (13)	1.0 (11)	-0.2 (11)	0.2 (11)
C21	12.4 (14)	12.5 (15)	13.4 (14)	2.8 (11)	3.4 (11)	-2.5 (11)
C00B	11.8 (14)	12.4 (15)	12.8 (14)	-0.4 (11)	0.8 (11)	0.6 (11)
C00C	13.8 (15)	17.4 (16)	10.1 (14)	-1.9 (12)	2.2 (11)	-1.0 (12)

Table 3 Anisotropic Displacement Parameters ($\text{\AA}^2 \times 10^3$) for solveheavy. The Anisotropic displacement factor exponent takes the form: $-2\pi^2[h^2a^{*2}U_{11}+2hka^*b^*U_{12}+\dots]$.

Atom	U ₁₁	U ₂₂	U ₃₃	U ₂₃	U ₁₃	U ₁₂
C00D	11.6(14)	14.4(15)	14.0(14)	-2.2(12)	1.1(11)	-0.4(11)
O00E	92(3)	29.9(17)	12.0(13)	-3.4(12)	-1.5(15)	20.8(17)
C00F	12.6(15)	17.5(16)	14.7(15)	-0.5(12)	1.8(12)	0.0(12)
C00G	12.0(14)	16.1(15)	8.9(13)	0.7(11)	-0.6(11)	-1.0(12)
C00H	26.1(18)	10.6(15)	17.6(16)	-3.2(12)	7.6(14)	-3.5(13)
C00I	14.7(15)	16.0(16)	14.7(15)	-1.6(12)	4.7(12)	1.9(12)
C00J	18.5(17)	26.6(19)	14.4(15)	2.4(13)	6.4(13)	-3.8(14)
C00K	12.3(14)	13.8(15)	11.7(14)	0.8(11)	1.0(11)	-1.3(11)
C00L	25.4(18)	13.9(16)	17.5(16)	-1.8(12)	8.6(14)	-4.0(13)
C00M	14.9(15)	17.5(16)	15.6(15)	2.1(12)	4.2(12)	2.6(12)
C00N	24.4(18)	21.6(18)	19.2(16)	3.6(14)	9.5(14)	0.3(14)
C00O	11.3(15)	25.4(18)	13.1(15)	0.9(13)	3.2(12)	0.9(13)
C00P	18.4(16)	20.5(17)	14.1(15)	-1.2(13)	1.6(13)	-1.5(13)
C00Q	22.0(17)	18.1(17)	19.4(16)	-2.7(13)	7.9(14)	4.0(13)
C00R	18.1(16)	14.4(16)	15.5(15)	0.7(12)	2.4(12)	-1.7(12)
C00S	22.2(17)	18.3(17)	16.8(16)	2.7(13)	3.3(13)	-7.0(13)
C00T	20.2(17)	24.6(18)	15.3(16)	-1.0(13)	3.0(13)	5.0(14)
C00U	12.9(14)	13.5(15)	12.0(14)	-1.7(11)	2.2(11)	-1.4(11)
C00V	21.2(18)	35(2)	20.2(17)	-3.7(15)	8.4(14)	5.3(15)
C00W	12.9(16)	30(2)	23.7(18)	0.0(15)	1.6(13)	3.3(14)
C00X	20.1(17)	19.6(17)	19.2(16)	-1.9(13)	6.8(13)	2.9(13)
C00Y	19.4(17)	16.1(16)	21.7(17)	0.9(13)	6.4(13)	-0.1(13)
C00Z	22.6(17)	15.8(16)	21.7(17)	0.5(13)	9.7(14)	0.9(13)
C010	17.8(16)	12.0(15)	15.2(15)	-3.3(12)	6.6(12)	1.0(12)
C011	23.6(17)	16.6(16)	14.7(15)	-0.1(12)	5.7(13)	1.1(13)
C012	21.8(18)	31(2)	17.2(16)	-1.6(15)	-0.9(14)	-3.7(15)
C013	15.0(16)	18.4(17)	21.6(17)	-0.3(13)	1.1(13)	-4.3(13)
C014	22.8(18)	26.6(19)	15.6(16)	-2.1(14)	2.3(13)	5.3(14)
C015	12.3(14)	17.4(16)	12.5(14)	-1.7(12)	0.8(11)	-1.6(12)
C016	16.2(16)	18.0(17)	16.6(15)	-1.8(13)	0.0(12)	0.8(13)
C017	32.2(13)	21.3(13)	15.7(11)	-0.3(10)	5.2(10)	0.4(11)
C018	17.4(16)	20.7(17)	12.7(15)	-0.8(12)	3.7(12)	0.4(13)
C019	25.0(18)	17.3(17)	20.1(16)	0.6(13)	10.6(14)	-1.4(14)
C01A	15.3(15)	12.1(15)	13.9(14)	-0.8(11)	3.7(12)	1.4(12)
C01B	31.8(15)	19.9(17)	14.9(14)	0.3(13)	7.2(12)	-2.7(14)
C01C	14.6(16)	38(2)	20.2(17)	2.3(15)	-3.5(13)	0.9(15)
C01D	50(3)	29(2)	21.3(19)	-4.4(16)	12.3(18)	-6.5(19)
C01E	25(2)	28(2)	36(2)	11.1(17)	-10.7(17)	-6.9(16)
C01F	38.2(14)	23.1(13)	17.4(11)	-0.7(10)	3.9(10)	1.7(11)

Table 3 Anisotropic Displacement Parameters ($\text{\AA}^2 \times 10^3$) for solveheavy. The Anisotropic displacement factor exponent takes the form: $-2\pi^2[h^2a^{*2}U_{11}+2hka^*b^*U_{12}+\dots]$.

Atom	U ₁₁	U ₂₂	U ₃₃	U ₂₃	U ₁₃	U ₁₂
C01G	30.7 (15)	20.2 (17)	15.2 (14)	-0.1 (13)	6.4 (12)	-1.8 (14)
C1	35.3 (16)	23.4 (16)	18.4 (14)	-0.5 (13)	2.6 (13)	2.1 (13)
C2	36.8 (16)	24.1 (16)	19.1 (14)	-0.7 (13)	2.5 (13)	2.2 (13)
C1A	36.1 (16)	24.8 (16)	18.7 (13)	-1.0 (13)	2.9 (13)	3.6 (13)
C2A	36.8 (16)	25.3 (16)	18.8 (14)	-1.0 (13)	2.4 (13)	3.9 (13)
C3	32.0 (15)	19.5 (17)	15.1 (14)	0.9 (13)	6.5 (12)	-1.7 (14)
C01H	30.6 (15)	18.7 (16)	14.3 (14)	0.6 (13)	6.2 (12)	-1.8 (13)

Table 4 Bond Lengths for solveheavy.

Atom	Atom	Length/ \AA	Atom	Atom	Length/ \AA
Ir01	O004	2.162 (2)	C00J	C018	1.386 (5)
Ir01	N10	2.053 (3)	C00K	C00U	1.404 (4)
Ir01	O006	2.165 (2)	C00M	C00Q	1.391 (5)
Ir01	N008	2.050 (3)	C00M	C01A	1.404 (4)
Ir01	C21	1.997 (3)	C00N	C00O	1.392 (5)
Ir01	C00G	1.996 (3)	C00N	C00Z	1.387 (5)
S002	C00B	1.726 (3)	C00O	C00X	1.379 (5)
S002	C00K	1.741 (3)	C00P	C012	1.397 (5)
S003	C00I	1.729 (3)	C00Q	C011	1.398 (5)
S003	C00M	1.737 (3)	C00R	C00S	1.383 (5)
O004	C016	1.271 (4)	C00T	C014	1.393 (5)
N10	C00B	1.326 (4)	C00T	C01A	1.394 (5)
N10	C00U	1.396 (4)	C00W	C01C	1.380 (5)
O006	C010	1.268 (4)	C00X	C019	1.401 (5)
O007	C00O	1.373 (4)	C00Y	C010	1.514 (5)
O007	C00V	1.424 (5)	C00Z	C015	1.400 (5)
N008	C00I	1.326 (4)	C010	C013	1.399 (5)
N008	C01A	1.400 (4)	C011	C014	1.418 (5)
C20	C00B	1.448 (4)	C011	C017	1.488 (5)
C20	C00G	1.414 (5)	C012	C01C	1.382 (6)
C20	C00R	1.403 (5)	C013	C016	1.404 (5)
C21	C00F	1.413 (5)	C015	C019	1.400 (5)
C21	C00P	1.401 (4)	C016	C01E	1.505 (5)
C00C	C00D	1.397 (5)	C017	C01G	1.350 (10)
C00C	C00L	1.413 (5)	C017	C1	1.466 (9)
C00C	C015	1.488 (4)	C017	C1A	1.377 (9)
C00DC00K		1.391 (4)	C017	C01H	1.422 (10)

Table 4 Bond Lengths for solveheavy.

Atom	Atom	Length/Å	Atom	Atom	Length/Å
O00E	C01D	1.424 (5)	C01B	C01F	1.286 (10)
O00E	C01F	1.378 (5)	C01B	C01G	1.392 (11)
C00F	C00I	1.444 (4)	C01F	C2	1.528 (10)
C00F	C00W	1.402 (5)	C01F	C2A	1.330 (9)
C00G	C018	1.410 (5)	C01F	C3	1.418 (9)
C00H	C00L	1.386 (5)	C1	C2	1.390 (11)
C00H	C00U	1.394 (5)	C1A	C2A	1.421 (11)
C00J	C00S	1.393 (5)	C3	C01H	1.412 (11)

Table 5 Bond Angles for solveheavy.

Atom	Atom	Atom	Angle/°	Atom	Atom	Atom	Angle/°
O004	Ir01	O006	87.45 (9)	C01A	C00M	S003	110.4 (2)
N10	Ir01	O004	89.27 (10)	C00Z	C00N	C00O	119.9 (3)
N10	Ir01	O006	97.81 (10)	O007	C00O	C00N	115.7 (3)
N008	Ir01	O004	96.90 (10)	O007	C00O	C00X	124.2 (3)
N008	Ir01	N10	171.79 (11)	C00X	C00O	C00N	120.1 (3)
N008	Ir01	O006	87.91 (10)	C012	C00P	C21	120.9 (3)
C21	Ir01	O004	176.32 (11)	C00M	C00Q	C011	119.4 (3)
C21	Ir01	N10	93.32 (12)	C00S	C00R	C20	119.1 (3)
C21	Ir01	O006	89.61 (11)	C00R	C00S	C00J	119.6 (3)
C21	Ir01	N008	80.78 (12)	C01A	C00T	C014	118.8 (3)
C00G	Ir01	O004	92.78 (11)	N10	C00U	C00K	113.6 (3)
C00G	Ir01	N10	80.34 (12)	C00H	C00U	N10	127.1 (3)
C00G	Ir01	O006	178.13 (11)	C00H	C00U	C00K	119.1 (3)
C00G	Ir01	N008	93.90 (12)	C01C	C00W	C00F	118.9 (3)
C00G	Ir01	C21	90.23 (13)	C00O	C00X	C019	119.1 (3)
C00B	S002	C00K	89.85 (16)	C00N	C00Z	C015	122.1 (3)
C00I	S003	C00M	89.67 (16)	O006	C010	C00Y	115.1 (3)
C016	O004	Ir01	125.5 (2)	O006	C010	C013	126.9 (3)
C00B	N10	Ir01	114.1 (2)	C013	C010	C00Y	118.0 (3)
C00B	N10	C00U	111.6 (3)	C00Q	C011	C014	118.2 (3)
C00U	N10	Ir01	134.3 (2)	C00Q	C011	C017	119.5 (3)
C010	O006	Ir01	125.4 (2)	C014	C011	C017	122.4 (3)
C00O	O007	C00V	117.4 (3)	C01C	C012	C00P	121.0 (3)
C00I	N008	Ir01	113.3 (2)	C010	C013	C016	127.8 (3)
C00I	N008	C01A	111.6 (3)	C00T	C014	C011	122.3 (3)
C01A	N008	Ir01	135.1 (2)	C00Z	C015	C00C	122.8 (3)
C00G	C20	C00B	112.8 (3)	C00Z	C015	C019	116.3 (3)

Table 5 Bond Angles for solveheavy.

Atom	Atom	Atom	Angle/°	Atom	Atom	Atom	Angle/°
C00R	C20	C00B	124.3 (3)	C019	C015	C00C	120.9 (3)
C00R	C20	C00G	122.8 (3)	O004	C016	C013	126.8 (3)
C00F	C21	Ir01	114.5 (2)	O004	C016	C01E	115.7 (3)
C00P	C21	Ir01	128.9 (3)	C013	C016	C01E	117.5 (3)
C00P	C21	C00F	116.6 (3)	C01G	C017	C011	124.4 (5)
N10	C00B	S002	114.9 (2)	C01G	C017	C1	115.9 (6)
N10	C00B	C20	117.5 (3)	C1	C017	C011	119.7 (5)
C20	C00B	S002	127.4 (2)	C1A	C017	C011	121.7 (5)
C00D	C00C	C00L	118.0 (3)	C1A	C017	C01H	118.7 (5)
C00D	C00C	C015	121.2 (3)	C01H	C017	C011	119.4 (4)
C00L	C00C	C015	120.8 (3)	C00J	C018	C00G	121.3 (3)
C00K	C00D	C00C	119.0 (3)	C00X	C019	C015	122.6 (3)
C01F	O00E	C01D	116.2 (3)	N008	C01A	C00M	113.3 (3)
C21	C00F	C00I	113.0 (3)	C00T	C01A	N008	127.4 (3)
C00W	C00F	C21	122.6 (3)	C00T	C01A	C00M	119.3 (3)
C00W	C00F	C00I	124.4 (3)	C01F	C01B	C01G	120.1 (8)
C20	C00G	Ir01	115.1 (2)	C00W	C01C	C012	120.1 (3)
C018	C00G	Ir01	128.9 (3)	O00E	C01F	C2	112.9 (4)
C018	C00G	C20	116.0 (3)	O00E	C01F	C3	124.8 (5)
C00L	C00H	C00U	118.3 (3)	C01B	C01F	O00E	125.5 (6)
N008	C00I	S003	115.0 (2)	C01B	C01F	C2	121.4 (6)
N008	C00I	C00F	118.0 (3)	C2A	C01F	O00E	115.3 (5)
C00F	C00I	S003	127.0 (3)	C2A	C01F	C3	119.8 (6)
C018	C00J	C00S	121.2 (3)	C017	C01G	C01B	125.1 (8)
C00D	C00K	S002	127.9 (3)	C2	C1	C017	121.8 (7)
C00D	C00K	C00U	122.2 (3)	C1	C2	C01F	115.1 (7)
C00U	C00K	S002	109.9 (2)	C017	C1A	C2A	119.8 (7)
C00H	C00L	C00C	123.0 (3)	C01F	C2A	C1A	122.2 (7)
C00Q	C00M	S003	127.6 (3)	C01H	C3	C01F	119.2 (7)
C00Q	C00M	C01A	122.0 (3)	C3	C01H	C017	120.0 (7)

Table 6 Torsion Angles for solveheavy.

A	B	C	D	Angle/°	A	B	C	D	Angle/°
Ir01	O004	C016	C013	1.0 (5)	C00N	C00O	C00X	C019	-0.8 (5)
Ir01	O004	C016	C01E	179.9 (3)	C00N	C00Z	C015	C00C	-178.2 (3)
Ir01	N10	C00B	S002	179.17 (14)	C00N	C00Z	C015	C019	-0.6 (5)
Ir01	N10	C00B	C20	-3.1 (4)	C00O	C00N	C00Z	C015	0.5 (6)

Table 6 Torsion Angles for solveheavy.

A	B	C	D	Angle/°	A	B	C	D	Angle/°
Ir01	N10	C00U	C00H	3.2 (5)	C00O	C00X	C019	C015	0.8 (5)
Ir01	N10	C00U	C00K	179.5 (2)	C00P	C21	C00F	C00I	-178.4 (3)
Ir01	O006	C010	C00Y	-173.2 (2)	C00P	C21	C00F	C00W	0.9 (5)
Ir01	O006	C010	C013	5.1 (5)	C00P	C012	C01C	C00W	0.8 (6)
Ir01	N008	C00I	S003	177.33 (15)	C00Q	C00M	C01A	N008	177.9 (3)
Ir01	N008	C00I	C00F	-4.3 (4)	C00Q	C00M	C01A	C00T	-2.7 (5)
Ir01	N008	C01A	C00M	-177.1 (2)	C00Q	C011	C014	C00T	-1.5 (6)
Ir01	N008	C01A	C00T	3.7 (6)	C00Q	C011	C017	C01G	-8.7 (6)
Ir01	C21	C00F	C00I	4.9 (4)	C00Q	C011	C017	C1	168.6 (4)
Ir01	C21	C00F	C00W	-175.9 (3)	C00Q	C011	C017	C1A	-161.4 (5)
Ir01	C21	C00P	C012	176.1 (3)	C00Q	C011	C017	C01H	13.4 (6)
Ir01	C00G	C018	C00J	179.9 (3)	C00R	C20	C00B	S002	-1.8 (5)
S002	C00K	C00U	N10	-2.6 (3)	C00R	C20	C00B	N10	-177.3 (3)
S002	C00K	C00U	C00H	174.1 (3)	C00R	C20	C00G	Ir01	-179.3 (2)
S003	C00M	C00Q	C011	-178.3 (3)	C00R	C20	C00G	C018	2.0 (5)
S003	C00M	C01A	N008	-1.7 (4)	C00S	C00J	C018	C00G	0.5 (5)
S003	C00M	C01A	C00T	177.7 (3)	C00U	N10	C00B	S002	-1.7 (3)
O006	C010	C013	C016	-2.5 (6)	C00U	N10	C00B	C20	174.4 (3)
O007	C00O	C00X	C019	179.3 (3)	C00U	C00H	C00L	C00C	1.1 (5)
C20	C00G	C018	C00J	-1.6 (5)	C00V	O007	C00O	C00N	-174.7 (3)
C20	C00R	C00S	C00J	0.0 (5)	C00V	O007	C00O	C00X	5.1 (5)
C21	C00F	C00I	S003	177.9 (3)	C00W	C00F	C00I	S003	-1.3 (5)
C21	C00F	C00I	N008	-0.3 (5)	C00W	C00F	C00I	N008	-179.5 (3)
C21	C00F	C00W	C01C	-0.9 (6)	C00Y	C010	C013	C016	175.8 (3)
C21	C00P	C012	C01C	-0.8 (6)	C00Z	C00N	C00O	O007	-179.9 (3)
C00B	S002	C00K	C00D	-179.7 (3)	C00Z	C00N	C00O	C00X	0.2 (5)
C00B	S002	C00K	C00U	1.3 (2)	C00Z	C015	C019	C00X	-0.1 (5)
C00B	N10	C00U	C00H	-173.5 (3)	C010	C013	C016	O004	-1.0 (6)
C00B	N10	C00U	C00K	2.8 (4)	C010	C013	C016	C01E	-179.9 (4)
C00B	C20	C00G	Ir01	3.6 (3)	C011	C017	C01G	C01B	178.7 (5)
C00B	C20	C00G	C018	-175.1 (3)	C011	C017	C1	C2	-178.9 (3)
C00B	C20	C00R	C00S	175.6 (3)	C011	C017	C1A	C2A	-179.4 (3)
C00C	C00D	C00K	S002	-177.7 (2)	C011	C017	C01H	C3	-179.6 (4)
C00C	C00D	C00K	C00U	1.2 (5)	C014	C00T	C01A	N008	-179.6 (3)
C00C	C015	C019	C00X	177.6 (3)	C014	C00T	C01A	C00M	1.2 (5)
C00D	C00C	C00L	C00H	-4.8 (5)	C014	C011	C017	C01G	171.1 (5)
C00D	C00C	C015	C00Z	-174.8 (3)	C014	C011	C017	C1	-11.6 (5)
C00D	C00C	C015	C019	7.7 (5)	C014	C011	C017	C1A	18.4 (6)
C00D	C00K	C00U	N10	178.4 (3)	C014	C011	C017	C01H	-166.8 (5)
C00D	C00K	C00U	C00H	-4.9 (5)	C015	C00C	C00D	C00K	-177.2 (3)

Table 6 Torsion Angles for solveheavy.

A	B	C	D	Angle/°	A	B	C	D	Angle/°
O00E	C01F	C2	C1	-176.2 (3)	C015	C00C	C00L	C00H	176.0 (3)
O00E	C01F	C2A	C1A	-179.2 (4)	C017	C011	C014	C00T	178.7 (4)
O00E	C01F	C3	C01H	-180.0 (5)	C017	C1	C2	C01F	-2.5 (2)
C00F	C21	C00P	C012	-0.1 (5)	C017	C1A	C2A	C01F	-2.5 (3)
C00F	C00W	C01C	C012	0.0 (6)	C018	C00J	C00S	C00R	0.3 (5)
C00G	C20	C00B	S002	175.3 (2)	C01A	N008	C00I	S003	-2.4 (4)
C00G	C20	C00B	N10	-0.2 (4)	C01A	N008	C00I	C00F	176.0 (3)
C00G	C20	C00R	C00S	-1.3 (5)	C01A	C00M	C00Q	C011	2.1 (5)
C00I	S003	C00M	C00Q	-179.3 (3)	C01A	C00T	C014	C011	0.9 (6)
C00I	S003	C00M	C01A	0.3 (3)	C01B	C01F	C2	C1	7.2 (5)
C00I	N008	C01A	C00M	2.6 (4)	C01D	O00E	C01F	C01B	13.9 (7)
C00I	N008	C01A	C00T	-176.7 (3)	C01D	O00E	C01F	C2	-162.5 (4)
C00I	C00F	C00W	C01C	178.3 (4)	C01D	O00E	C01F	C2A	169.1 (4)
C00K	S002	C00B	N10	0.2 (3)	C01D	O00E	C01F	C3	-8.0 (7)
C00K	S002	C00B	C20	-175.4 (3)	C01F	C01B	C01G	C017	3.5 (7)
C00L	C00C	C00D	C00K	3.6 (5)	C01F	C3	C01H	C017	0.2 (7)
C00L	C00C	C015	C00Z	4.4 (5)	C01G	C017	C1	C2	-1.4 (2)
C00L	C00C	C015	C019	-173.2 (3)	C01G	C01B	C01F	O00E	176.2 (5)
C00L	C00H	C00U	N10	179.9 (3)	C01G	C01B	C01F	C2	-7.7 (7)
C00L	C00H	C00U	C00K	3.7 (5)	C1	C017	C01G	C01B	1.3 (6)
C00M	S003	C00I	N008	1.3 (3)	C1A	C017	C01H	C3	-4.6 (7)
C00M	S003	C00I	C00F	-177.0 (3)	C2A	C01F	C3	C01H	3.1 (5)
C00M	C00Q	C011	C014	0.0 (5)	C3	C01F	C2A	C1A	-2.0 (3)
C00M	C00Q	C011	C017	179.8 (3)	C01H	C017	C1A	C2A	5.7 (5)

Table 7 Hydrogen Atom Coordinates ($\text{\AA} \times 10^4$) and Isotropic Displacement Parameters ($\text{\AA}^2 \times 10^3$) for solveheavy.

Atom	x	y	z	U(eq)
H00D	1558.83	7699.81	8864.18	16
H00H	2390.45	6117.41	7687.48	21
H00J	6218.65	7543.68	4004.72	23
H00L	1430.77	6189.17	8986.92	22
H00N	-581.85	6292.21	11327.45	25
H00P	5584.2	6695.02	7879.71	22
H00Q	5451.72	4952.62	2811.93	23
H00R	4314.82	8217.57	5835.96	20
H00S	5637.72	8270.55	4705.86	23
H00A	-2724.33	7638.21	11658.94	37

Table 7 Hydrogen Atom Coordinates ($\text{\AA}\times 10^4$) and Isotropic Displacement Parameters ($\text{\AA}^2\times 10^3$) for solveheavy.

Atom	<i>x</i>	<i>y</i>	<i>z</i>	U(eq)
H00B	-1290.27	7737.27	12461.19	37
H00C	-2571.26	7443.05	12717.16	37
H00W	8272.36	5511.45	6726.08	27
H00X	-862.04	7790.1	10989.51	23
H00E	2008.64	4901.37	6770.33	28
H00F	357.01	4981.25	6283.78	28
H00G	1089.56	5263.89	7250.92	28
H00Z	576.17	6236.31	10122.99	23
H012	7797.45	6441.41	8800.32	29
H013	-384.21	5602.88	5227.02	23
H018	5498.43	6768	4405.58	20
H019	344.27	7730.23	9798.81	24
H01C	9123.57	5848.59	8242.81	31
H01A	3075.43	3956.69	-2268.2	49
H01B	3320.6	3761.13	-1201.99	49
H01D	4361.17	4171.27	-1451.38	49
H01E	-1224.14	6609.11	4256.89	49
H01F	-1411.38	6039.66	3921.35	49
H01G	-512.41	6414.19	3448.96	49

Table 8 Atomic Occupancy for solveheavy.

Atom	Occupancy	Atom	Occupancy	Atom	Occupancy
C01B	0.493 (8)	C01G	0.493 (8)	C1	0.493 (8)
C2	0.493 (8)	C1A	0.507 (8)	C2A	0.507 (8)
C3	0.507 (8)	C01H	0.507 (8)		

Experimental

Single crystals of $\text{C}_{45}\text{H}_{29}\text{IrN}_2\text{O}_4\text{S}_2$ [solveheavy] were [extracted]. A suitable crystal was selected and [mounted] on a Bruker APEX-II CCD diffractometer. The crystal was kept at 99.99 K during data collection. Using Olex2 [1], the structure was solved with the SHELXS [2] structure solution program using Direct Methods and refined with the SHELXL [3] refinement package using Least Squares minimisation.

1. Dolomanov, O.V., Bourhis, L.J., Gildea, R.J., Howard, J.A.K. & Puschmann, H. (2009), J. Appl. Cryst. 42, 339-341.
2. Sheldrick, G.M. (2008). Acta Cryst. A64, 112-122.
3. Sheldrick, G.M. (2015). Acta Cryst. C71, 3-8.

Crystal structure determination of [solveheavy]

Crystal Data for $\text{C}_{45}\text{H}_{29}\text{IrN}_2\text{O}_4\text{S}_2$ ($M=918.02$ g/mol): monoclinic, space group $P2_1/c$ (no. 14), $a = 9.7527(11)$ \AA , $b = 26.827(3)$ \AA , $c = 14.5853(16)$ \AA , $\beta = 104.776(2)^\circ$, $V = 3689.9(7)$ \AA^3 , $Z = 4$, $T = 99.99$ K, $\mu(\text{MoK}\alpha) = 3.780$ mm^{-1} , $D_{\text{calc}} = 1.653$ g/cm^3 , 32867 reflections measured ($3.036^\circ \leq 2\theta \leq 55.84^\circ$), 8727 unique ($R_{\text{int}} =$

0.0315, $R_{\text{sigma}} = 0.0268$) which were used in all calculations. The final R_1 was 0.0276 ($I > 2\sigma(I)$) and wR_2 was 0.0664 (all data).

Refinement model description

Number of restraints - 198, number of constraints - unknown.

Details:

1. Fixed Uiso

At 1.2 times of:

All C(H) groups

At 1.5 times of:

All C(H,H,H) groups

2. Restrained planarity

C1A, C2A, C01F, C3, C01H, C017

with sigma of 0.01

C017, C1, C2, C01F, C01B, C01G

with sigma of 0.01

3. Uiso/Uanisotropy restraints and constraints

$C017 \approx C01G \approx C01B \approx C01H \approx C3 \approx C2A \approx C1A \approx C1$

$\approx C2 \approx C01F$: within 2A with sigma of 0.002 and sigma for terminal atoms of 0.004 within 2A

4. Rigid body (RIGU) restraints

C3, C01H, C01G, C01B, C01F, C2, C1, C2A, C1A, C017

with sigma for 1-2 distances of 0.002 and sigma for 1-3 distances of 0.002

5. Others

$\text{Sof}(C1A) = \text{Sof}(C2A) = \text{Sof}(C3) = \text{Sof}(C01H) = 1 - \text{FVAR}(1)$

$\text{Sof}(C01B) = \text{Sof}(C01G) = \text{Sof}(C1) = \text{Sof}(C2) = \text{FVAR}(1)$

6.a Aromatic/amide H refined with riding coordinates:

C00D(H00D), C00H(H00H), C00J(H00J), C00L(H00L), C00N(H00N), C00P(H00P),

C00Q(H00Q), C00R(H00R), C00S(H00S), C00W(H00W), C00X(H00X), C00Z(H00Z),

C012(H012), C013(H013), C018(H018), C019(H019), C01C(H01C)

6.b Idealised Me refined as rotating group:

C00V(H00A,H00B,H00C), C00Y(H00E,H00F,H00G), C01D(H01A,H01B,H01D), C01E(H01E,

H01F,H01G)

This report has been created with Olex2, compiled on 2020.11.12 svn.r5f609507 for OlexSys. Please [let us know](#) if there are any errors or if you would like to have additional features.

APPENDIX I

CRYSTAL DATA FOR Ir[(6-(3,5-difluorophenyl)-2-pbt)₂(acac)]

Table 1 Crystal data and structure refinement for Ir[(6-(3,5-difluorophenyl)-2-pbt)₂(acac)]

Identification code	6-(3,5-difluorophenyl)-2-pbt
Empirical formula	C ₅₀ H ₄₃ F _{7.3} IrN ₂ O ₂ S ₂
Formula weight	1098.88
Temperature/K	99.96
Crystal system	triclinic
Space group	P-1
a/Å	12.6414(9)
b/Å	13.1546(9)
c/Å	15.0581(10)
α/°	89.988(2)
β/°	74.036(2)
γ/°	70.8660(10)
Volume/Å ³	2263.3(3)
Z	2
ρ _{calc} /cm ³	1.612
μ/mm ⁻¹	3.115
F(000)	1095.0
Crystal size/mm ³	0.31 × 0.29 × 0.24
Radiation	MoKα (λ = 0.71073)
2θ range for data collection/°	3.294 to 55.956
Index ranges	-14 ≤ h ≤ 16, -16 ≤ k ≤ 17, -19 ≤ l ≤ 19
Reflections collected	36113
Independent reflections	10044 [R _{int} = 0.0209, R _{sigma} = 0.0215]
Data/restraints/parameters	10044/0/574
Goodness-of-fit on F ²	1.066
Final R indexes [I ≥ 2σ (I)]	R ₁ = 0.0200, wR ₂ = 0.0480
Final R indexes [all data]	R ₁ = 0.0241, wR ₂ = 0.0498
Largest diff. peak/hole / e Å ⁻³	1.25/-0.71

Table 2 Fractional Atomic Coordinates ($\times 10^4$) and Equivalent Isotropic Displacement Parameters ($\text{\AA}^2 \times 10^3$) for 6-(3,5-difluorophenyl)-2-pbt. U_{eq} is defined as 1/3 of the trace of the orthogonalised U_{ij} tensor.

Atom	<i>x</i>	<i>y</i>	<i>z</i>	$U(\text{eq})$
Ir1	2322.1 (2)	4560.0 (2)	7246.8 (2)	13.95 (3)
S002	4501.1 (5)	4240.1 (5)	4283.7 (4)	19.33 (11)
S1	-61.9 (5)	3637.9 (5)	9670.1 (4)	20.07 (11)
F6	1783.3 (8)	10549.1 (8)	5522.1 (7)	35.9 (4)
F5	875.5 (10)	11031.4 (9)	7535.7 (7)	42.4 (4)
O1	1314.2 (14)	6219.4 (12)	7791.3 (11)	18.1 (3)
O2	3781.3 (14)	4807.6 (12)	7574.1 (11)	17.6 (3)
F2	488.1 (16)	10831.4 (13)	3308.2 (12)	45.2 (5)
F3	1190.9 (19)	2911.2 (15)	14280.4 (11)	51.8 (5)
F1	4461.2 (16)	9176.4 (16)	1722.2 (12)	45.4 (4)
F4	5191.8 (17)	1452.2 (15)	12678.8 (14)	48.6 (5)
N2	1610.3 (16)	4105.7 (14)	8515.3 (13)	15.6 (4)
N1	3006.0 (16)	4856.2 (14)	5912.2 (12)	15.2 (4)
C15	3333.5 (18)	3053.6 (17)	6698.8 (15)	16.0 (4)
C11	3549.9 (19)	5579.7 (18)	4506.2 (15)	16.6 (4)
C7	2644 (2)	7404.8 (18)	4219.2 (15)	18.4 (4)
C13	3853.0 (19)	4002.2 (18)	5396.2 (15)	16.4 (4)
C25	909.8 (19)	4367.3 (16)	7020.4 (15)	15.9 (4)
C28	-1257 (2)	4181 (2)	6996.0 (18)	25.4 (5)
C17	4218 (2)	1099.1 (19)	6625.0 (19)	27.4 (5)
C30	117 (2)	4183.6 (17)	7817.8 (15)	17.2 (4)
C26	581 (2)	4418.4 (18)	6201.9 (16)	20.5 (5)
C31	564.8 (19)	4023.7 (17)	8614.3 (15)	17.3 (4)
C35	2457 (2)	3185.8 (18)	10965.4 (16)	19.6 (5)
C12	3508 (2)	6391.4 (18)	3913.7 (15)	18.3 (4)
C9	1914 (2)	6770.4 (18)	5717.8 (16)	20.0 (5)
C16	3415 (2)	2077.9 (18)	7101.5 (17)	21.6 (5)
C5	3567 (2)	8313 (2)	2920.2 (17)	24.7 (5)
C18	4970 (2)	1058.0 (19)	5742.7 (18)	26.5 (5)
C39	1808 (2)	3048.7 (19)	12679.4 (17)	26.1 (5)
C38	2714 (2)	2827.3 (18)	11847.8 (16)	20.7 (5)
C27	-475 (2)	4320.1 (19)	6188.7 (17)	24.2 (5)
C33	1177.5 (19)	3553.8 (17)	10004.6 (15)	17.2 (4)
C41	3195 (3)	2166 (2)	13516.7 (19)	35.5 (7)
C10	2791.7 (19)	5762.3 (17)	5414.9 (15)	16.4 (4)
C3	1524 (2)	9156.8 (19)	3725.9 (17)	24.2 (5)
C14	4079.0 (19)	2977.6 (18)	5788.9 (15)	17.6 (4)
C8	1857 (2)	7575.5 (18)	5118.1 (16)	21.0 (5)

Table 2 Fractional Atomic Coordinates ($\times 10^4$) and Equivalent Isotropic Displacement Parameters ($\text{\AA}^2 \times 10^3$) for 6-(3,5-difluorophenyl)-2-pbt. U_{eq} is defined as 1/3 of the trace of the orthogonalised U_{ij} tensor.

Atom	x	y	z	$U(eq)$
C29	-961 (2)	4104.3 (19)	7819.9 (17)	22.3 (5)
C34	1381 (2)	3255.0 (18)	10850.2 (15)	19.0 (4)
C23	1720 (2)	6897.6 (18)	8042.6 (16)	20.8 (5)
C40	2080 (3)	2701 (2)	13481.4 (18)	32.5 (6)
C36	3286 (2)	3432.4 (19)	10246.3 (17)	22.8 (5)
C4	2574 (2)	8302.7 (19)	3607.4 (16)	20.0 (5)
C32	1994.5 (19)	3811.0 (17)	9296.2 (15)	16.3 (4)
C37	3074 (2)	3747.8 (19)	9412.9 (16)	20.6 (5)
C43	3862 (2)	2266 (2)	11847.7 (19)	25.9 (5)
C19	4905 (2)	2000.0 (19)	5315.8 (17)	23.2 (5)
C2	1512 (2)	9998 (2)	3171.4 (18)	28.0 (5)
C6	3489 (2)	9174 (2)	2384.5 (18)	29.6 (6)
C1	2472 (3)	10039 (2)	2496.0 (18)	29.4 (6)
C24	871 (3)	8052 (2)	8306 (2)	31.9 (6)
C21	4869 (2)	5648 (2)	8159.3 (18)	27.8 (5)
C42	4068 (3)	1967 (2)	12686 (2)	33.0 (6)
C47	7181 (3)	11477 (2)	-250 (2)	36.6 (6)
C20	3769 (2)	5694.7 (19)	7918.4 (15)	19.8 (5)
C48	7560 (3)	12252 (3)	-905 (2)	42.4 (7)
C22	2871 (2)	6675 (2)	8115.1 (18)	27.9 (6)
C49	6548 (3)	13248 (3)	-937 (2)	43.5 (7)
C46	8179 (3)	10465 (3)	-221 (2)	45.6 (8)
C44	6854 (4)	9369 (3)	399 (3)	63.8 (11)
C50	1133 (3)	11550 (2)	6463 (2)	44.5 (8)
C45	7836 (4)	9727 (3)	500 (3)	59.6 (10)

Table 3 Anisotropic Displacement Parameters ($\text{\AA}^2 \times 10^3$) for 6-(3,5-difluorophenyl)-2-pbt. The Anisotropic displacement factor exponent takes the form: - $2\pi^2[h^2a^{*2}U_{11}+2hka^*b^*U_{12}+\dots]$.

Atom	U_{11}	U_{22}	U_{33}	U_{23}	U_{13}	U_{12}
Ir1	14.68 (4)	14.78 (4)	12.67 (4)	1.67 (3)	-2.44 (3)	-6.68 (3)
S002	18.9 (3)	20.8 (3)	13.7 (2)	0.1 (2)	-0.6 (2)	-4.0 (2)
S1	17.1 (3)	26.9 (3)	18.5 (3)	7.4 (2)	-4.3 (2)	-11.2 (2)
F6	31.8 (5)	31.3 (6)	36.3 (6)	-19.7 (4)	7.8 (4)	-14.6 (4)
F5	53.6 (7)	43.6 (7)	30.7 (6)	5.9 (4)	-7.3 (5)	-21.4 (5)
O1	19.4 (8)	17.7 (7)	15.7 (7)	1.5 (6)	-2.3 (6)	-6.6 (6)

Table 3 Anisotropic Displacement Parameters ($\text{\AA}^2 \times 10^3$) for 6-(3,5-difluorophenyl)-2-pbt.
The Anisotropic displacement factor exponent takes the form: -
 $2\pi^2[h^2a^{*2}U_{11}+2hka^*b^*U_{12}+\dots]$.

Atom	U_{11}	U_{22}	U_{33}	U_{23}	U_{13}	U_{12}
O2	18.3(7)	20.3(8)	15.6(7)	0.1(6)	-2.6(6)	-10.5(6)
F2	47.3(10)	30.6(9)	37.9(9)	10.9(7)	-4.4(8)	5.8(8)
F3	71.1(13)	50.8(11)	16.6(7)	3.7(7)	-2.9(8)	-7.3(10)
F1	37.4(9)	63.7(12)	40.2(9)	28.9(9)	-7.7(8)	-27.1(9)
F4	47.0(11)	53.2(11)	65.7(12)	33.4(10)	-39.4(10)	-24.3(9)
N2	14.7(8)	17.0(9)	15.1(8)	1.9(7)	-3.4(7)	-6.0(7)
N1	15.5(8)	17.3(9)	12.7(8)	1.5(7)	-2.0(7)	-7.2(7)
C15	14.0(10)	18.3(10)	18.4(10)	0.3(8)	-7.5(8)	-6.8(8)
C11	14.1(10)	19.6(10)	15.5(10)	-0.7(8)	-3.2(8)	-5.8(8)
C7	21.1(11)	22.2(11)	16.1(10)	4.3(8)	-6.1(9)	-12.3(9)
C13	15.3(10)	20.8(10)	12.9(9)	0.2(8)	-3.0(8)	-6.8(9)
C25	17.0(10)	11.7(9)	18.0(10)	1.0(8)	-5.3(9)	-3.4(8)
C28	24.1(12)	29.7(13)	29.1(13)	4.9(10)	-12.8(11)	-13.8(10)
C17	32.6(13)	18.2(11)	35.9(14)	4.1(10)	-15.5(12)	-9.9(10)
C30	19.0(10)	16.5(10)	18.6(10)	3.8(8)	-6.4(9)	-8.5(9)
C26	21.8(11)	22.0(11)	17.6(10)	1.4(9)	-5.6(9)	-7.4(9)
C31	17.7(10)	16.4(10)	18.1(10)	2.4(8)	-3.1(9)	-8.1(9)
C35	24.5(11)	17.4(10)	17.2(10)	1.8(8)	-6.6(9)	-7.1(9)
C12	18.3(10)	24.5(11)	13.2(10)	0.2(8)	-2.8(9)	-10.3(9)
C9	21.0(11)	21.1(11)	14.9(10)	0.9(8)	-1.1(9)	-6.6(9)
C16	24.8(12)	19.1(11)	23.1(11)	3.6(9)	-7.9(10)	-9.6(9)
C5	24.5(12)	31.1(13)	23.0(12)	8.6(10)	-9.2(10)	-13.5(10)
C18	28.3(13)	17.1(11)	31.6(13)	-5.7(10)	-10.9(11)	-2.5(10)
C39	36.4(14)	19.6(11)	19.0(11)	1.8(9)	-8.6(11)	-4.8(10)
C38	30.2(12)	17.0(10)	19.9(11)	4.4(8)	-10.5(10)	-11.9(9)
C27	28.6(12)	24.9(12)	23.6(12)	2.9(9)	-13.5(10)	-10.0(10)
C33	15.5(10)	17.5(10)	17.7(10)	1.7(8)	-4.0(9)	-5.4(8)
C41	64(2)	28.6(13)	28.3(14)	10.7(11)	-29.0(15)	-21.4(14)
C10	18.0(10)	19.1(10)	14.1(10)	1.9(8)	-5.0(9)	-8.9(9)
C3	27.5(12)	24.5(12)	18.6(11)	3.4(9)	-3.5(10)	-9.1(10)
C14	18.3(10)	18.7(10)	18.3(10)	1.3(8)	-7.1(9)	-7.9(9)
C8	22.3(11)	18.5(11)	18.7(11)	0.8(9)	-2.8(9)	-4.9(9)
C29	21.3(11)	24.8(12)	23.5(11)	5.0(9)	-6.2(10)	-11.9(10)
C34	20.6(11)	19.5(10)	15.0(10)	3.8(8)	-2.0(9)	-7.1(9)
C23	27.2(12)	17.7(11)	16.2(10)	1.2(8)	-4.8(9)	-7.2(9)
C40	52.1(17)	25.9(13)	18.3(12)	2.0(10)	-9.1(12)	-12.5(12)
C36	23.2(12)	26.4(12)	24.1(12)	6.5(9)	-10.6(10)	-12.4(10)
C4	25.4(12)	22.7(11)	16.9(10)	3.3(9)	-8.0(9)	-13.2(10)

Table 3 Anisotropic Displacement Parameters ($\text{\AA}^2 \times 10^3$) for 6-(3,5-difluorophenyl)-2-pbt.
The Anisotropic displacement factor exponent takes the form: -
 $2\pi^2[h^2a^{*2}U_{11}+2hka^*b^*U_{12}+\dots]$.

Atom	U_{11}	U_{22}	U_{33}	U_{23}	U_{13}	U_{12}
C32	18.7 (10)	16.5 (10)	13.7 (9)	2.4 (8)	-4.1 (8)	-6.6 (8)
C37	20.2 (11)	26.3 (12)	18.3 (11)	6.2 (9)	-4.8 (9)	-12.5 (10)
C43	31.4 (13)	24.6 (12)	30.0 (13)	11.0 (10)	-14.4 (11)	-16.0 (11)
C19	21.0 (11)	24.8 (12)	22.2 (11)	-3.8 (9)	-7.4 (10)	-5.1 (10)
C2	34.2 (14)	21.9 (12)	26.0 (12)	3.5 (10)	-10.4 (11)	-5.6 (11)
C6	33.7 (14)	40.2 (15)	23.3 (12)	11.0 (11)	-7.8 (11)	-23.7 (12)
C1	45.4 (16)	26.5 (13)	24.8 (12)	10.1 (10)	-15.2 (12)	-19.0 (12)
C24	34.6 (14)	20.2 (12)	38.0 (15)	-1.7 (11)	-9.1 (12)	-6.9 (11)
C21	28.9 (13)	31.8 (13)	28.8 (13)	-0.2 (10)	-12.1 (11)	-15.4 (11)
C42	40.8 (16)	27.7 (13)	47.3 (17)	16.5 (12)	-29.6 (14)	-19.6 (12)
C47	41.9 (16)	39.9 (16)	29.9 (14)	-1.9 (12)	-9.4 (13)	-17.3 (13)
C20	22.8 (11)	23.5 (11)	12.9 (10)	1.2 (8)	-1.7 (9)	-10.7 (10)
C48	34.8 (15)	45.9 (18)	53.3 (19)	10.4 (15)	-13.0 (15)	-22.4 (14)
C22	29.8 (13)	31.4 (13)	27.7 (13)	-10.1 (10)	-3.4 (11)	-21.1 (11)
C49	32.8 (15)	43.2 (17)	53.1 (19)	8.8 (15)	-5.1 (15)	-17.2 (14)
C46	48.7 (19)	46.3 (18)	46.0 (18)	4.4 (15)	-20.4 (16)	-16.0 (15)
C44	70 (3)	35.1 (18)	66 (2)	11.6 (17)	7 (2)	-14.9 (18)
C50	51.0 (19)	30.9 (15)	56 (2)	-2.4 (14)	-23.6 (17)	-12.7 (14)
C45	77 (3)	49 (2)	45 (2)	11.8 (16)	-18 (2)	-11 (2)

Table 4 Bond Lengths for 6-(3,5-difluorophenyl)-2-pbt.

Atom	Atom	Length/ \AA	Atom	Atom	Length/ \AA
Ir1	O1	2.1595 (15)	C30	C31	1.449 (3)
Ir1	O2	2.1554 (15)	C30	C29	1.400 (3)
Ir1	N2	2.0548 (19)	C26	C27	1.389 (3)
Ir1	N1	2.0500 (18)	C35	C38	1.494 (3)
Ir1	C15	2.000 (2)	C35	C34	1.391 (3)
Ir1	C25	2.000 (2)	C35	C36	1.405 (4)
S002	C11	1.747 (2)	C9	C10	1.398 (3)
S002	C13	1.729 (2)	C9	C8	1.388 (3)
S1	C31	1.727 (2)	C5	C4	1.394 (4)
S1	C33	1.744 (2)	C5	C6	1.384 (4)
F6	C50	1.751 (3)	C18	C19	1.385 (4)
F5	C50	1.743 (4)	C39	C38	1.399 (4)
O1	C23	1.269 (3)	C39	C40	1.383 (3)
O2	C20	1.271 (3)	C38	C43	1.396 (4)

Table 4 Bond Lengths for 6-(3,5-difluorophenyl)-2-pbt.

Atom	Atom	Length/Å	Atom	Atom	Length/Å
F2	C2	1.357 (3)	C33	C34	1.399 (3)
F3	C40	1.357 (3)	C33	C32	1.393 (3)
F1	C6	1.354 (3)	C41	C40	1.369 (4)
F4	C42	1.355 (3)	C41	C42	1.380 (4)
N2	C31	1.329 (3)	C3	C4	1.396 (3)
N2	C32	1.400 (3)	C3	C2	1.385 (3)
N1	C13	1.329 (3)	C14	C19	1.401 (3)
N1	C10	1.398 (3)	C23	C24	1.520 (3)
C15	C16	1.405 (3)	C23	C22	1.422 (3)
C15	C14	1.415 (3)	C36	C37	1.389 (3)
C11	C12	1.388 (3)	C32	C37	1.399 (3)
C11	C10	1.406 (3)	C43	C42	1.388 (4)
C7	C12	1.397 (3)	C2	C1	1.369 (4)
C7	C8	1.409 (3)	C6	C1	1.377 (4)
C7	C4	1.492 (3)	C21	C20	1.514 (3)
C13	C14	1.445 (3)	C47	C48	1.517 (4)
C25	C30	1.415 (3)	C47	C46	1.516 (4)
C25	C26	1.400 (3)	C20	C22	1.377 (3)
C28	C27	1.395 (4)	C48	C49	1.513 (4)
C28	C29	1.385 (3)	C46	C45	1.524 (5)
C17	C16	1.395 (3)	C44	C45	1.507 (6)
C17	C18	1.394 (4)			

Table 5 Bond Angles for 6-(3,5-difluorophenyl)-2-pbt.

Atom	Atom	Atom	Angle/°	Atom	Atom	Atom	Angle/°
O2	Ir1	O1	87.64 (6)	C19	C18	C17	119.7 (2)
N2	Ir1	O1	88.16 (6)	C40	C39	C38	118.6 (3)
N2	Ir1	O2	96.79 (7)	C39	C38	C35	120.3 (2)
N1	Ir1	O1	97.07 (7)	C43	C38	C35	120.1 (2)
N1	Ir1	O2	87.97 (7)	C43	C38	C39	119.5 (2)
N1	Ir1	N2	173.09 (7)	C26	C27	C28	121.1 (2)
C15	Ir1	O1	176.53 (8)	C34	C33	S1	126.81 (19)
C15	Ir1	O2	90.01 (7)	C32	C33	S1	110.81 (16)
C15	Ir1	N2	94.65 (8)	C32	C33	C34	122.4 (2)
C15	Ir1	N1	80.30 (8)	C40	C41	C42	116.0 (2)
C25	Ir1	O1	90.17 (7)	N1	C10	C11	113.34 (19)
C25	Ir1	O2	176.58 (7)	N1	C10	C9	127.2 (2)
C25	Ir1	N2	80.51 (8)	C9	C10	C11	119.4 (2)

Table 5 Bond Angles for 6-(3,5-difluorophenyl)-2-pbt.

Atom	Atom	Atom	Angle/°	Atom	Atom	Atom	Angle/°
C25	Ir1	N1	94.91 (8)	C2	C3	C4	118.8 (2)
C25	Ir1	C15	92.29 (8)	C15	C14	C13	112.59 (19)
C13	S002	C11	89.70 (11)	C19	C14	C15	123.0 (2)
C31	S1	C33	89.22 (11)	C19	C14	C13	124.4 (2)
C23	O1	Ir1	125.26 (15)	C9	C8	C7	122.2 (2)
C20	O2	Ir1	125.02 (15)	C28	C29	C30	118.6 (2)
C31	N2	Ir1	113.71 (15)	C35	C34	C33	118.0 (2)
C31	N2	C32	111.50 (19)	O1	C23	C24	115.8 (2)
C32	N2	Ir1	134.72 (15)	O1	C23	C22	126.4 (2)
C13	N1	Ir1	113.62 (15)	C22	C23	C24	117.8 (2)
C13	N1	C10	111.86 (19)	F3	C40	C39	118.0 (3)
C10	N1	Ir1	134.52 (14)	F3	C40	C41	118.2 (2)
C16	C15	Ir1	128.79 (17)	C41	C40	C39	123.8 (3)
C16	C15	C14	116.5 (2)	C37	C36	C35	122.4 (2)
C14	C15	Ir1	114.73 (16)	C5	C4	C7	120.3 (2)
C12	C11	S002	127.75 (17)	C5	C4	C3	118.9 (2)
C12	C11	C10	122.1 (2)	C3	C4	C7	120.7 (2)
C10	C11	S002	110.14 (17)	C33	C32	N2	113.23 (19)
C12	C7	C8	119.2 (2)	C33	C32	C37	119.7 (2)
C12	C7	C4	120.3 (2)	C37	C32	N2	127.0 (2)
C8	C7	C4	120.5 (2)	C36	C37	C32	118.0 (2)
N1	C13	S002	114.90 (17)	C42	C43	C38	118.4 (3)
N1	C13	C14	117.8 (2)	C18	C19	C14	118.7 (2)
C14	C13	S002	127.16 (16)	F2	C2	C3	118.0 (2)
C30	C25	Ir1	114.43 (15)	F2	C2	C1	118.2 (2)
C26	C25	Ir1	129.59 (18)	C1	C2	C3	123.8 (2)
C26	C25	C30	115.9 (2)	F1	C6	C5	118.6 (2)
C29	C28	C27	119.7 (2)	F1	C6	C1	118.1 (2)
C18	C17	C16	121.3 (2)	C1	C6	C5	123.3 (3)
C25	C30	C31	113.10 (19)	C2	C1	C6	116.0 (2)
C29	C30	C25	123.3 (2)	F4	C42	C41	118.7 (2)
C29	C30	C31	123.5 (2)	F4	C42	C43	117.7 (3)
C27	C26	C25	121.4 (2)	C41	C42	C43	123.6 (3)
N2	C31	S1	115.17 (16)	C46	C47	C48	113.6 (3)
N2	C31	C30	117.5 (2)	O2	C20	C21	115.3 (2)
C30	C31	S1	127.16 (17)	O2	C20	C22	127.8 (2)
C34	C35	C38	119.0 (2)	C22	C20	C21	116.8 (2)
C34	C35	C36	119.6 (2)	C49	C48	C47	112.8 (3)
C36	C35	C38	121.4 (2)	C20	C22	C23	127.4 (2)
C11	C12	C7	118.5 (2)	C47	C46	C45	114.4 (3)

Table 5 Bond Angles for 6-(3,5-difluorophenyl)-2-pbt.

Atom	Atom	Atom	Angle/°	Atom	Atom	Atom	Angle/°
C8	C9	C10	118.4 (2)	F5	C50	F6	113.32 (18)
C17	C16	C15	120.7 (2)	C44	C45	C46	114.2 (3)
C6	C5	C4	119.2 (2)				

Table 6 Torsion Angles for 6-(3,5-difluorophenyl)-2-pbt.

A	B	C	D	Angle/°	A	B	C	D	Angle/°
Ir1	O1	C23	C24	173.63 (16)	C16	C15	C14	C19	-3.2 (3)
Ir1	O1	C23	C22	-7.6 (4)	C16	C17	C18	C19	-1.7 (4)
Ir1	O2	C20	C21	175.32 (16)	C5	C6	C1	C2	-0.9 (4)
Ir1	O2	C20	C22	-3.0 (3)	C18	C17	C16	C15	0.8 (4)
Ir1	N2	C31	S1	179.75 (10)	C39	C38	C43	C42	-1.5 (4)
Ir1	N2	C31	C30	4.2 (2)	C38	C35	C34	C33	-177.7 (2)
Ir1	N2	C32	C33	179.43 (15)	C38	C35	C36	C37	178.8 (2)
Ir1	N2	C32	C37	0.0 (3)	C38	C39	C40	F3	-179.3 (2)
Ir1	N1	C13	S002	176.88 (10)	C38	C39	C40	C41	1.3 (4)
Ir1	N1	C13	C14	7.2 (2)	C38	C43	C42	F4	-178.0 (2)
Ir1	N1	C10	C11	176.55 (15)	C38	C43	C42	C41	2.0 (4)
Ir1	N1	C10	C9	-5.4 (4)	C27	C28	C29	C30	0.8 (4)
Ir1	C15	C16	C17	176.95 (17)	C33	S1	C31	N2	-1.07 (17)
Ir1	C15	C14	C13	-7.1 (2)	C33	S1	C31	C30	174.0 (2)
Ir1	C15	C14	C19	175.60 (17)	C33	C32	C37	C36	-0.4 (3)
Ir1	C25	C30	C31	-8.0 (2)	C10	N1	C13	S002	2.6 (2)
Ir1	C25	C30	C29	175.38 (17)	C10	N1	C13	C14	173.30 (18)
Ir1	C25	C26	C27	176.41 (17)	C10	C11	C12	C7	-3.3 (3)
S002	C11	C12	C7	177.68 (17)	C10	C9	C8	C7	0.5 (4)
S002	C11	C10	N1	1.8 (2)	C3	C2	C1	C6	0.2 (4)
S002	C11	C10	C9	176.46 (17)	C14	C15	C16	C17	1.6 (3)
S002	C13	C14	C15	175.58 (16)	C8	C7	C12	C11	0.8 (3)
S002	C13	C14	C19	1.7 (3)	C8	C7	C4	C5	153.3 (2)
S1	C33	C34	C35	176.85 (17)	C8	C7	C4	C3	-25.3 (3)
S1	C33	C32	N2	2.1 (2)	C8	C9	C10	N1	179.2 (2)
S1	C33	C32	C37	177.36 (17)	C8	C9	C10	C11	-2.9 (3)

Table 6 Torsion Angles for 6-(3,5-difluorophenyl)-2-pbt.

A	B	C	D	Angle/°	A	B	C	D	Angle/°
O1	C23	C22	C20	0.9 (5)	C29	C28	C27	C26	-2.1 (4)
O2	C20	C22	C23	5.2 (4)	C29	C30	C31	S1	4.1 (3)
F2	C2	C1	C6	-180.0 (2)	C29	C30	C31	N2	179.0 (2)
F1	C6	C1	C2	179.7 (2)	C34	C35	C38	C39	-30.5 (3)
N2	C32	C37	C36	-179.8 (2)	C34	C35	C38	C43	149.4 (2)
N1	C13	C14	C15	-0.2 (3)	C34	C35	C36	C37	0.0 (3)
N1	C13	C14	C19	177.0 (2)	C34	C33	C32	N2	178.98 (19)
C15	C14	C19	C18	2.3 (3)	C34	C33	C32	C37	1.6 (3)
C11	S002	C13	N1	-1.36 (18)	C40	C39	C38	C35	179.8 (2)
C11	S002	C13	C14	174.1 (2)	C40	C39	C38	C43	0.0 (4)
C13	S002	C11	C12	178.9 (2)	C40	C41	C42	F4	179.2 (2)
C13	S002	C11	C10	-0.28 (17)	C40	C41	C42	C43	-0.8 (4)
C13	N1	C10	C11	-2.8 (3)	C36	C35	C38	C39	150.8 (2)
C13	N1	C10	C9	175.3 (2)	C36	C35	C38	C43	-29.3 (3)
C13	C14	C19	C18	-174.7 (2)	C36	C35	C34	C33	1.1 (3)
C25	C30	C31	S1	172.54 (16)	C4	C7	C12	C11	179.5 (2)
C25	C30	C31	N2	2.4 (3)	C4	C7	C8	C9	-178.1 (2)
C25	C30	C29	C28	1.8 (3)	C4	C5	C6	F1	179.7 (2)
C25	C26	C27	C28	0.9 (4)	C4	C5	C6	C1	0.4 (4)
C17	C18	C19	C14	0.2 (4)	C4	C3	C2	F2	-178.8 (2)
C30	C25	C26	C27	1.5 (3)	C4	C3	C2	C1	1.1 (4)
C26	C25	C30	C31	173.73 (19)	C32	N2	C31	S1	2.4 (2)
C26	C25	C30	C29	-2.9 (3)	C32	N2	C31	C30	173.09 (18)
C31	S1	C33	C34	-179.5 (2)	C32	C33	C34	C35	-1.9 (3)
C31	S1	C33	C32	-0.61 (17)	C2	C3	C4	C7	177.0 (2)
C31	N2	C32	C33	-2.9 (3)	C2	C3	C4	C5	-1.6 (3)
C31	N2	C32	C37	176.5 (2)	C6	C5	C4	C7	-177.7 (2)
C31	C30	C29	C28	-174.5 (2)	C6	C5	C4	C3	0.9 (3)
C35	C38	C43	C42	178.6 (2)	C24	C23	C22	C20	179.7 (3)
C35	C36	C37	C32	-0.4 (3)	C21	C20	C22	C23	-173.1 (3)
C12	C11	C10	N1	-177.4 (2)	C42	C41	C40	F3	179.7 (2)
C12	C11	C10	C9	4.3 (3)	C42	C41	C40	C39	-0.9 (4)
C12	C7	C8	C9	0.5 (4)	C47	C46	C45	C44	56.4 (4)
C12	C7	C4	C5	-25.3 (3)	C48	C47	C46	C45	174.5 (3)
C12	C7	C4	C3	156.1 (2)	C46	C47	C48	C49	179.0 (3)
C16	C15	C14	C13	174.16 (19)					

Table 7 Hydrogen Atom Coordinates ($\text{\AA}\times 10^4$) and Isotropic Displacement Parameters ($\text{\AA}^2\times 10^3$) for 6-(3,5-difluorophenyl)-2-pbt.

Atom	<i>x</i>	<i>y</i>	<i>z</i>	U(eq)
H28	-1987.34	4138.11	6980.83	30
H17	4252.42	447.59	6907.12	33
H26	1092.05	4522.64	5643.28	25
H12	4054.66	6260.43	3313.56	22
H9	1369.69	6901.09	6319.15	24
H16	2919.03	2084.68	7705.04	26
H5	4288.56	7735.24	2820.83	30
H18	5525.74	386.27	5435.6	32
H39	1021.22	3430.19	12692.74	31
H27	-669.15	4348.32	5620.6	29
H41	3357.39	1945.73	14079.95	43
H3	829.52	9160.53	4178.49	29
H8	1266.91	8264.57	5320.58	25
H29	-1479.5	4000.36	8374.4	27
H34	802.91	3103.89	11331.13	23
H36	4017.02	3381.73	10333.06	27
H37	3644.31	3915.35	8936.94	25
H43	4487.18	2092.75	11287.84	31
H19	5410.16	1983.64	4713.87	28
H1	2439.23	10627.78	2126.7	35
H24A	350.87	8214.68	7908.44	48
H24B	1311.02	8552.57	8221.33	48
H24C	405.27	8131.53	8956.3	48
H21A	4948.95	5201.31	8674.4	42
H21B	4820.82	6380.21	8342.17	42
H21C	5551.13	5330.63	7617.16	42
H47A	6803.64	11856.81	382.76	44
H47B	6588.63	11264.86	-444.18	44
H48A	8139.71	12477.79	-705.61	51
H48B	7947.57	11871.5	-1537.62	51
H22	3039.17	7270.53	8322.82	33
H49A	6825.07	13681.09	-1417.07	65
H49B	6224.3	13678.8	-333	65
H49C	5939.91	13028.78	-1083	65
H46A	8805.09	10680.21	-89.32	55
H46B	8505.32	10050.66	-841.09	55
H44A	7040.74	9060.29	-240.46	96
H44B	6126.93	9991.74	547.01	96
H44C	6757.3	8821.18	825.5	96

Table 7 Hydrogen Atom Coordinates ($\text{\AA}\times 10^4$) and Isotropic Displacement Parameters ($\text{\AA}^2\times 10^3$) for 6-(3,5-difluorophenyl)-2-pbt.

Atom	<i>x</i>	<i>y</i>	<i>z</i>	U(eq)
H50A	1648.71	11982.01	6444.12	53
H50B	381.15	12042	6397.77	53
H45A	8530.9	9077.83	453.38	72
H45B	7599.58	10110.61	1126.02	72

Table 8 Atomic Occupancy for 6-(3,5-difluorophenyl)-2-pbt.

Atom	Occupancy	Atom	Occupancy	Atom	Occupancy
F6	1.649 (6)	F5	1.651 (6)		

Experimental

Single crystals of $\text{C}_{50}\text{H}_{43}\text{F}_{7.3}\text{IrN}_2\text{O}_2\text{S}_2$ [6-(3,5-difluorophenyl)-2-pbt] were [1]. A suitable crystal was selected and [1] on a 'Bruker APEX-II CCD' diffractometer. The crystal was kept at 99.96 K during data collection. Using Olex2 [1], the structure was solved with the Unknown [2] structure solution program using Unknown and refined with the Unknown [3] refinement package using Unknown minimisation.

1. Dolomanov, O.V., Bourhis, L.J., Gildea, R.J, Howard, J.A.K. & Puschmann, H. (2009), *J. Appl. Cryst.* 42, 339-341.
- 2.
- 3.

Crystal structure determination of [6-(3,5-difluorophenyl)-2-pbt]

Crystal Data for $\text{C}_{50}\text{H}_{43}\text{F}_{7.3}\text{IrN}_2\text{O}_2\text{S}_2$ ($M=1098.88$ g/mol): triclinic, space group P-1 (no. 2), $a = 12.6414(9)$ \AA , $b = 13.1546(9)$ \AA , $c = 15.0581(10)$ \AA , $\alpha = 89.988(2)^\circ$, $\beta = 74.036(2)^\circ$, $\gamma = 70.8660(10)^\circ$, $V = 2263.3(3)$ \AA^3 , $Z = 2$, $T = 99.96$ K, $\mu(\text{MoK}\alpha) = 3.115$ mm^{-1} , $D_{\text{calc}} = 1.612$ g/cm^3 , 36113 reflections measured ($3.294^\circ \leq 2\theta \leq 55.956^\circ$), 10044 unique ($R_{\text{int}} = 0.0209$, $R_{\text{sigma}} = 0.0215$) which were used in all calculations. The final R_1 was 0.0200 ($I > 2\sigma(I)$) and wR_2 was 0.0498 (all data).

Refinement model description

Number of restraints - 0, number of constraints - unknown.

Details:

1.a Secondary CH2 refined with riding coordinates:

C47 (H47A, H47B), C48 (H48A, H48B), C46 (H46A, H46B), C50 (H50A, H50B), C45 (H45A, H45B)

1.b Aromatic/amide H refined with riding coordinates:

C28 (H28), C17 (H17), C26 (H26), C12 (H12), C9 (H9), C16 (H16), C5 (H5), C18 (H18), C39 (H39), C27 (H27), C41 (H41), C3 (H3), C8 (H8), C29 (H29), C34 (H34), C36 (H36), C37 (H37), C43 (H43), C19 (H19), C1 (H1), C22 (H22)

1.c Idealised Me refined as rotating group:

C24 (H24A, H24B, H24C), C21 (H21A, H21B, H21C), C49 (H49A, H49B, H49C), C44 (H44A, H44B, H44C)

This report has been created with Olex2, compiled on 2022.04.07 svn.rca3783a0 for OlexSys. Please [let us know](#) if there are any errors or if you would like to have additional features.